MECHANICAL MODEL OF AN EARLY STAGE OSTEOARTHRITIS

by

Venkat S. Chiravuri

A thesis submitted to the Faculty of the University of Delaware in partial fulfillment of the requirements for the degree of Master of Science in Mechanical Engineering.

Fall 2009

MECHANICAL MODEL OF AN EARLY

STAGE OSTEOARTHRITIS

by
Venkat S. Chiravuri

Approved: _____

John E. Novotny, Ph.D.
Professor in charge of thesis on behalf of the Advisory Committee

Approved: _____

Anette M. Karlsson, Ph. D.
Chair, Department of Mechanical Engineering

Approved: _____

Michael J. Chajes, Ph. D.
Dean, College of Engineering

Approved: _____

Debra H. Norris, M S.
Vice Provost for Graduate and Professional Education

ACKNOWLEDGMENTS

I would like to express my gratitude to my advisor Dr. John Novotny whose encouragement, guidance and support led me to the successful completion of this project. I would also like to thank Dr. Liyun Wang and Dr. Jill Higginson for serving as committee members and providing additional insights and understanding.

I would also like to thank Phillip Holcombe and Jennifer Docimo for their support during the progression of the project at several stages. I also appreciate assistance provided by several other Professors; who provided with different insights throughout my Masters.

Lastly I would thank my family and friends for their unending support in completing my Masters.

TABLE OF CONTENTS

LIST OF TABLES

LIST OF FIGURES

ABSTRACT

Osteoarthritis (OA) is a common degenerative disease which affects the articular surfaces and adjacent tissues of human synovial joints. More than 20 million Americans are estimated to have OA. OA changes the entire joint; morphologically, biochemically, structurally and biomechanically. The early stages of OA are characterized by a roughened articular surface, with possible partial thickness defects. This may worsen with fibrillation and eventually full thickness damage on both surfaces resulting in bone on bone contact. Animal models are commonly used to study the pathophysiology of OA, providing us the insight into cartilage degeneration. There have been numerous surgery-based models of OA, which induce OA by some sort of trauma to the knee such as meniscectomy or anterior cruciate ligament transection. To overcome some of the problems inherent in these models, a mechanically induced model of uni-compartmental OA was developed that altered the mechanical loading of the knee of New Zealand white rabbit.

The overall purpose of the research project was to develop a model of early-stage OA, to look for early adaptation in the cartilage and subchondral bone and to assess possible treatments. The research objectives of the current thesis are to determine changes in the knee articular cartilage and subchondral bone from tissue that underwent the mechanically induced OA model. To further interpret the experimental results of the animal model, a mathematical model is formulated that is used to predict the joint load and stress state at the articular surfaces.

One of the specific purposes of the research is to determine the changes in material properties of the articular cartilage, mineral and trabecular structure of the subchondral bone and histology of the femoral and tibial joint surfaces in tissue under two different loading time periods of 2 and 4 weeks. The contralateral knees are to be used as internal controls. Correlations with the cartilage material properties to the subchondral bone changes are made.

The second specific aim of the research is to formulate an analytical model of the knee joint of the New Zealand white rabbit under the mechanically induced loading model of OA that incorporates accurate three-dimensional geometry, external joint loading, deformable

articular contact and non-linear ligament properties. The model is implemented to determine the loads and stresses on the tibial and femoral articular surfaces given the changing articular cartilage material properties at the 2 and 4 week loading time periods and in the contralateral control.

The results of the testing showed that the properties of cartilage as well as the trabecular bone morphology were altered. For articular cartilage, aggregate moduli and permeability values showed significant changes towards an OA-like degeneration that increased with the time of loading. The bone mineral density and concentration was altered also in the subchondral bone with exposure to the altered loading. Histological evaluation showed surface damage only and loss of proteoglycan, but little full thickness damage. The results of the analytical model showed increased stresses in the femur which have led to the changes in the properties of both the cartilage and the trabecular bone morphology. The results in general indicate signs of early stage OA, formulating in a new mechanical model for early stage OA.

Chapter 1

INTRODUCTION

1.1 Osteoarthritis

Osteoarthritis (OA) is a common joint degenerative disease which affects the joint surfaces and adjacent tissues. More than 20 million Americans are estimated to have OA. The World Health Organization projects that 10% of the world population over 60 years suffers from OA. OA prevalence will only increase given that the percentage of the elderly population above 65 is growing [1].

OA brings about changes encompassing the entire joint; morphologically, biochemically, structurally and biomechanically. The extracellular matrix (ECM) and chondrocytes are greatly affected [72]. The early stages of OA are characterized by a roughened articular surface with possible partial thickness defects. This may worsen with fibrillation increasing into full thickness fissures and eventually full thickness damage on both surfaces resulting in bone on bone contact (Fig. 1.1) [1]. OA presents with joint pain and may be visualized on radiographs with joint space narrowing and osteophyte formation. In severe cases, the pathology can progress to include joint contracture, muscle atrophy and limb deformity.

Buckwalter and Martin [1] have detailed an OA diagnosis methodology using radiographs and noting the clinical symptoms of chronic joint pain, restricted motion, crepitus with motion and joint effusion. Patients usually seek medical attention complaining of joint pain. They often describe the pain as a deep aching poorly localized discomfort that has been present for years. The pain may increase with activity or changes in the weather, especially storms or a drop in temperature. Secondarily the person may notice a decrease in the freedom of active joint movement. This may be attributed to a loss of cartilage, ligament and capsular contractures, muscle spasm and contractures, osteophytes or intra-articular fragments of cartilage, bone or menisci.

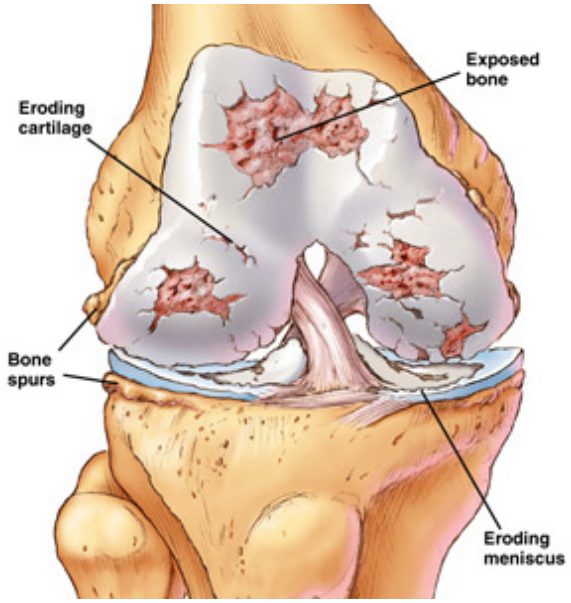

Figure 1.1: Manifestation of osteoarthritis during different stages as shown in one diagram (http://me.queensu.ca/people/deluzio/images/OsteoarthritisKnee 1.jpg)

Severe cases may present with joint deformities and subluxations. Joint grinding, effusions and tenderness may also accompany the above mentioned symptoms. The radiographs usually indicate the joint space narrowing with a loss of cartilage thickness, increased density of sub-chondral bone and the presence of osteophytes (Fig. 1.2). Sometimes cysts or cavities develop with OA. Joint subluxation and deformity may occur with advanced cases especially the varus or bow-

leggedness characterizing medial compartment OA (Fig. 1.3). Computerized tomography (CT) or magnetic resonance imaging (MRI) can also be used for examination purposes.

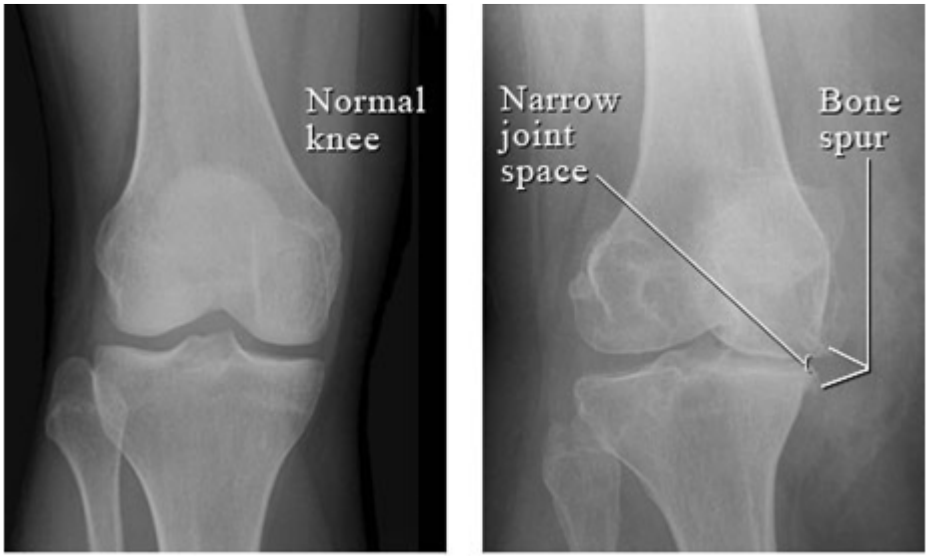

Figure A Figure B

Figure 1.2: Figure A indicates a normal knee x-ray as indicated by the spacing and lack of spurs in contrast with figure B; knee where the bone spur and narrow joint spacing are an indicators of OA (http://64.143.176.9/library/healthguide/en-us/support/topic.asp?hwid=zm6052)

The exact pathophysiology of OA is still relatively unknown compounding the problems to treat it. Due to that, many treatments aiming to slow down the progression are based more on speculation than science. Once the patient develops OA he or she will have it for the rest of their life and the severity generally increases. There are many risk factors associated with both the onset and progression of OA, such as obesity, repetitive occupational or elite athletic physical activity [2], knee injury, select lower limb characteristics like varus limb alignment, quadriceps weakness, joint laxity, and increasing age [3].

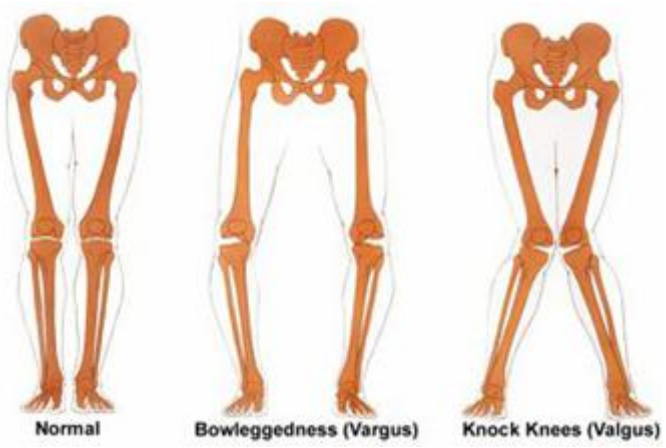

Figure 1.3: Different loading patterns which might lead to increased loading in one compartment of the knee when compared to others, varus or vargus increases the loading in the medial side where as valgus increases the load in the lateral side of the knee (http://www.pharmainfo.net/files/images/stories/article_ Images/ArthriticKnee JointSurfaces3.jpg).

Mechanical factors such as such as knee alignment have been identified as the causative factor, and are thought to play important roles in OA [4]. Knee alignment determines the load distribution across the knee. During normal gait, ~70% of the load is transmitted through the medial compartment due to the ground reaction force passing through the medial condyle of the knee [5]. It has been identified that abnormal dynamic loading of the knee during the gait results in the increased forces, and thereby stresses on the medial plane which may result in OA [6]. Varus mal-alignment of the knee serves to increase the moment arm of the ground reaction force in the frontal plane and further increases the loading in the medial compartment [64]. When applied repetitively, an abnormally large external adduction moment is thought to accelerate the breakdown of the knee joint's medial aspect [7]. It is also suggested that the mal-aligned knee might not be able to evenly distribute the muscle forces causing greater structural progression in these joints [8]. One example of that would be greater quadriceps compression increasing the force across the knee joint [7]. In simple terms in the event of local conditions muscle forces can become pathogenic. It is also found that the abduction moment in people with OA is greater than the normal people, added to that this moment increases progressively with OA [6].

This abnormal frontal plane loading of the knee has been related to a common form of OA known as uni-compartmental OA. As the name suggests only one compartment of the knee, usually the medial, is compromised resulting in the impediment of the normal functioning of cartilage and hence impeding the normal functioning of the affected person. A model of uni-compartmental OA will enhance our understanding of the disease and also help in providing better treatment solutions.

An important step in understanding the patho-mechanics of this disease is to study the articular cartilage micro- to macro-levels so that we can have a better picture of its functioning.

1.2 Articular Cartilage

Martel-Pelletier [9] has detailed articular cartilage as a specialized, avascular, aneural connective tissue that protects the bones of diarthrodial joints. It serves as a load-bearing material, distributes impact and is capable of sustaining shearing forces. The unique nature of this tissue is attributed to the composition and structure of its extracellular matrix, which is composed of a high concentration of proteoglycans, especially aggrecan, entangled in a dense network of collagen fibers and a large amount of water. This structure allows for near frictionless motion of the joint and distribution of the load. The active builders of the articular cartilage are called chondrocytes. They are a sparse population of cells, which are responsible for the synthesis and maintenance of the extracellular matrix.

1.2.1 Chondrocytes

Chondrocytes are the single cell type in adult articular cartilage. They are highly specialized and cannot be further differentiated. In normal cartilage, chondrocytes are surrounded by a layer of a pericellular matrix which is rich in type IV collagen and proteoglycans. The chondrocyte and its pericellular matrix are called chondron. The cells work to maintain the stability of the super structure, by synthesis, assembly and maintenance of homeostasis in the tissue. [65].

As the only cell type present in articular cartilage, these unique and resilient cells are accustomed to living in an avascular environment, where they obtain oxygen and nutrients by diffusion through the ECM. As the normal oxygen concentration in articular cartilage is less than 5%, chondrocytes are able to survive at low oxygen concentrations. This means they are likely one of the last cells in the body to die after the heart stops beating and circulation ceases [10]. This highlights the need to do further research to determine the conditions that lead to their death and dysfunction in OA.

1.2.2 Structure

Cartilage is divided into four zones with different functions: the superficial, middle or transitional, deep or radial, and calcified cartilage zones. The superficial zone is the thinnest of the four and consists of fine collagen fibrils and elongated chondrocytes aligned parallel to the surface and low proteoglycan content. It is in contact with the synovial fluid. The middle zone represents 40–60% of the total cartilage height. It is formed by proteoglycans and thicker collagen fibrils that are more randomly organized. The deep zone contains the largest collagen fibrils in a radial disposition upward from the surface. The radial zone is separated from other zones by tidemark. Its main function seems to be to anchor the cartilage to the bone as collagen fibrils from the radial zone penetrate into the calcified cartilage. In this zone, the cell population is very scarce and chondrocytes are hypertrophic.

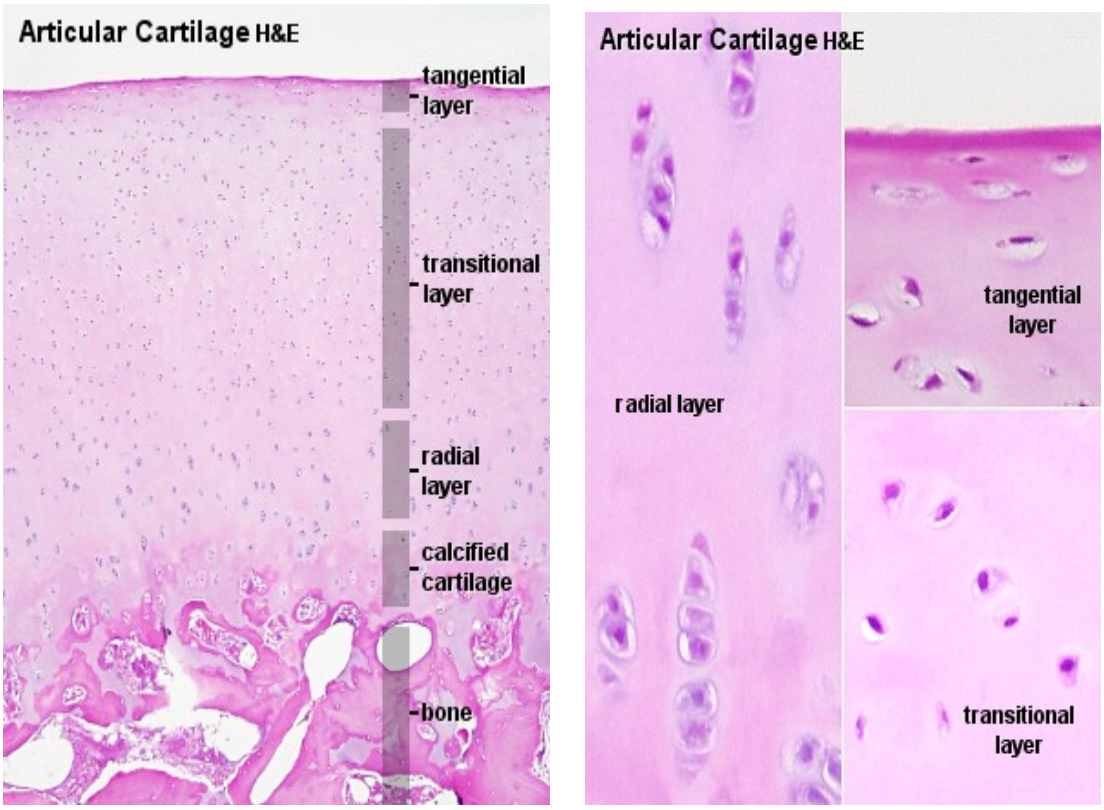

Figure 1.40: Structure of a stained sample of Articular Cartilage from top to bottom indicating the different layers. On the right side the figure indicates how chondrocytes are arranged in different layers. In tangential layer chondrocytes are rather small and flattened parallel to the surface. The most superficial part (lamina splendens) is devoid of cells. Collagen fibers in the matrix of the tangential layer are very fine. They run parallel to the surface of the cartilage. In the transitional zone chondrocytes are slightly larger, are round and occur both singly and in isogenous groups. Collagen fibers take an oblique course through the matrix of the transitional zone. In the radial zone fairly large chondrocytes form radial columns, i.e. the stacks of cells are oriented perpendicular to the articulating surface. The calcified region rests on the underlying cortex of the bone. The matrix of the calcified cartilage layer stains slightly darker (H&E) than the matrix of the other layers (http://www.lab.anhb.uwa.edu.au/mb140/CorePages/Cartilage/Images/arc 22he.jpg).

1.2.3 Composition

In engineering terms, cartilage is a porous, viscoelastic material consisting of three principal phases (a phase represents all of the chemical compositions with similar physical properties):

1) A solid phase, which is composed predominately of a densely woven, strong, collagen (mainly type I) fibrillar network (15-22% by wet weight) entangled with proteoglycan macromolecules (PG, 4-7% by wet weight), molecular weight of approximately 200 million daltons,

2) A fluid phase, which is water (normally < 80% by wet weight); and

3) An ion phase, which has many ionic species of dissolved electrolytes with positive and negative charges (Na+, Ca++, Cl-, etc; << 1% by wet weight). [11]

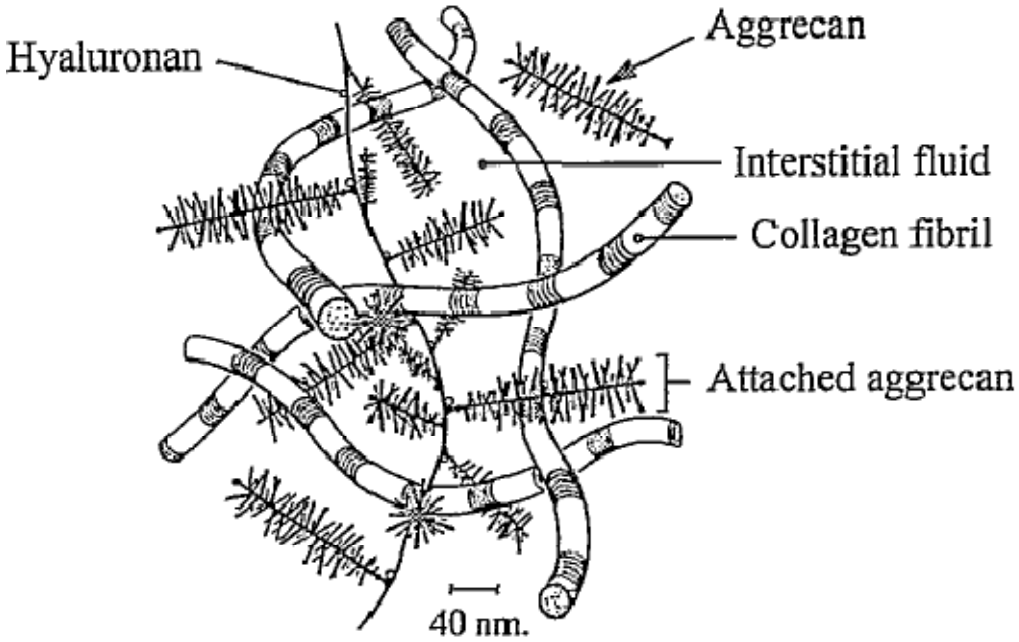

Figure 1.5: A general representation of the collagen network interacting with the proteoglycan network, forming a porous, fiber reinforced, composite solid matrix in articular cartilage. The spaces of this porous solid matrix are filled with water and dissolved ions. The "average" pore size for interstitial fluid flow is approximate 60 A^0 [Mow and Lu. 2008].

1.2.3.1 Collagen

In articular cartilage and meniscus the collagen serves to provide the tensile stiffness and strength for the tissue.

1.2.3.2 Type II collagen

The major component of cartilage is type II collagen; it consists of three identical polypeptide chains-alpha1 (II) polypeptide chains combined to form a triple helix. The primary function of collagen fibrils in cartilage is to support the tissue with tensile stiffness and strength to the tissue. Also the collagen network also functions to restrain the selling pressure of the embedded proteoglycans, which provide compressive stiffness.

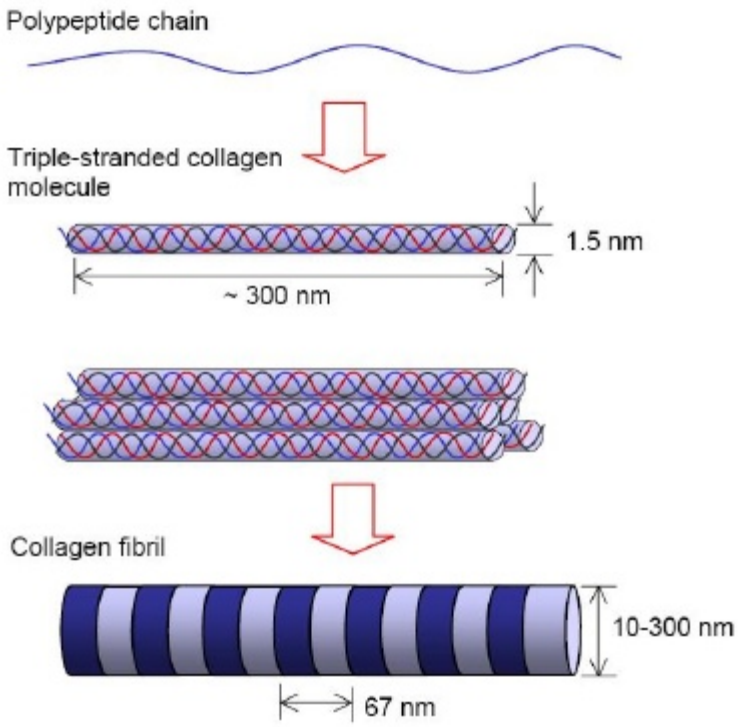

Figure 1.6: Structure of a Collagen fibril as seen from a single polypeptide chain to triple stranded collagen molecule to Collagen fibril (http://www.azonano.com/images/Article_Images/ImageForArticle_2267(2).jpg).

There are other types of collagen like type XI collagen which is around 3% in adult cartilage which consists of 3 different alpha chains, type IX collagen, which are around 3% and 1% in adult cartilage consists of 3 different alpha chains respectively.

OA can be characterized by the enhanced degradation that occurs in the type II collagen-based fibrils. The proteolytic enzymes know as collagenases cleave only within the type II collagen triple helix of the heterotypic fibrils, and do not cleave within the triple helices of type IX or type XI collagen [12].

1.2.3.3 Proteoglycans

Proteoglycans (PGs) are large complex molecules each formed by a core protein and one or more covalently attached GAG (glycosaminoglycan) chains. PGs are important for cartilage assembly and cartilage structure. There are as many as 30 types of proteoglycans available.

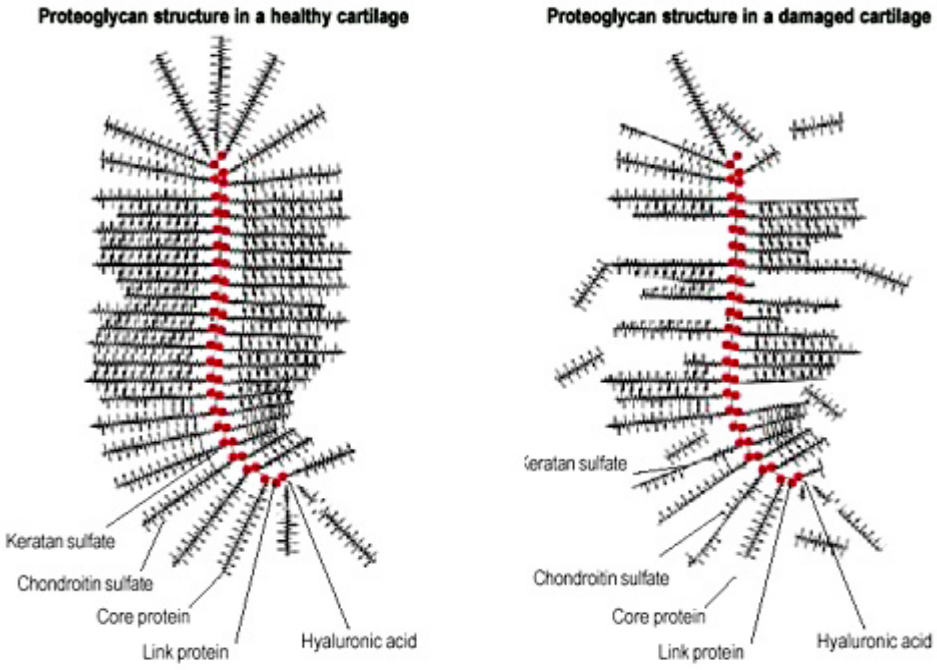

Figure 1.7: Structure of proteoglycan as seen in a normal healthy cartilage where the individual components are intact as compared to the OA cartilage where they are not (http://dolenio.com/PATHOPHYSIOLOGY.htm).

1.2.3.4 Aggrecan

Normal cartilage consists of a high content of aggrecan, which exists in association with hyaluronic acid (HA) and link protein in the form of proteoglycan aggregates that provide the osmotic properties needed for articular cartilage to resist compressive loads. Each aggregate is composed of up to 100 aggrecan molecules radiating from a central filament of HA. Proteoglycan aggregates exist in two predominant molecular forms, which differ in their link protein content and probably their functional characteristics, as link protein stabilizes the aggrecan/HA interaction. Proteoglycan aggregate structure is influenced by the length of the HA, the proportion of link protein, and the degree of aggrecan processing. Aggrecan morphology is not constant throughout life, with decreases in HA length, aggrecan size, and possibly link protein stabilization being evident. Aggrecan possesses a core protein with three globular regions, termed G1, G2 and G3, which are stabilized by disulfide bonds. [9]

High concentrations of aggrecan are necessary for articular cartilage to resist compressive loads. This functional ability depends on the aggrecan molecules possessing a high GAG content in order to bind and hold water within the ECM. A decrease in aggrecan GAG content in the ECM can result in over compression of the cartilage under load, causing an adverse response by the chondrocytes with increased protease secretion and subsequent tissue degeneration [13].

1.2.3.5 Hyaluronan

HA is a nonsulfated GAG characterized by its long length. It is synthesized at the plasma membrane of the cell via a hyaluronan synthase and extruded directly into the extracellular space where proteoglycan aggregate formation occurs in the pericellular matrix. It is not clear how the proteoglycan aggregates move from this environment to the more remote parts of the ECM. The HA content in articular cartilage increases with age and its size decreases [14]. The increase in HA content might reflect an accumulation of partially degraded proteoglycan aggregates, and the decrease in size is probably a consequence of degradation. HA degradation might have an adverse metabolic effect on the cells, as HA oligosaccharides can promote cell mediated catabolism [9].

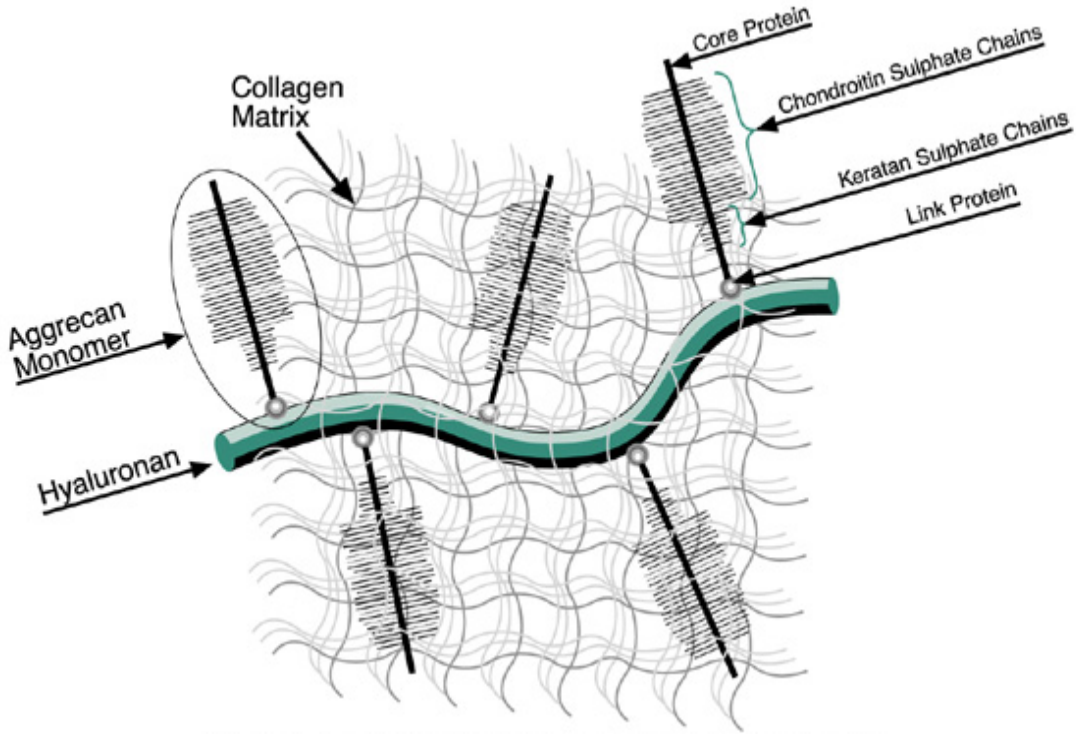

Figure 1.8: Schematic of Aggrecan and Hyaluronan molecules in the ECM of cartilage (http://www.peprotech.co.kr/fa_sub/img/chart-2.jpg).

There are many other types of proteoglycans such as leucine-rich repeat proteoglycans, decorin, versican, etc.

One of the first cartilage matrix constituents affected during OA is aggrecan, which depletes as the severity of the disease increases. At one point of time in the disease progression, the chondrocytes appear unable to compensate fully for proteoglycan loss even in the presence of increased synthesis, resulting in a net loss of matrix. The structure of the proteoglycan remaining in the cartilage is altered in different ways [15].It appears that the presence of aggregates can reduce the vulnerability of proteoglycans to enzymatic attack. In OA, certain proteases are able to attack the proteoglycan monomer. Such degraded fragments can rapidly diffuse from cartilage, leaving behind normal proteoglycan still capable of aggregation. As soon as the degradation occurs, the products are either further degraded by chondrocyte enzymes or rapidly diffused into the synovial fluid. Alternatively, the reduction in the HA content of OA cartilage, which causes a reduction in the size of the proteoglycan aggregates, could favor a loss of proteoglycan breakdown products from the tissue.

1.3 Material Properties of the ECM of the Cartilaginous Tissue

To describe the intrinsic or flow independent properties of the ECM of cartilage, parameters required are Young's modulus (E_s), compressive aggregate modulus (H_a), shear modulus (G) and Poisson's ratio (v_s). Young's modulus and aggregate modulus describe the stiffness of the cartilage. Normal values of aggregate modulus have been found to be in the range of 0.7+/-0.4 MPa. Poisson's ratio is defined as the ratio of lateral strain to axial strain, theoretically υ can be from 0.5, an incompressible material to 0 for a highly compressible material. Permeability is also an important flow dependent parameter that quantifies the interstitial fluid flow that occurs during creep and stress relaxation behaviors. To determine the permeability (κ): which is a measure of the ease with which fluid flows through the matrix. The diffusive drag coefficient (K) is inversely related to the permeability coefficient (κ) by

(1.1)

The porosity for cartilage is around .75, hence $\mathbf{K}$ ranges from 10^{14} to 10^{15} N-sec/m^4. A large value of K indicates that interstitial fluid flow will cause large drag forces to be generated in these tissues.

Studies have determined the aggregate modulus and the Young's modulus, using unconfined compression test, confined compression test, or indentation test. In unconfined and confined compression, the Young's modulus (E_S) and the aggregate modulus (H_A) respectively, are determined from the linear range of the stress–strain curve Fig. 1 (b).

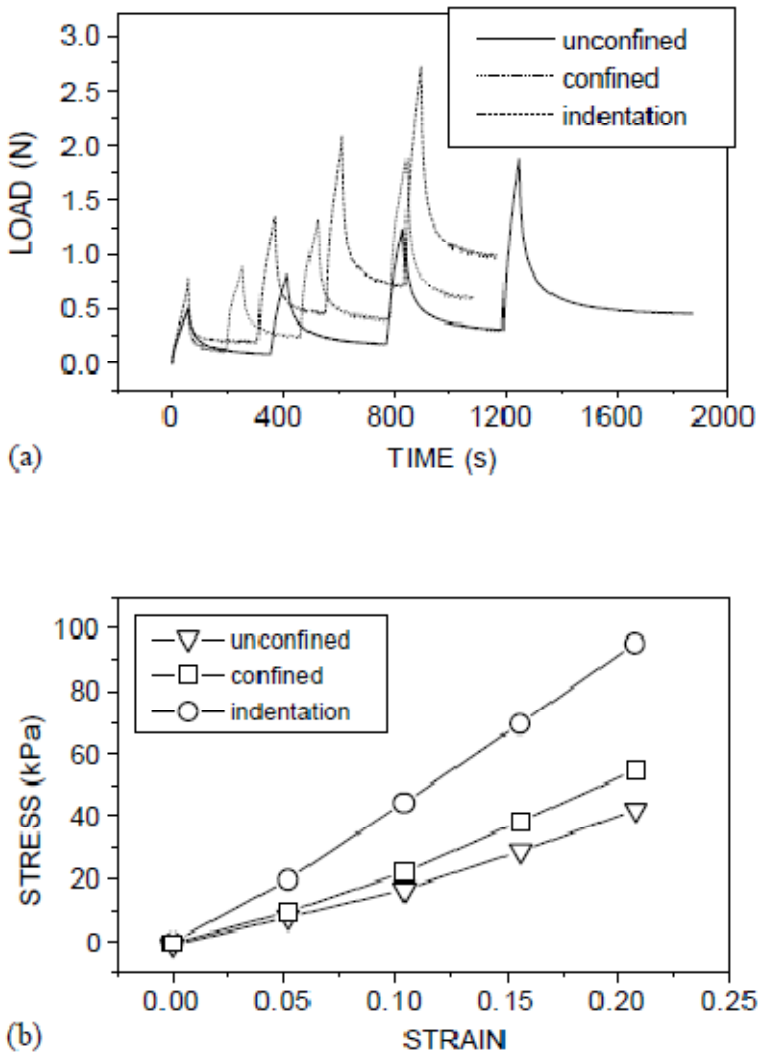

Figure 1.9: The graph (a) represents the amount of load applied during the specified test with time. The graph (b) represents the relation between stress and strain amongst various tests [73].

The Young's modulus (E_s) can also be determined from the linear range of the stress-strain curve in an unconfined compression tests also, it can be determined indirectly from the confined compression test from the equation:

$$E_s = \frac{(1+\upsilon_s)(1-2\upsilon_s)}{(1-\upsilon_s)} H_A \qquad (1.2)$$

where H_A is the aggregate modulus and υ_s is the Poisson's ratio.

In a confined compression test, a small cylindrical cartilage-bone plug is placed against a porous cylinder head of similar diameter. The chamber prevents lateral expansion. When a constant load compressive in nature is applied on to the surface of the cartilage the interstitial fluid is redistributed and any excess fluid in the cartilage must exude through the porous cylinder head resulting in a creep deformation. When equilibrium is reached the aggregate modulus is calculated.

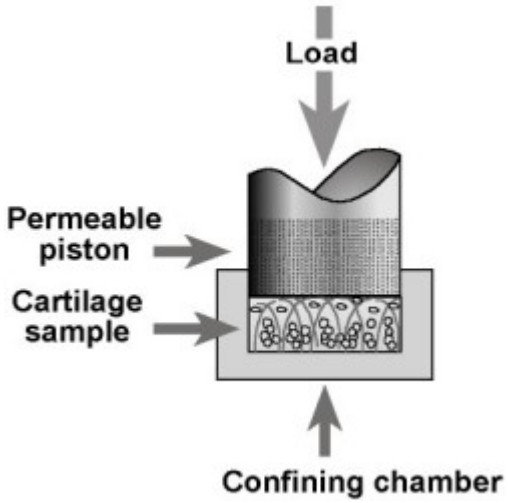

Figure 1.10 : The schematic representing the confined compression test, where a cartilage sample is placed in the chamber where it is confined from all around except at the top where the load is applied using a permeable piston (http://luotain.uku.fi/bbc/research_fields/biomechanics/).

In indentation test the Young's modulus is determined using the equation derived from the solution of Hayes et al., 1972 for a single-phase elastic material:

$$E_s = \frac{(1-\upsilon_s^2\ )\pi a}{2\kappa h} H_A \tag{1.3}$$

Where a is the radius of the indenter, h is the cartilage thickness, υ_s is the Poisson's ratio, E is the slope of the equilibrium stress-strain curve and κ is the theoretical scaling. An updated scaling factor is used taking finite deformation into account from the finite element simulation [16]. In the current research creep indentation test is used to determine the material properties as there was no need to cut the articular surface and test each block separately. Rather we can use a porous indenter to test different sites on the surface of the articular surface. Also it preserves the surface integrity there by allowing for staining and histological analysis. Another advantage of indentation experiment is that we can measure the value of Poisson's ratio with the experiment as compared to the confined compression which doesn't allow for the measurement of the Poisson's ratio due to 1-d nature of the experiment.

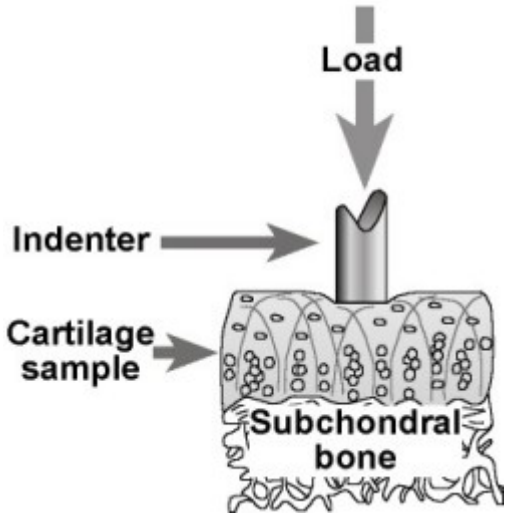

Figure 1.11: The diagram represents the indentation test where the sample of cartilage with the bone is placed under the indenter; the indenter is usually porous (http://luotain.uku.fi/bbc/research_fields/biomechanics/).

1.4 Existing Models of Articular Cartilage

In light of the above discussion, a mathematical model is necessary to process the mechanical testing data and determines the properties of the cartilage. Constituent equations serve our purpose in determining the material properties under specific testing conditions. Previously, the common assumption which was used to model the instantaneous and equilibrium indentation behavior of articular cartilage was to model cartilage as single phase, linear isotropic, homogenous, and elastic solid. For a linear elastic material, the generalized Hooke's law can be written in direct tensor notation as

$$\sigma = C : \varepsilon \tag{1.4}$$

Where σ and ε are stresses and infinitesimal strains, C is a stiffness tensor and the operator ":" denotes a double inner product. The model has its disadvantages when it comes to account for the time dependence of mechanical response. In spite of this, it has been

applied to the study of cartilage, particularly in the analysis of indentation tests [17]. In such situations, linear elastic solutions may be interpreted as representing instantaneous (time, t → 0) or equilibrium responses (t) [18].

There were many models which attempted to explain the time and strain dependent response of the mechanical test. One is a monophasic viscoelastic model, and is based on analogies of arrangements of mechanical spring and dashpot (viscous dampers) elements [19]. These one dimensional models were discarded but laid the basis for the upcoming models. A second finite deformation biphasic theory for intrinsically incompressible mixtures was first put forth by Mow et al., 1980 [20]. In these models the articular cartilage was described in terms of an incompressible solid phase mainly composed of collagen, proteoglycans, chondrocytes, etc and an intrinsically incompressible fluid phase mainly composed of interstitial water and dissolved electrolytes. The fluid is free to move under an imposed pressure gradient, stress and strain of the tissue causes pressurization and flow of interstitial fluid. The time dependence of the mechanical responses such as the creep and stress relaxation can be explained by the dissipative effects of this fluid flow. The basic isotropic linear elastic biphasic model is explained in more detail. It was solved in the previous investigations using a finite element model.

1.4.1 Isotropic Linearly Elastic Biphasic Model

The mathematical model of the cartilage was developed based on the basic conservation equations of mass, momentum and the constitutive equations, which in turn were based on the binary mixture theory [20]. The development of the model assumed an incompressible, isotropic, linearly elastic solid and an incompressible, inviscid fluid.

(1.5)

(1.6)

$$\pi^f = -\pi^s = K\left(v^s - v^f\right) \tag{1.7}$$

The continuity equation and equation of motion governing the behavior of the biphasic material are given by equations (1.5) and (1.6). The continuity equation is the sum of the incompressible solid and fluid phases, where α is the solid content defined as the ratio of solid volume to fluid volume, and v^f and v^s represent the velocity of the fluid and solid phase, respectively. The momentum equation (1.6) has been derived based on quasi-static conditions, and is seen as the balance between the stress field $\sigma^{s,f}$ and the diffusive body forces $\pi^{s,f}$ which result from frictional drag forces. Equation (1.7) provides a definition of the counteracting solid and fluid body forces, where K represents the diffusive drag coefficient.

$$\sigma^s = -\alpha pI + \lambda_s eI + 2\mu_s e \tag{1.8}$$

$$\sigma^f = -pI \tag{1.9}$$

Equations 1.8 and 1.9 represent the constitutive equations that have been derived from the linear bi-phasic model. Equation 1.8 represents the solid phase and equation 1.9 represents the fluid phase. For the solid phase, σs is the stress tensor, p is the pressure, I is the identity tensor, λs and μs are the Lame constants for the solid matrix, and e and e are the infinitesimal strain tensor and dilatation of the solid matrix respectively [21].

1.5 Animal Models

Animal models are commonly used to study the pathophysiology of OA, providing us insight into cartilage degeneration. Ideally they could also create experimental pathways for therapeutic mediation of the disease occurring either naturally or surgically. Animal models are not expensive and help to understand the changes happening at both mechanical and biochemical level. They are beneficial in the way that they isolate the age factor when it comes

to cartilage degeneration. There is a large body of literature on animal models of OA being tested for potential anti-OA agents and disease modifying effects.

Animal models of OA generally include surgically induced or naturally occurring models. Methods include spontaneous OA, anterior cruciate ligament transection, meniscectomy, injections and osteotomy.

1.5.1 Spontaneous OA

Certain species such as the Hartley albino guinea pig have been reported to spontaneously develop focal lesions on the medial plateau as early as 3 months of age [22]. The reasons attributed to the phenomenon are obesity and varus position the animal adopts. The pathogenesis consists of fibrillation and loss of proteoglycan, clustering of chondrocytes, presence of osteophytes and subchondral bone sclerosis which is similar to the pathophysiology in humans [22]. It occurs in both males and females. Since males grow quickly they tend to show more pronounced characteristics. The OA is symmetrical bilaterally in terms of incidences and severity. Initial stages consist of lesions on the medial side not under the meniscus, but there is no change in the subchondral bone properties. The chondrocytes do not exhibit cloning.

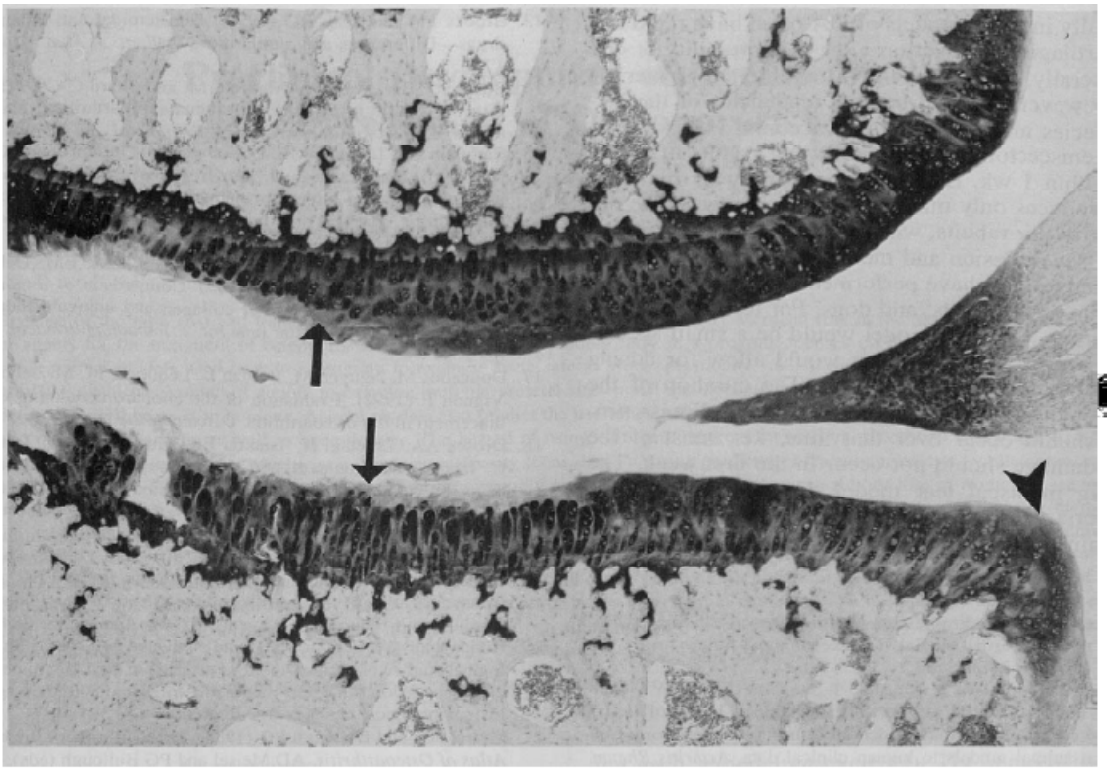

Figure 1.12: Medial view of 9-month old guinea pig which developed spontaneous OA. Tibia and femoral degeneration extended into middle zone and was characterized by loss of proteoglycan, fibrillation and chondrocytes cloning (arrows) [23].

As the OA-animals reach 6 months of age, 90-100% of medial tibial plateau has minimal to moderate lesions. This includes chondrocytes death/loss extending into the upper middle zone, fibrillation and proteoglycan loss, and cloning in the middle to deep zones [22]. With the 1 year olds, cartilage degeneration is prominent in all aspects of the medial compartment. Cell deaths in deep zone, subchondral bone sclerosis, and synovial hypercellularity have also been seen. With 18 months to 2 year olds, major surface changes in the medial compartment, bone sclerosis, bone cyst formation and large osteophytes which have undergone near complete endochondral ossification have been observed.

Other models of spontaneous OA include Syrian hamsters and many strains of mice. The STR/ort mouse spontaneously develops degenerative changes of the knee joints including the loss of hyaline cartilage, osteophyte formation, calcification and ossification of cruciate ligaments and chondroid metaplasia [24], 85% of the 35 weeks old male mice showed OA like lesions [25]. In addition, they become obese and show elevated serum levels of the

cartilage oligomeric matrix protein (COMP). Elevated levels of serum COMP are of particular interest, as serum COMP has also been found in human knee OA patients and has been suggested as a prognostic marker [26].

The major disadvantage of these type of spontaneous models are their variability in severity. There are often other systemic, endocrine-related problems that the animal may also be undergoing. The length of time to develop defects also affects the genetic models which make it unsuitable experimentally.

1.5.2 Meniscectomy

The menisci are a C-shaped fibro-cartilage structure that is located between the femoral conydles and tibial plateau. When viewed in cross-section they appear wedge shaped, with the convex outer margin thicker than the inner margin [27]. The surface in contact with the femur is concave whereas the surface in contact with the tibia is flat to convex. The composition of the adult menisci is 70% water; 75% of its dry weight is collagen, 8%-13% is non-collagenous protein and 1% is hexosamine [28]. The proteoglycans present in it are 40%-chondroitin6-sulfate, 10%-20%-chondroitin4-sulfate, 20%-30%-dermatan sulfate and 15% keratin sulfate [29]. One of the most important functions of the meniscus is load transmission; 70% of the load in the lateral compartment and 50% of the load in the medial compartment is transmitted through the menisci. Also 50% of the compressive load is transmitted through the posterior horns in extension and 85% transmission at 90^0 flexion [30]. The meniscus increases the contact area resulting in the decrease of the pressure across the central area in each compartment.

Meniscectomy is a surgical procedure by which a part or the entire meniscus is removed in an event of meniscal injury or tear. Partial or total meniscectomy results in altered joint kinematics, decreased contact area, and an increase in the magnitude and gradient of contact stresses. This model is used to simulate OA in animals such as rabbits, mice, hamsters, goats and dogs. Meniscectomy results in changes at the cartilage as well as the subchondral bone. Partial medial meniscectomy in rabbits resulted in mild, focal lesions and PG depletion that was partially reversible [31]. Bendele, [69] reported one of the reasons for that is rabbits tend to load their lateral side as opposed to medial side. In the case of partial lateral meniscectomy, the lesions produced were very consistent in both location and severity.

After six weeks post-operation, the histological analysis showed severe focal chondrocytes loss, PG loss, fibrillation, osteophyte formation and trabeculae thickening. The mechanical properties also changed with the procedure. There was a decrease of 20-50% in the compressive and shear moduli of tibia1 cartilage in both equilibrium and dynamic modes of testing. There was also a decrease in the GAG concentration at the sites adjacent to those tested mechanically [32]. The study also reinforced the fact that the shear modulus depends on collagen network's degree of organization since the shear modulus was less around the areas with maximum degeneration.

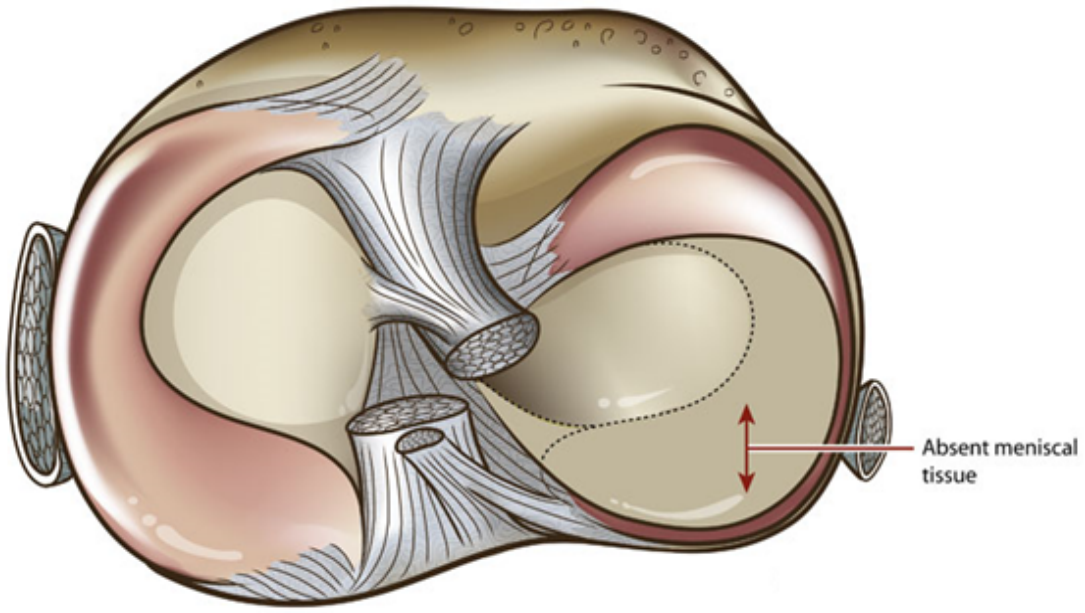

Figure 1.13: Partial meniscectomy performed where the posterior horn of lateral meniscus is removed (http://www.cartilagerestoration.org/graphics/about/big_illu
strations/partial_meniscectomy.jpg).

In rats, the meniscectomy model has shown rapid and consistent disease progression with proteoglycan and collagen changes. The lesions were severe and highly localized but are comparable to that in humans [33]. The changes also include fibrillation, osteophyte formation and chondrocyte cloning [69]. Bendele, 1999 [23] reported in the guinea pig meniscal tear model that after 3 weeks post-surgery, cartilage degeneration was evident up to 1/3 of the medial tibial surface with chondrophytes formation. At 6 week post-surgery the cartilage degeneration extended into middle zone of the medial tibial plateau, cloning was evident, as well as large tibial chondrophytes undergoing endochondral ossification. By 12 week post-surgery degeneration extended into deep zone cartilage, cloning as well as extensive ossification of chondrocytes were also noticed.

There are other models such as dog meniscectomy and goat meniscectomy. For goat OA model, the surgical procedure produced mild changes [31]. Dogs unlike rodents have an altered gait and loading pattern post-surgically, resulting in more instability. One such surgical procedure as described by Bendele [23] consists of 1/2 of the anterior portion of the meniscus

being removed. The histological analysis has shown focal chondrocytes and proteoglycan loss, fibrillation, clonal proliferations of chondrocytes in the area surrounding it, osteophyte formation, and subchondral bone thickening around the 3 months post-surgery. The major advantage with the beagle model is the thickness of the cartilage. Due to thickness we can scrutinize the depth of lesions in a better and perform surgical repairs.

1.5.3 Anterior Cruciate Ligament Transection

Humans often develop OA following a traumatic injury and it can also be simulated in the animals by ACL transection. The pathogenesis is similar as the lesions progress slowly towards OA. ACLT model is generally used to experimentally induce joint instability. Surgery is performed by arthroscopy or, direct visualization through an incision or, blind cut through a stab incision. The model was first developed and characterized for dogs. Guilak [70] had summarized the following. In dogs, transection of the anterior cruciate ligament produced extensive changes in all of the measured mechanical properties and hydration of articular cartilage as early as 6 weeks after surgery. Properties such as stiffness in compression (aggregate modulus), tension and shear decreased significantly after transection of the anterior cruciate ligament. The testing was done for both full-thickness cartilage and for samples harvested from the surface zone and the results were the same in terms of the direction of change. By the end 6 weeks, the aggregate and shear modulus reached stable values in the case of tibial cartilage, but in case of the tensile modulus, it decreased at all sites at 6 weeks and decreased further with time. By 12 weeks, the reductions in the compressive and tensile modulus were approximately 24 and 64%, respectively. They also found that permeability increased significantly by the end of 12 weeks. The water content also increased by the end of 6 weeks. Gross inspection of the articular surface revealed some discoloration and fibrillation in comparison with the control joints. These changes were not severe or focal in nature. Histological analysis showed extensive fibrillation and cleft formation into the middle zone and hypo-cellularity.

The model has also been implemented to produce OA in rabbits. In rabbits, the procedure resulted in gradual and progressive changes in the gross morphological, histological and biochemical properties of the articular cartilage. This is similar to that of human OA [34]. At the end of 9 weeks post-surgery, the mechanical properties in the medial side were different from the lateral side. The confined compression modulus was reduced

compared to the control side. The equilibrium modulus determined here by confined compression testing of control rabbit cartilage is of the order 0.75 ± 0.28 MPa. 6-24 weeks post-surgery, articular gross properties included fibrillation of the articular cartilage with increased India ink staining. Development of areas of full-thickness erosion of cartilage and formation of osteophytes was noted. Histological analysis showed fissures and chondrocytes cloning.

1.5.4 Chemically Induced OA

There are different ways one could induce OA in an animal, one of them is by using chemicals that lead to the degeneration of the cartilage. Usually the chemicals consist of enzymes, collagenase, etc. Papain is one of the proteolytic enzymes used for induction of experimental OA.

Kikuchi et al., 1998 have documented a larger amount of collagenase was detected in OA cartilage than in normal cartilage. Cytokines such as interleukin (IL)-1 and tumor necrosis factor (TNF), which are secreted from inflammatory cells and synovial cells of OA patients, stimulate the production of proteolytic enzymes such as collagenase and stromelysin, and the release of proteoglycans from cartilage. The release of such chemicals results in further damage to the cartilage. Hence a model of OA was developed which consisted of injecting chemicals such as collagenase or papain intra-articularly.

The advantage with these models is that there is no need for surgery and also the time it takes to induce OA is less. The changes can be classified as time related or dose related. With an increase in the dose of collagenase, the cartilage layer showed signs of increased degeneration [35]. With an increase to a 2 mg dose there was even abrasion of the cartilage layer. The cartilage degeneration at the weight bearing regions was more severe with dosage. Surface irregularities, diffusion of cells into transitional and radial zones and slight reduction in staining with safranin O were observed with 0.5 ml dosage. With 1 ml dosages, clefts and cloning in radial zones and moderate reduction in staining were observed. With 2 ml dosage loss in the radial zone, cell cloning in the radial zone and extensive reduction in staining with safranin O were observed.

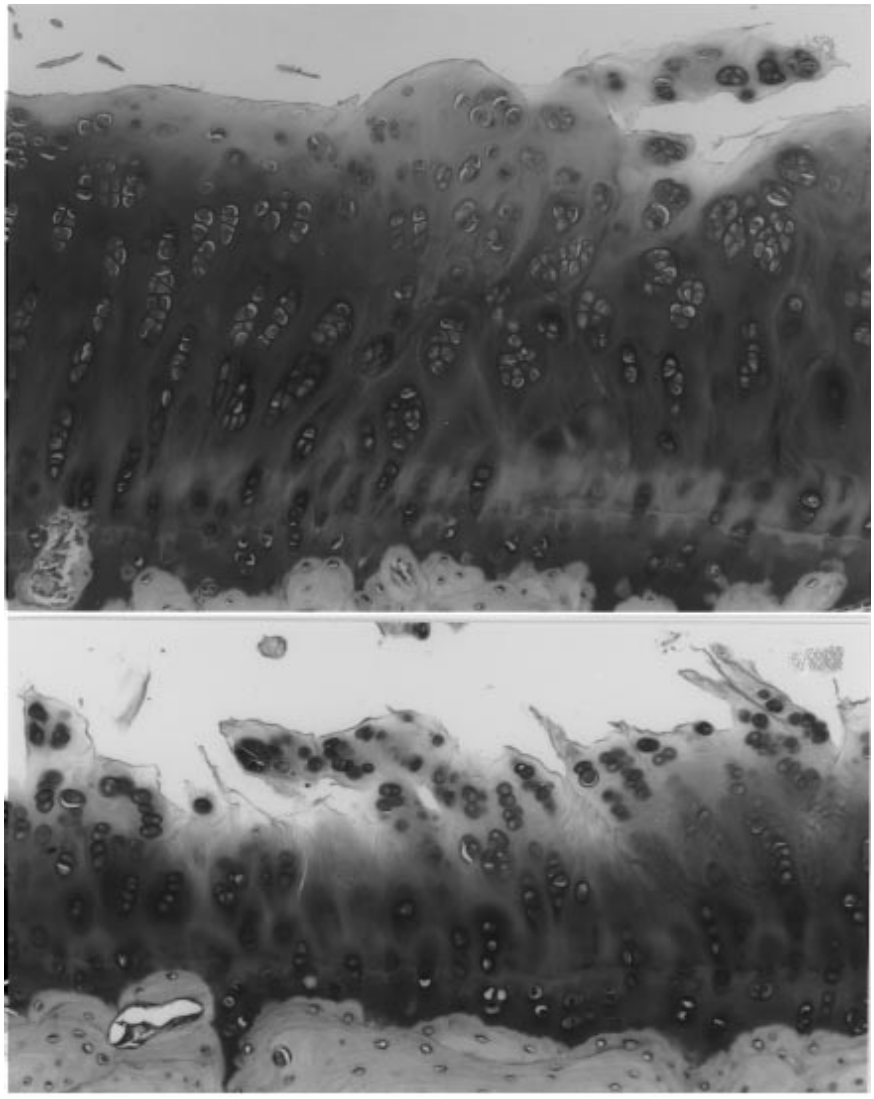

Figure 1.14: stained cartilage (safranin-O staining) of the lateral femoral condyle from rabbits which were injected with top 1.0 and bottom 2.0 mg of collagenase, surface fibrillation and clefts can be seen in the figures (Kikuchi et al., 1998).

Previously, it was assumed that the way by which collagenase degrades the cartilage is by attacking the ligaments and tendons, which are made up of collagen type I and not attacking the cartilage directly which is collagen type-II. The damage to

the ligaments and tendons causes an indirect damage to the cartilage [36]. But with this model, it is assumed that the inflammatory reaction in the joint causes the degeneration of the early stages. It can be concluded that a collagenase injection into the knee joint will not only directly destroy the cartilage, but cause the inflammatory reaction of synovial tissues and accelerate cartilage degeneration.

1.6 Joint Modeling

Mathematical representation of the knee is an important step towards determining the equilibrium forces and moments which are important in evaluation in surgical and diagnostic procedures and for the design of prostheses. One of the earliest models was designed to simulate the quasi-static behavior of the tibio-femoral joint by calculating the relative equilibrium positions of the tibia and femur for given external loads and constraints [37]. The model consisted of non-linear representation of the ligaments and a rigid cartilage surface approximated by polynomials. It is assumed that any deformations within the cartilage will not have any effect on the relative motion and forces in the joint. This assumption is based on another assumption stating that the deformation in the cartilage is very small when compared to the ranges of motion in the knee joint.

The major drawback with the rigid contact is that there is no way to analyze the stress in cartilage or pressure distribution between the contacting surfaces. In order to get around this Blankevoort [38] proposed a deformable articular contact model. In this model the assumptions pertaining to deformable articular contact are based on the simplified theory of contact for thin layers of isotropic linear-elastic materials bonded to a rigid foundation [66]. The assumptions made in this model are:

1) The characteristic length of the area under contact is assumed to be relatively large when compared to the cartilage thickness.

2) The cartilage length is assumed to be isotropic and linear elastic material. This goes against the more complicated biphasic theory proposed be Mow et al., 1985 where in the cartilage is modeled as non linear and visco-elastic. But in this case it is assumed that there is no time dependencies so that deformable contact as a first- order approximation of the behavior of the articular contact.

3) The subchondral bone is modeled as rigid in comparison with the cartilage surface.

Given these, a simplified relation between the normal surface stress (σ_n) and the surface displacement is:

$$\sigma_n = S\left(\frac{u_n}{b}\right) \tag{4.1}$$

Where S is the aggregate modulus represented by,

$$S = \frac{(1-\upsilon)E}{(1+\upsilon)(1-2\upsilon)} \tag{4.2}$$

Also u_n is the surface displacement and b is the surface thickness, E is the elastic modulus and υ is the Poisson's ratio. This relation is linear and only applicable to the small deformations. To account for the large deformations and geometric non-linear behavior, integration over the total displacement of the incremental stress increase as a function of the incremental displacement is given by

$$d\sigma_n = S\left(\frac{du_n}{b-u_n}\right) \tag{4.3}$$

Dividing the right hand side by b and integrating over the relative surface displacement u_n/b results in:

$$\sigma_n = S\int_0^{u_n/b}\left(\frac{d(\frac{u_n}{b})}{1-(u_n/b)}\right) = -S\,ln(1-(u_n/b)) \tag{4.4}$$

This relation is similar to strain hardening, since the stiffness increases with increasing surface displacement.

$$\frac{d\sigma_n}{d\epsilon_n} = \frac{S}{1-\epsilon_n} \tag{4.5}$$

, where $\epsilon_n = u_n/b$.

With all the assumptions made for the cartilage surface, we can model the ligaments. Here the ligaments are assumed to be non-linear line elements, which means that the tension in a ligament is a function only of the length or strain.

$$f_j = f_j(\varepsilon_j)$$

Where $f_j$represents the force in the ligament j which is a function of ε_j.

Strain can be represented as follows,

$$\varepsilon = (L - L_0)/L_0$$

The way the function $f_j(\varepsilon_j)$ is modeled is that it is assumed to be non-linear for small strains and linear for strains higher than a specified level [37].

$$f = 1/4(k)\left(\frac{\epsilon^2}{\epsilon_1}\right) \qquad 0 \leq \varepsilon \leq 2\epsilon_1 \tag{4.6}$$

$$f = k(\epsilon - \epsilon_1) \qquad \varepsilon > 2\epsilon_1 \tag{4.7}$$

$$f = 0 \qquad \varepsilon < 0 \qquad (4.8)$$

Where f represents the tensile force in a line element, k represents the ligament stiffness and ε represents the strain in the ligament calculated from its length L and the zero-load length L_0.

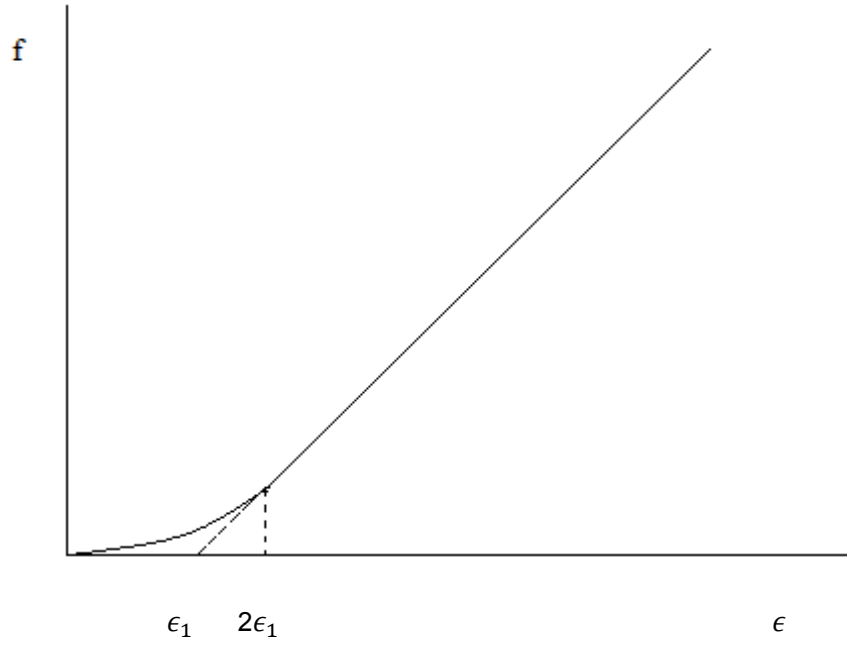

Figure 1.15: The force strain relationship for a ligament. A quadratic relationship is assumed below $2\epsilon_1$ and linear relationship for strains above $2\epsilon_1$.

1.7 Research Objective

The overall purpose of the research project was to develop a model of early-stage OA in order to understand the development of the pathology, to look for early adaptation in the cartilage and subchondral bone and to assess possible treatments. Towards this end, a mechanically induced model of uni-compartmental OA was developed that altered the mechanical loading of the knee of New Zealand white rabbit. This is described in the previous work of Ms. Turka [67], and was improved to avoid any surgical intervention by Mr. Kreidler and Mr. Holcombe. The loading pattern was selected to induce uni-compartmental osteoarthritis on the medial compartment of the knee. Uni-compartmental osteoarthritis is one of the most common forms of joint degenerative disease resulting in changes in the biomechanical and biochemical as well as structural changes in the articular cartilage.

The research objectives of the current thesis are to determine changes in the knee articular cartilage and subchondral bone from tissue that underwent the mechanically induced OA model. To further interpret the experimental results of the animal model, a mathematical model will be formulated that will be used to predict the joint load and stress state at the articular surfaces.

The thesis will meet the following two specific aims and address the stated hypotheses:

Specific Aim 1: To determine the changes in material properties of the articular cartilage, mineral and trabecular structure of the subchondral bone and histology of the femoral and tibial joint surfaces in tissue that underwent two different loading time periods of 2 and 4 weeks. The contralateral knees will be used as internal controls. Correlations with the cartilage material properties to the subchondral bone changes will be made.

Hypothesis 1.1: The aggregate modulus will decrease and the permeability will increase significantly in 2 and 4 week joints compared to contralateral control;

Hypothesis 1.2: Subchondral bone mineral density will increase and trabecular structure will be altered significantly in 2 and 4 week joints compared to contralateral control;

Hypothesis 1.3: Articular cartilage and subchondral bone histology will be graded significantly lower in 2 and 4 week joints compared to contralateral control;

Hypothesis 1.4: Changes in the material properties of the articular cartilage will be correlated to changes in the subchondral bone mineral density and trabecular structure with greater loading time period.

Specific Aim 2: To formulate an analytical model of the knee joint of the New Zealand white rabbit under the mechanically induced loading model of OA that incorporates accurate three-dimensional geometry, external joint loading, deformable articular contact and non-linear ligament properties. The model will be implemented to determine the loads and stresses on the tibial and femoral articular surfaces given the changing articular cartilage material properties at the 2 and 4 week loading time periods and in the contralateral control.

Hypothesis 2.1: Contact loads and stresses will be significantly higher in the joints in 2 and 4 week joints compared to contralateral control;

Increased medial loading has been cited as a major factor in the development of uni-compartmental OA [39]. With the progression of OA, the biomechanical properties will change as well as the properties of subchondral bone. Aggregate modulus which is an indicator of stiffness will reduce [34]. Similarly, other properties such as bone mineral density increase with the progression of OA [40]. Histological analysis is an important tool in understanding the changes occurring at the tissue level. With the progression of OA the cartilage starts losing its integrity. The surface of cartilage is usually fibrillated with the loss of proteoglycan in the whole cartilage [23].

Chapter 2

PREVIOUS INVESTIGATIONS

In this section the previous methods which formed the basis of the research are described. Christina Turka was involved in designing and validating the initial loading device which was surgically attached to the tibia. Next, the finite element method used for calculating the mechanical properties of the articular cartilage under the indentation test is described. This model was developed by Fulin Lei. The mechanical properties results obtained by using the finite element model and μCT on healthy rabbits are tabulated. The feasibility and drawbacks of the surgically implanted device are described and a newer device presented. This was implemented by Jason Kreidler and Phillip Holcombe and was used to generate the loaded tissue in the current research.

2.1 Load Induced Uni-compartmental OA Model

The main objective of these previous studies was to mechanically induce uni-compartmental OA in an animal model using an altered joint loading mechanism. As described in the introduction, the models previously used to induce OA were often surgically induced and directly compromised the tissue of the knee joint including the skin, blood vessels, synovium, meniscus or ligaments. Though this may be a good model of post-traumatic OA, the more gradual changes in cartilage and bone physiology that occurs in non-traumatic OA may be different. Hence a method that alters only the loading applied to the joint was devised. The ability to modulate the magnitude of the load and the dose should allow for gradation in the changes in the physiology of the knee externally would be a more suitable model to study the early initiation and progression of OA.

New Zealand white rabbits were selected for the model under consideration. Rabbits provide enough articular cartilage surface area to enable mechanical testing as compared to mice or guinea pigs. They are a commonly used model in both ligament transaction and menisectomy studies. At the same time they are relatively inexpensive in comparison to larger animals. The average age of the rabbits chosen was at least 1 year and their weight was between 4 -5 Kg. This insured that they were adult.

The methodology adopted to create uni-compartmental OA was to apply a pure varus moment about the knee so as to increase joint loads in the medial side of the knee. The initial device was developed by Christina Turka in her Master's thesis [67]. A pin was surgically inserted into the tibia of the rabbit and the moment was applied to it using an externally mounted motor. The external device applied a cyclical adduction moment to the knee, increasing the loading to the medial compartment of the knee. As shown in the figure 2.1 the intended device will increase the moment in the medial compartment by increasing the varus angle.

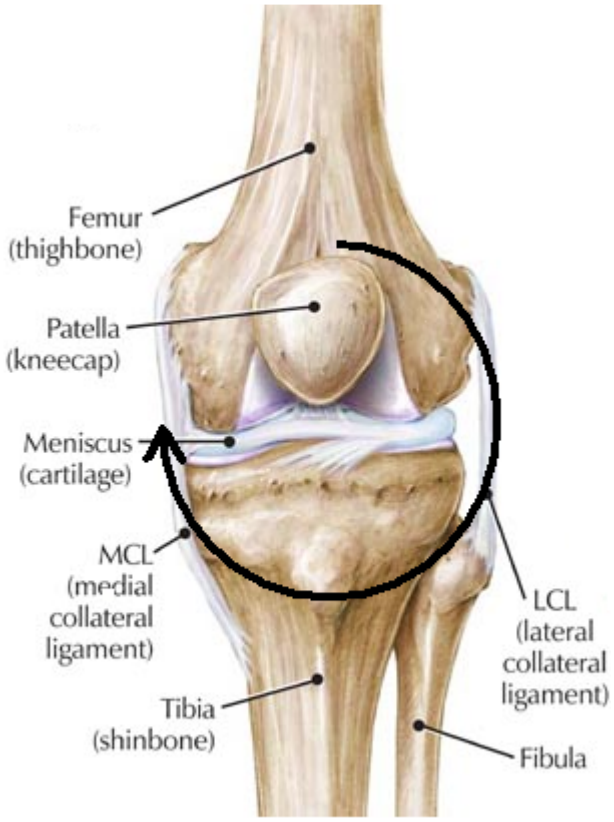

Figure 2.1: Frontal view of the knee with the desired loading pattern (http://prehealthfig2007.wikispaces.com/II.+Elizabeth+Crew+&+Madison+Miller).

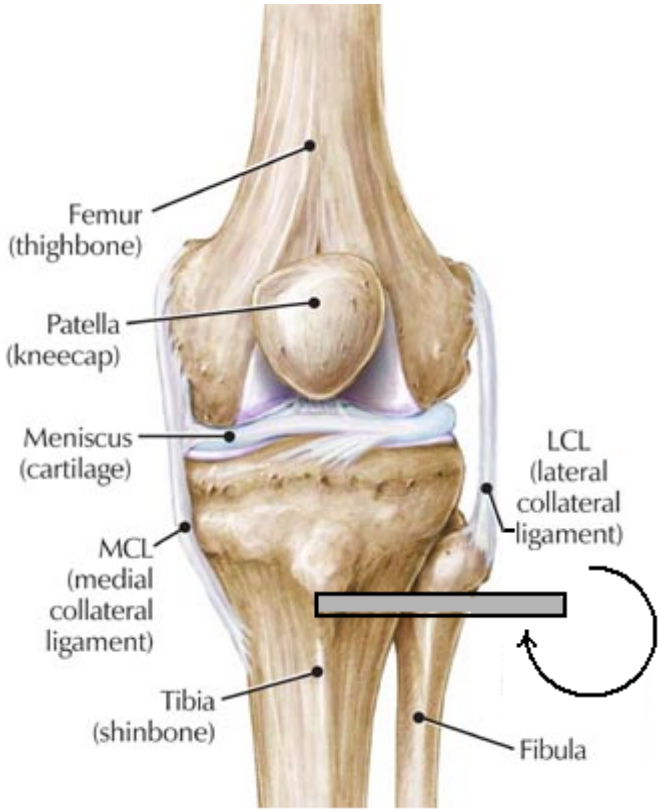

Figure 2.2: Frontal view of the knee of the rabbit leg with the surgically implanted pin through which the moment is transferred to the tibia (http://prehealthfig2007.wikispaces.com/II.+Elizabeth+Crew+&+Madison+Miller).

Figure 2.2 depicts the intended surgical pin in the tibia through which the applied will be applied. The primary requirement of this device was to apply a maximum moment of equivalent to one and a half times the body weight of the rabbit on the femur applied at a moment arm from the midline of the knee to the middle of the medical compartment. Assuming a weight to be 5 Kg multiplied with g (9.81 m/s^2), the moment due to weight would be 73.6 N. Assuming that the force would be transmitted through the centerline of the knee joint, and multiplying the maximum

force by the maximum moment arm (found from the cadaveric calculations), it was found out that the maximum moment due to the weight was 0.3 N-m or 300 N-mm.

The motor chosen was a 6V DC motor with a 12/4-1024:1 reduction ratio gearbox (MicroMo Electronics, Clearwater, FL). The motor was secured to a custom-designed L-shaped aluminum bracket, which was attached to an aluminum plate designed to mount the motor onto two twin pillow blocks. The pillow blocks were free to slide along cylindrical rails which were held in the place using four support blocks. The device sub-assembly allowed the motor to achieve linear translation in the direction of the motor shaft. The device sub-assembly was mounted such that the cylindrical rails were parallel to the side wall of the animal restrainer, therefore the translation capabilities of the device allowed the rabbit to safely move in a forward/backward motion. The principal mode of operation of the motor is running at a stall condition in order to develop the required torque. A stall condition occurs when a current is applied to the motor, but the shaft is refrained from rotating, resulting in the development of torque on the motor shaft. As a reaction to this an opposing torque is experienced in the object that restrains the motor shaft.

2.2 Finite Element Model Solution

A finite element method of solution was created by doctoral student Fulin Lei using ABAQUS (ABAQUS, Inc., Providence, RI) for the indentation creep problem [68]. This solution was based on the biphasic model of Lei, 2005 [63]. The finite element model consisted of articular cartilage modeled using bilinear porous elements, while the indenter was modeled using rigid elastic elements. The articular cartilage surface was modeled with 28 elements in the radial direction and 12 elements in the thickness direction while the indenter was modeled with 2 elements in the thickness direction and 12 elements in the radial direction (Figure 2.3). The radius of the

articular cartilage was set at four times the radius of the indenter, which for our experiments was 1 millimeter. Articular cartilage elements were finely meshed in the area of the indenter and were made coarse further away from the indenter.

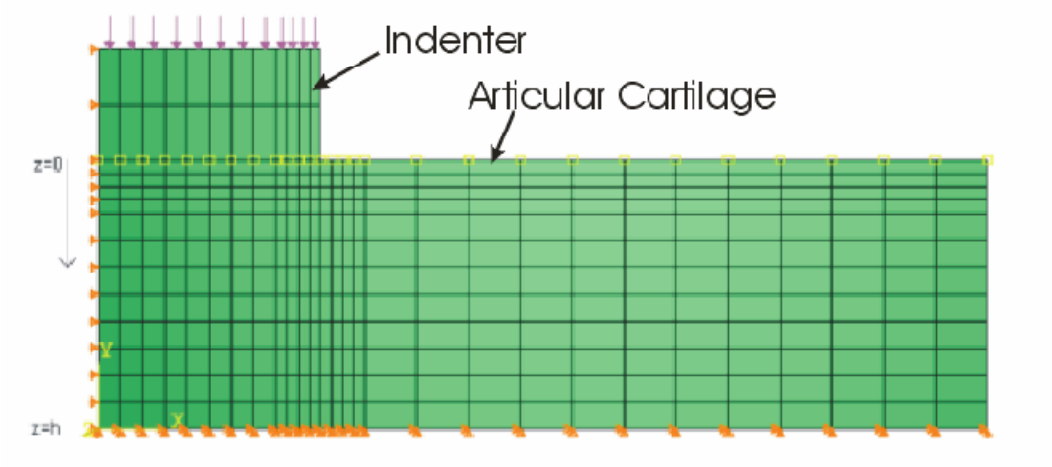

Figure 2.3: Finite element mesh of articular cartilage with indenter.

All boundary conditions within the finite element model were prescribed based on the boundary conditions described by the biphasic model [20].

$$\sigma_{zz}^{f} = 0 \; z = 0, r \geq 0 \tag{2.1a}$$

$$\sigma_{rz}^{s} = 0 \quad z = 0, r \geq 0 \tag{2.1b}$$

$$u_z(r,t) = u(t) \quad z = 0, r \leq a \tag{2.2}$$

$$\sigma_{zz}^{s} = 0 \quad z = 0, r > a \tag{2.3}$$

$$u_r^s = u_z^s = \frac{\partial p}{\partial z} = 0 \;\; z = h, r \geq 0 \tag{2.4}$$

$$P_0 = -\iint_A \sigma_{zz}^{s} dA \qquad z = 0, r \leq a, t > 0 \tag{2.5}$$

Equations 2.1a and b describe the boundary conditions of free-draining and frictionless surface on the top surface in the biphasic model , where σ_{zz}^{f} represents the normal stress component of the fluid along the thickness direction and σ_{rz}^{s} is the shear stress component of the solid on the top surface. The indenter is rigid (Equation 2.2), hence the velocity component is along the thickness direction; $u_z(r, t)$ is equal to the total velocity u(t) .

Equation 2.3 represents no loading on the top surface. σ_{zz}^{s}, the normal stress component of the solid is along the thickness direction, which is zero on the top surface for all r>a. At the cartilage-bone interface, a rigid, impervious interface condition exists, resulting in zero velocity of the solid component in both the radial, u_r^s and thickness, u_z^s directions (Equation 2.4). There is no pressure change in the thickness direction along z. For the creep indentation problem, u(t) is unknown, but the loading condition is a step compressive loading PoH(t) over the indented area, where Po is the applied constant load over the area A (Equation 2.5).

$$f(x) = \frac{1}{2}\sum_i f_i^2(x) = \frac{1}{2}\left\|\overline{u_{exp}} - \overline{u_{com}}\right\|^2 \quad (2.6)$$

$$\Delta f = |f(x)_{n+1} - f(x)_n| \leq 10^{-7} \quad (2.7)$$

In the finite element model, the load is modeled to be a uniform pressure distributed over the indenter area. Initial guesses are used for aggregate modulus, permeability, and Poisson's ratio. The finite element model in ABAQUS interfaces with FORTRAN and MATLAB to arrive at the final solution. Once the solution is obtained, a nonlinear least squares optimization program (Equation 2.7) is used to iterate the material properties to determine the best fit for the experimental data set. The optimization program uses the trust region method for nonlinear minimization, and the convergence criterion is set as a change in the function value between two iterations of less than 10^{-7} (Equation 2.6).

The output from the finite element model includes the history of the iterated material properties and the modeled u(t) creep curve. The mechanical properties of the articular cartilage obtained using the finite element model may then be compared to the properties determined from the analytical solution based on the biphasic model to identify the performance of each model.

2.3 Mechanical Properties of Normal Tissue

Utilizing μCT and indentation tests for the bone and biomechanical properties, respectively were determined and are tabulated below.

Location	BMD (mg/cc)		BVF		Tb. T (μm)		Tb. N		Tb. Sp (μm)	
	Mean	SD	Mean	SD	Mean	SD	Mean	SD	Mean	SD
FLA	491.6	56.7	0.47	0.07	0.16	0.03	2.8	0.32	0.2	0.04
FLC	547.2	25	0.52	0.08	0.19	0.06	2.78	0.39	0.18	0.03
FLP	548.2	26.5	0.55	0.06	0.21	0.05	2.69	0.32	0.17	0.02
FMA	523.4	36.5	0.51	0.03	0.17	0.03	3.1	0.32	0.16	0.01
FMC	542.7	39.8	0.49	0.05	0.16	0.02	3.02	0.23	0.17	0.02
FMP	570.7	29.8	0.49	0.05	0.17	0.03	3.02	0.25	0.17	0.01
TLA	539.8	75.1	0.53	0.08	0.18	0.04	3.06	0.45	0.15	0.03
TLC	562.6	60.2	0.53	0.03	0.18	0.03	3.06	0.33	0.16	0.02
TLP	524.3	42.4	0.52	0.03	0.17	0.03	3.11	0.41	0.16	0.02
TMA	503.9	38.8	0.51	0.05	0.19	0.03	2.66	0.14	0.19	0.02
TMC	536.9	62.2	0.52	0.05	0.18	0.02	2.82	0.21	0.17	0.03
TMP	554.1	80.9	0.54	0.05	0.19	0.03	2.81	0.26	0.17	0.02

Table 2.1: Bone properties of the healthy rabbits; where BMD is bone mineral density, BVF is bone volume fraction, Tb. T is trabecular thickness, Tb. N is trabecular number and Tb. S is trabecular separation. The letters in locations are F for femur, T for Tibia, L for lateral, M for medial, A for anterior, C for center and P represents posterior.

Location	Thickness(mm)		Ha (MPa)		k (m^4/Ns) ($X10^{-15}$)		v		R^2	
	Mean	SD	Mean	SD	Mean	SD	Mean	SD	Mean	SD
FLA	0.162	0.038	0.167	0.065	1.538	1.351	0.26	0.086	0.979	0.024
FLC	0.192	0.045	0.232	0.078	1.599	0.477	0.285	0.073	0.993	0.002
FLP	0.244	0.051	0.309	0.101	2.827	0.653	0.305	0.026	0.976	0.022
FMA	0.289	0.05	0.292	0.046	1.916	0.522	0.28	0.022	0.974	0.023
FMC	0.27	0.06	0.33	0.054	2.465	1.082	0.306	0.022	0.987	0.009
FMP	0.393	0.115	0.437	0.164	13.11	22.79	0.361	0.056	0.978	0.017
TLA	0.215	0.079	0.235	0.22	1.369	0.454	0.274	0.111	0.981	0.014
TLC	0.317	0.083	0.236	0.107	6.83	8.051	0.287	0.046	0.932	0.136
TLP	0.411	0.095	0.297	0.114	3.732	3.065	0.309	0.029	0.98	0.012
TMA	0.315	0.088	0.306	0.136	4.253	1.908	0.351	0.063	0.973	0.014
TMC	0.632	0.048	0.592	0.103	6.335	1.449	0.344	0.028	0.978	0.005
TMP	0.571	0.09	0.518	0.234	22.25	44.59	0.348	0.057	0.974	0.009

Table 2.2: Mechanical properties of the healthy rabbits. Ha represents aggregate modulus, k presents permeability, v represents Poisson's ratio and R^2 is the coefficient of determination. The letters in locations are F for femur, T for Tibia, L for lateral, M for medial, A for anterior, C for center and P represents posterior.

2.4 Modified loading device

In spite of the fact that the surgery was not interfering in any way with the joint capsule, a surgery was performed and it did result in a trauma to the animal in a manner which might affect its behavior and put it at risk of infection. Hence this design was abandoned for a new design (by Jason Kreidler and Phillip Holcombe) where an external brace was attached to the tibia to which the motor applied the cyclic varus moment. The brace was designed using SolidWorks and machined out of Delrin. The brace was designed to fit the tibia and to make sure that it would be snugly fit. It had a Velcro strap to hold it around the tibia.

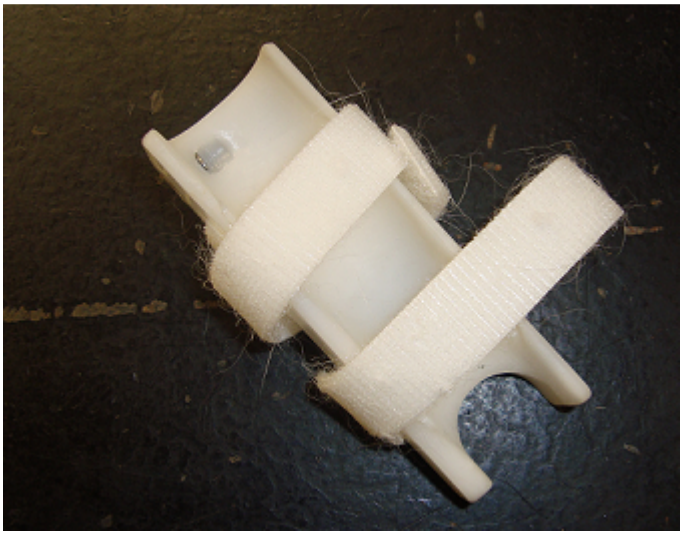

Figure 2.4: The brace which was used to apply the external varus moment to the tibia.

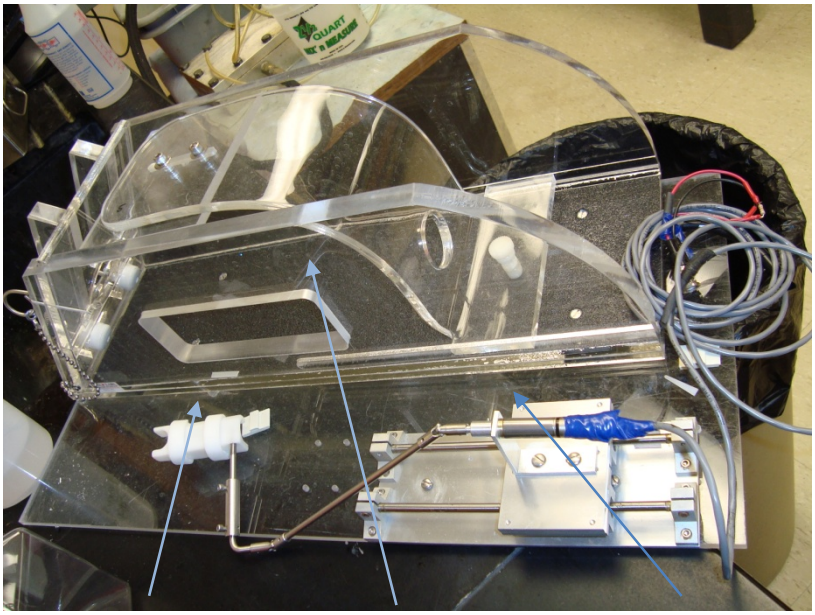

Figure 2.5: The brace with the motor attached to it. Next to it is the restrainer in which the rabbit was housed during the loading duration.

The very idea of choosing an external device to load the knee is to eliminate any kind of surgical trauma to the animal. One might never know what kind of effect any sort of surgery might bring to the knee joint. Also we did not have to use any anesthesia or antibiotics on the rabbit. The loading might create inconvenience but not intolerable pain. Hence it becomes a purely mechanical method which loads the knee in the manner we want.

Chapter 3

TESTING AND ANALYSIS OF ARTICULAR CARTILAGE AND TRABECULAR BONE MORPHOLOGY

In this section the testing protocol which was used to generate the current tissue is described followed by the tests which are used to determine the bone as well as mechanical properties. Histological techniques are described which are essential in grading the progression of OA from the morphology point of view. After biomechanical and histological analysis, is the joint modeling which helps us estimating the forces acting on the femur throughout the loading period.

3.1 Testing Protocol

Eight New Zealand white rabbits underwent the loading induced OA protocol. Each was at least one year old and from 4 to 5 kg in weight. Only female animals were chosen to decrease animal to animal interaction. The protocol was reviewed and approved by the Institutional Animal Use and Care Committee of the University of Delaware. Four animals each were placed under loading for two weeks or four weeks for five days a week. Each day the rabbit was loaded for four hours each day. After the loading period was complete the animals were euthanized and the whole body was wrapped and kept in the freezer at -55^0C. These experiments were performed by Jason Kreidler and Phillip Holcombe under the direction of the University of Delaware Animal Care Facility and its director Frank Warren.

3.2 Experimental Methods

3.2.1 Micro-computerized tomography

In order to detect changes in the subchondral trabecular bone, mineral content and structure were quantified using micro-computerized tomography (μCT) scans. These were performed on the eight loaded New Zealand White rabbit legs (4 four weeks and 4 two weeks loaded) and the eight contralateral unloaded legs. Below the articular layer the bone is called subchondral trabecular bone where as the trabecular, or cancellous, bone is located inside the cortical bone. It is comprised of rods, plates and bars separated by cavities that contain red bone marrow.

The important structural quantities of subchondral bone are bone mineral density (BMD), bone volume fraction (BVF), trabecular plate thickness (Tb. T), trabecular plate separation (Tb. S), and trabecular plate number (Tb. N). The bone mineral density is defined as the ratio of bone mineral content and the total bone volume, while the bone volume fraction is the ratio of volume of bone material to the total volume. The trabecular thickness represents an average thickness of trabeculae. Trabecular separation is the average distance between trabeculae. Trabecular number is the number of continuous trabecular elements per unit area.

These are all important properties as bone mineral density; geometry, micro-architecture, and quality of trabecular bone all effect the bone strength and stiffness. The trabeculae properties are interrelated; an increase in trabecular thickness and number will result in a decrease in trabecular separation, which consequently affects the bone mineral density and bone volume. Studies have shown an increase in mechanical properties of trabecular bone by increasing the bone volume through increased trabecular thickness [71]. Characterizing structural bone properties is useful in comparison with diseased tissue. It has been shown that the progression of OA will result in thickening and hardening of the subchondral trabecular bone, resulting in an increase in bone density [40].

Before scanning the rabbit legs were kept frozen at -55° C and then were thawed. Specimens consisted of only the femur and tibia with the joint capsule intact. The μCT scans were performed using a GE eXplore Locus Micro CT Scanner (General Electric Medical Systems, London, ON, Canada) (Figure 3.1). Scans were performed at a 27 μm resolution for 160 minutes. Half-resolution reconstructions were then performed separately for the tibia and

femur of each leg. The reconstructions were viewed in MicroView (GE Healthcare, Chalfont St. Giles, United Kingdom), a 3-dimensional image viewer with a bone analysis package. Six 1 mm^3 cuboid regions of interest (ROI) were established within the subchondral trabecular bone, approximately underneath the locations that underwent indentation testing described later. A 3-D bone analysis was then performed by the program for each ROI.

Figure 3.1: µ-CT setup used to perform the scaning of the cadaver legs.

3.2.2 Mechanical Testing

Biphasic creep indentation tests were performed on the eight loaded New Zealand White rabbit legs (4 four weeks and 4 two weeks loaded) following µCT scanning. Before the testing each specimen had be dissected to remove non-articular soft tissues and disarticulated. The ligaments and menisci were carefully removed. During the dissection, care

was taken not damage the articular surfaces. The specimens were kept moist with phosphate buffered saline (PBS) periodically, thereby maintaining the cartilage hydration. Each of the tibia and femur samples was attached

to an aluminum mounting plate that would interface with the material testing machine. Tibial and femoral samples were mounted as shown in the figure 3.2 and figure 3.3 respectively with the proper orientations. Once they were mounted on the plate the samples were wrapped in paper towels soaked with PBS, placed in individually labeled containers and frozen at -55° C until the day of mechanical testing. On the day of testing, each specimen was removed from the freezer and allowed to thaw at room temperature for one hour.

Figure 3.2: A tibial sample mounted on the plate, with proper orientation.

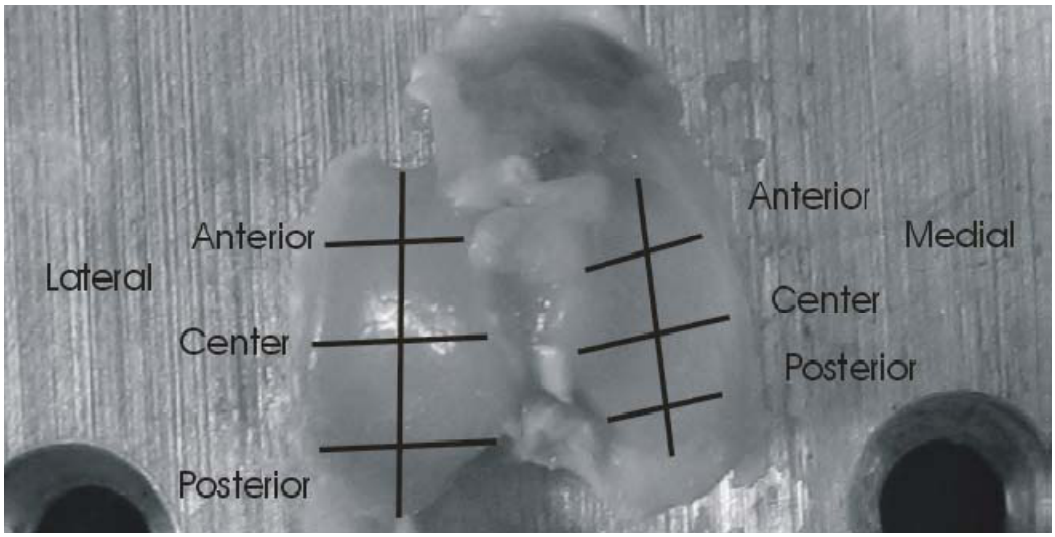

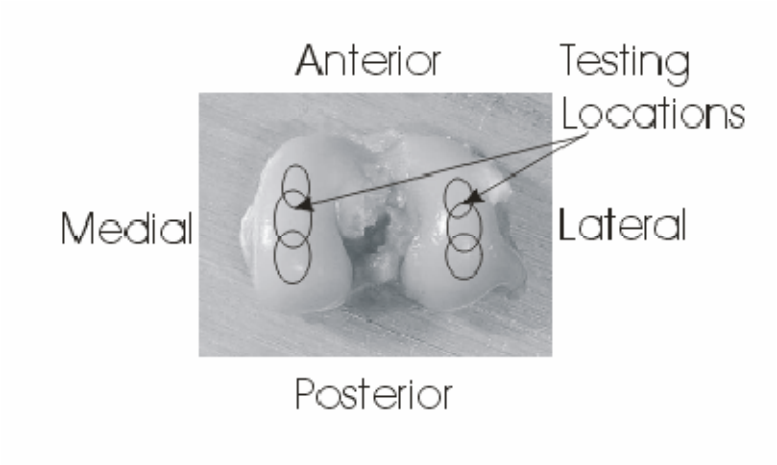

Figure 3.3: A femur sample mounted on the plate with the proper orientations.

The specimen with plate was aligned so that the anterior tibia and femur were oriented toward a mounting hole on the base plate (Figure 3.4). This alignment simplified the procedure of adjusting the translation and tilt tables. The base plate was then mounted into the fluid bath. The fluid bath was attached to the translation stage beneath the 5848 MicroTester (Instron, Canton, MA) (Figure 3.5). The chamber was filled with PBS until the specimen was fully submerged.

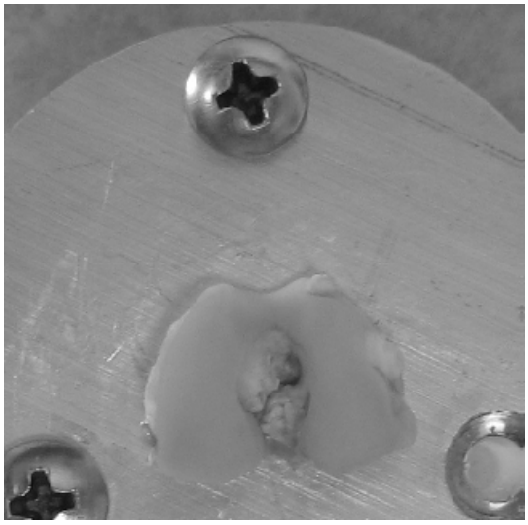

Figure 3.4: Example of proper specimen mounting onto the aluminum base Plate.

Figure 3.5: Instron 5848 Microtester used to perform the creep indentation experiments

After mounting the specimen, the initial indention testing location was identified by adjusting the translation stage. The surface at each testing location then needed to be aligned so that it would be perpendicular to the porous indenter. This alignment was achieved using a 200 N six degree-of-freedom load cell (ATI Industrial Automation, Apex, NC) and the adjustment of the surface with the goniometer tables

on top of the translation stage. The load cell was interfaced using a Labview program which provided real time magnitudes of the three orthogonal forces and moments from the load cell.

A solid, circular ended indenter was mounted onto the load cell, its reading was balanced, and the crosshead slowly lowered until the indenter contacted the cartilage surface. After contact was made, the moments and loads were observed. In order to minimize the moments and have force only in the direction of the indenter the goniometer tables were adjusted. Surface angle was changed until there were no moments in any direction and only force along the axis of the indenter (Figure 3.6).

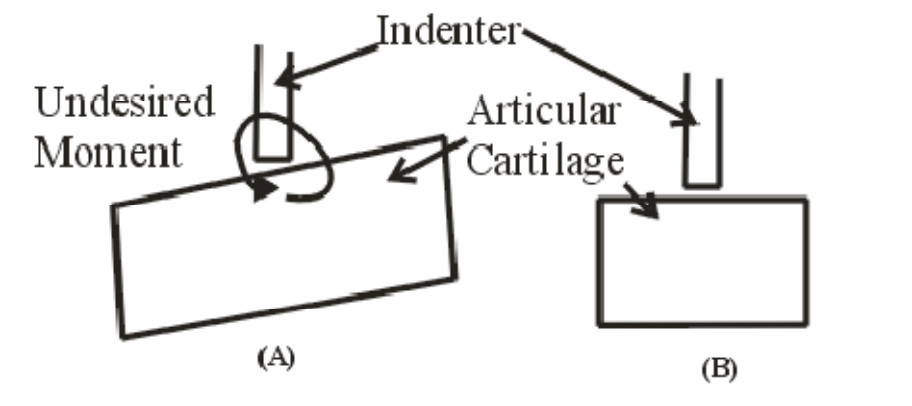

Figure 3.6: Indenter aligned as shown in the diagram.

Once the surface was perpendicularly oriented, the six degree-of-freedom load cell was replaced with a 5 N load cell (Instron, Canton, MA) to be used for the creep indentation test. The 5 N load cell was selected for the higher accuracy (± 0.01N). The specimen was allowed to equilibrate for 5 minutes following alignment to allow for the tissue to regain any fluid loss. The 2 mm diameter, circular ended, porous indenter was mounted onto the 5 N load cell, and the load cell was balanced and calibrated.

The creep indentation test consisted of an initial tare load of 0.06 N. The purpose of the tare load is to provide a tissue thickness that is a function of the specimen's biphasic equilibration and not just the amount it has swelled during its time in the PBS. This tare load

was determined from preliminary testing to be sufficient to counteract the swelling pressure of rabbit cartilage and the load control accuracy of the material testing machine.

Following the tare load, a creep indentation test was performed based on the linear biphasic model [20]. The creep indentation test consisted of applying an instantaneous load of 0.11 N to make the total load equal to 0.17 N. This load was determined to satisfy the assumption of the infinitesimal strain theory used in the linear biphasic model [41]. After the load was applied, the sample was allowed to attain equilibrium, which was defined when the change in displacement decreased to less than 0.15 micron over a time period of 300 seconds. Data was sampled in a manner such that the data points collected were more during initial phase and less during the later part where equilibrium was being attained.

After the creep indentation test the porous indenter was replaced with a needle probe to estimate the thickness of the cartilage at the same location as before. The needle test consisted of a needle probe which was inserted into the load cell and it descended slowly at a constant rate of 167μm/s [42]. The load cell was re-balanced in order to account for the change in weight between the indenter and the needle probe. The thickness was measured as the displacement from the point where it made contact with cartilage to a point where it reached the top of the calcified zone by observing the change in force output of the load cell.

After the thickness was determined the needle probe was removed and the same procedure was carried out at each of the six different locations on the sample as seen from the figure 3.3 and figure 3.2. As a general rule the testing was finished within 36 hours over all locations so as to preserve the tissue material properties. After every test was completed the sample was wrapped in a paper towel and soaked in PBS and stored in the freezer at -55^{0}C.

3.2.3 Post Processing

After the experiments the data were saved in files corresponding to their locations. The thickness was determined using a MATLAB program where the thickness was determined by identifying the change in slope on the load versus displacement plot between the calcified zone and the articular cartilage layer. For the numerical solution of the linear biphasic model,

the total load was subtracted from the tare load since it was responsible for the deformation. In order to determine the mechanical properties of the sample under load, a finite element model developed in ABAQUS by Fulin Lei at the University of Delaware was used as described in the Previous Investigations section. The model required an indention test's experimental data file, an input file containing the specimen thickness, radius of indenter, and loading profile, and a file containing initial guesses of the mechanical properties. Analysis using the finite element model was performed to optimize the material properties that most closely match the experimental deformation curve.

3.3 Histology

Histology is also an important step in studying the morphology of the cartilage with OA, in conjunction with biomechanical testing. Histological grading systems have been used to identify changes occurring at tissue level for such as surface fissures, cell changes such as number, size and shape, and changes in the proteoglycan content [43] ,[44]. There are problems associated with grading a sample, since there is no consensus system and since grading is qualitative. One might see what may not be seen by another. Nonetheless histology offers an insight into the changes happening at the cellular as well as tissue level.

3.3.1 Sample Preparation

After μ-CT and mechanical testing, the sample was cut into half along the notch so as to separate the medial and lateral condyles and the medial and lateral tibial plateaus using a scalpel blade. Once samples were cut they were labeled according to the following convention: R (Rabbit) Animal #Leg (L-loaded, R-Not loaded) Bone (F-Femur, T-Tibia) Condyle (L-Lateral, M-Medial). For example a specimen could be R70LFM, where the rabbit # would be 70 and sample being loaded medial femur.

Once naming was done the samples were put into 40 ml of formalin for four days with one change under constant agitation. After the containers were thoroughly rinsed and the

containers were filled with 1X PBS and the samples agitated. After one more day the samples were removed from the PBS and the containers were thoroughly rinsed. The containers were filled with Cal-Ex Decal solution to remove the calcium from the bone mineral in the samples. The solution was changed twice daily. In order to determine if the end point of decalcification was reached, 5 ml of 5% ammonium hydroxide and 5 ml of 5% ammonium oxalate was added to 5 ml of the decalcifying solution just before changing the solution and allowed to sit for 15 min. If there was precipitate then further decalcifying was still necessary. Otherwise the process of decalcifying was over.

After decalcifying the samples were to be embedded into paraffin wax. Jennifer Docimo was involved in this process with embedding performed at the Nemours/A.I. Dupont Children's Hospital biology department. After embedding the samples were sectioned in microtome into sections of 6 microns at the University of Delaware Department of Biological Sciences histology core facility.

3.3.2 Paraffin removal, Re-Hydration and Staining

To visualize the cellularity, collagen structure and proteoglycan content the tissue sections were stained using common protocols from the literature [45]. The overall goal of performing was to utilize the Mankin scoring system for cartilage degeneration. For the purpose of staining the tissue sections, the solutions that were made and kept aside in separate dishes include the following: Iron Hematoxylin (Weighert's) Working Solution made from the mixture provided in the box; 0.001% Fast Green FCF Solution which consisted of 0.1gm fast green FCF in 1Liter distilled water; 1% Acetic Acid Solution made from mixing 1mL glacial acetic acid with 99mL distilled water and 0.1% Safranin O Solution which consisted of 0.1gm Safranin O in 100mL distilled water.

Next was the process of de-paraffinization, rehydration and staining; the procedure followed step by step in this order:

1. Samples were deparaffinized and hydrated to water by 3 changes of Petroleum Ether, 100% alcohol, 95% alcohol, 70% alcohol, distilled water, 5 min each, 10 min for water.

2. Next samples were stained with Weighert's iron Hemotoxylin working solution for 7 minutes.

3. After staining the samples were washed in running tap water for 10 minutes.

4. Once washed the samples were stained with fast green (FCF) solution for 3 minutes.

5. The stained samples were rinsed quickly with 1% acetic acid solution for no more than 10 to 15 seconds.

6. Rinsed sample were stained in 0.1% safranin O solution for 5 minutes.

7. After the staining was completed the samples were dehydrated with 95% ethyl alcohol, absolute alcohol, and citrosolve (xylene substitute) using 2 changes each for 2 minutes each.

8. After dehydration each slide was mounted using a resinous medium and a cover slip.

The grading was based on structural, cellular, tidemark based and staining based aspects of the given slide. The grading for each of the aforementioned characteristic property is described in the table (Table 3.1) below. At the end of each slide the individual scores are added to give a cumulative score. Depending upon the score the grade of OA was determined divided into six grades of OA.

Structure		Cell		Staining		Tidemark	
Grade & Description		Grade & Description		Grade & Description		Grade & Description	
0	Normal	0	Normal	0	Normal	0	Intact
1	Surface irregularities	1	Diffuse hypercellularity	1	Slight reduction	1	Crossed by blood vessels
2	Pannus and surface irregularities	2	Cloning	2	Moderate reduction		
3	Clefts to transitional zone	3	Hypocellularity	3	Severe reduction		
4	Clefts to radial zone			4	No dye		
5	Clefts to calcified zone						
6	Complete disorganization						

Table 3.1: The different characteristic properties of the stained sample which have their grade across which is their description.

3.4 Mathematical model of knee

To meet the second specific aim the forces and stress acting on the articular cartilage surfaces would have to be determined in order to estimate the changes caused by the tissue degeneration. In order to estimate the loads we would require a three-dimensional mathematical model of the knee with which to perform the equilibrium analysis. Due to the complexity of the model, representative models using a common geometry and average material properties will be used.

3.4.1 Device Description : Bird

There are many methods to generate a three-dimensional model of the surfaces such as computerized tomography or magnetic resonance imaging scans from which a joint surface can be generated. In our lab an electromagnetic measurement system (miniBIRD, Ascension Tech Corp), which consists of a transmitter and a receiver, was used to digitize points on the articular cartilage surface.

Figure 3.7: The transmitter as shown in the figure generates electro-magnetic field. The arrow points in the positive x direction and the positive z direction is going through the transmitter from top to bottom.

The transmitter generates a 3-d electro-magnetic field, with a radius of approximately 3 feet. It has a coordinate system as shown in the figure with positive z pointing downwards, positive x in the direction of arrow and y in the direction as defined by the cross product of z and x (Figure 3.7).

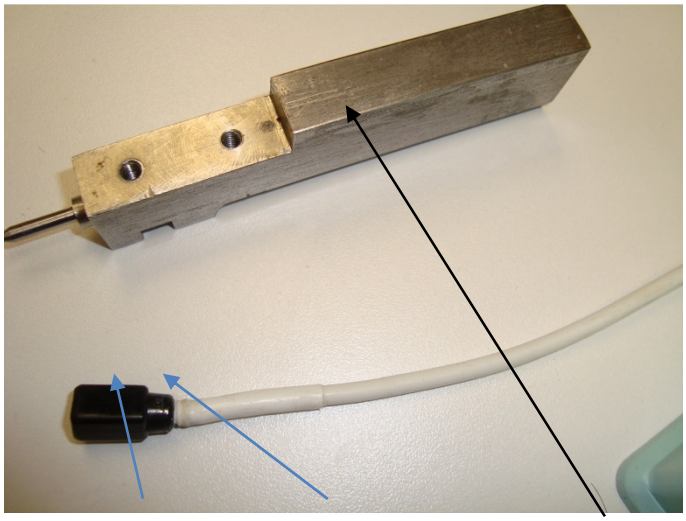

Figure 3.8: The receiver consists of a stylus with a pointed end and the actual receiver fixed into the grooves.

The receiver generates a current when placed in the magnetic field of the transmitter and has its own coordinate system. The groove shows +ve direction of z as coming out of the receiver and +ve x direction is along the length of the wire through the receiver.

3.4.2 Offset in Bird

The receiver stylus is made of a stainless steel which when moved within the magnetic field in different directions causes a misalignment in the axes of the stylus and the receiver which in turn creates an offset. In order to overcome that it was necessary to find out how much was the tip offset from the receiver, which was found out by fixing the tip of the stylus and rotating it in the magnetic field and collecting the data points in stream mode. Once this is done the offset is determined by the sphere that fits the data using a simple MATLAB program.

3.4.3 Data Collection

A frozen rabbit leg was kept out to thaw for 3-4 hours and later carefully dissected to remove all the skin, fat and muscle until just the knee capsule was left with the ligaments and joint. After that the ligaments were cut and the menisci were also carefully removed making sure not to nick the cartilage surface. Once the tibia and femur were separated, about two inches from the respective surface using a hand saw, excessive bone was cut out. After that superglue was used to stick the bone on a delrin surface.

With the bird switched to fly mode, data was collected on the surface roughly along a line so that later this data could be fitted using polynomials. The data was taken along the surface and the respective ligament insertions were recorded. When the experiment was completed the tibia and femur were wrapped in paper towels soaked in PBS and kept in the freezer.

The results of the data collection consisted of a position and transformation matrix, and as discussed before the offset points will have to be transformed to a point on the surface of the tibia or femur. Hence the transformation matrix comes into the picture with the offset; which is given with the output.

$$X = (X^1 - O)T^{-1}$$

Where X^1 represents the point obtained from the data collection from which the offset O is subtracted and multiplied by the inverse of the transformation matrix gives X which is the point on the either the femur or tibia. It turns out as seen from the graph below one set of points on the surface of the femur when fitted using a polynomial of order 7, the surface was distorted. There could have been many reasons for the distortion, such as interference from the surroundings and the stylus was made up of stainless steel which could also induce the distortions in the data collection systems. Also if one were to click on the same point with everything held constant the point and the transformation matrix would be different for no apparent reason.

Hence a slightly different method was used to collect the points on the surface. This method consisted of moving the stylus parallel to one of the axis and perpendicular to one

axis, i.e., the surface from anterior to posterior was chosen as the x axis and surface from medial to lateral was chosen as z axis and y axis was chosen was axis of femur or tibia. While collecting points it was necessary to choose a plane perpendicular to z axis, and then moving from anterior to posterior in keeping all the other axes of the receiver as parallel as possible to the corresponding axis of the transmitter. To determine if the axes are parallel or not, we can look at the transformation matrix and check if it is very close to the identity matrix. And if it was close then the point was accepted as a valid point on the surface and once the point was accepted five points were collected to take the average of all the points to minimize the slight change in the same point effect as discussed above.

$$\begin{matrix} 1 & 0 & 0 \\ 0 & 1 & 0 \\ 0 & 0 & 1 \end{matrix}$$

The methodology would be repeated by increasing the distance along the z axis by a small amount and then going from anterior to posterior in small steps and at the same time keeping the axes parallel to complete the data collection for femur and then tibia.

3.4.4 Curve fitting digitized data

After the data collection was complete the points were curve fitted using polynomials of 6^{th} or 7^{th} or 8^{th} order using a MATLAB program. First the points were fitted in the x axis direction from anterior to posterior and then later from medial to lateral for each condyle separately. This process of using polynomials resulted in a curve which was not smooth.

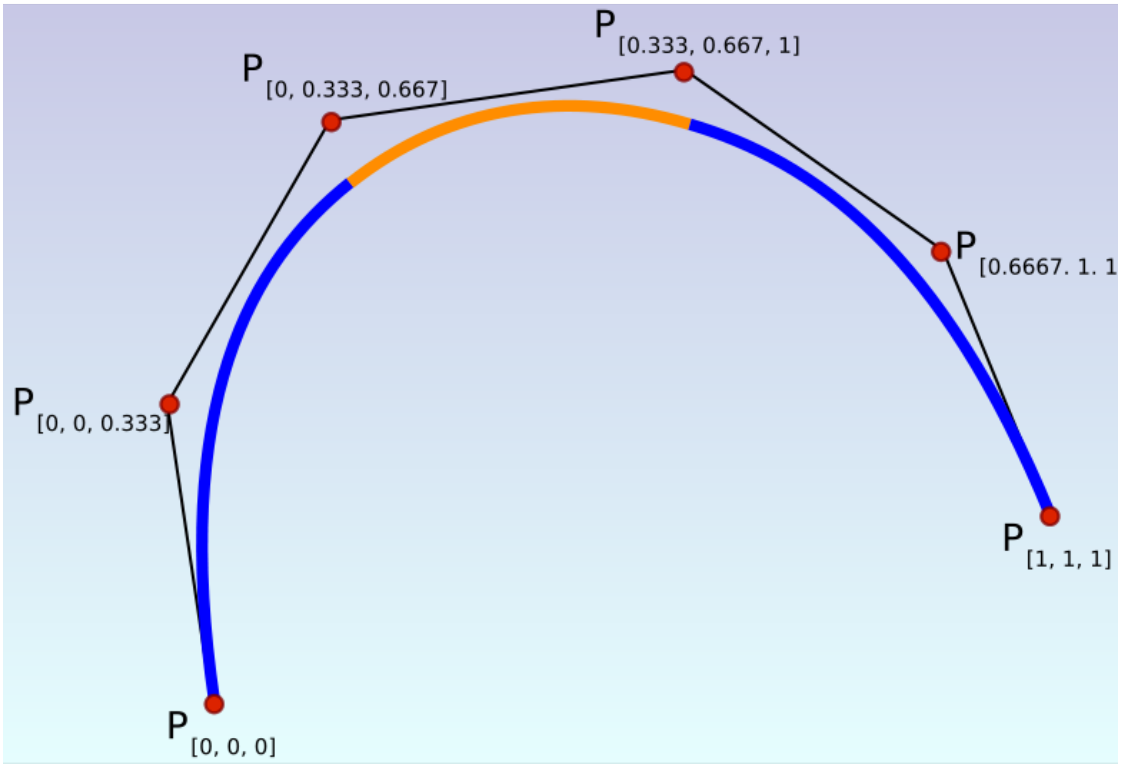

Figure 3.9: A spline interpolation of leading to smooth fit (http://upload.wikimedia.org/wikipedia/commons/5/55/Parametic_Cubic_Spline.svg).

Since in both the tibia and femur each condyles and plateaus were of different lengths and widths, sometimes only 3 or 4 points were available to be fitted along the medial to lateral curvature. Even when using a least square approximation or increasing the order of the polynomial, the fitting procedure resulted in a shape which might or might not represent the shape of the condyle or plateau at the location. Hence the idea of using polynomials for curve fitting was abandoned and use of the splines as a method of interpolation was used. Splines have the advantage that the curve fitting does not depend on the number of points. Also the resulting curve was able to be smoothed using the function csaps (Figure 3.9); which is a cubic smoothing spline was used so that we can select how smooth we want to have points interpolated using the variable 'p' while using this function in MATLAB. The value of p ranges from 0-1 where 0 being the state when the interpolation is a least squared straight line fit to the data and 1 corresponds to the state where the interpolation consists of natural or cubic spline interpolation. A value of p was chosen to be 0.7 where the curves were quite smooth.

One more advantage of choosing spline interpolation was it takes a lot less computation time to calculate the total curve fitting process. A completely curve fitted figure of the rabbit knee was then generated with the ligament insertions (Figure 3.11).

3.4.5 Ligament Properties

After geometric models of the joint surfaces were ready the ligaments lengths and stiffness were found from the literature. After some preliminary analysis it was found that only PCL and LCL were under strain and hence in order to find their stiffness and ϵ_1 values, a test protocol as described by Komatsuda et al., 2006 was used to estimate the stiffness of PCL and LCL. After careful dissection of two more rabbits and keeping intact the PCL and LCL in separate rabbits, holes were drilled into both tibia and femur and then tibia was fixed to the bottom of the Instron table and the femur was inserted into the Instron head and held in its place using a screw. 0.5 N preload was applied to each specimen and cyclic preconditioning from 0.0 to 0.3 mm of extension was performed and when the load was just zero from this cyclic load using calipers the initial length of the ligaments was found out. Later a strain rate of 10 mm/min was applied till failure but in our case the bone broke towards the end of the experiment.

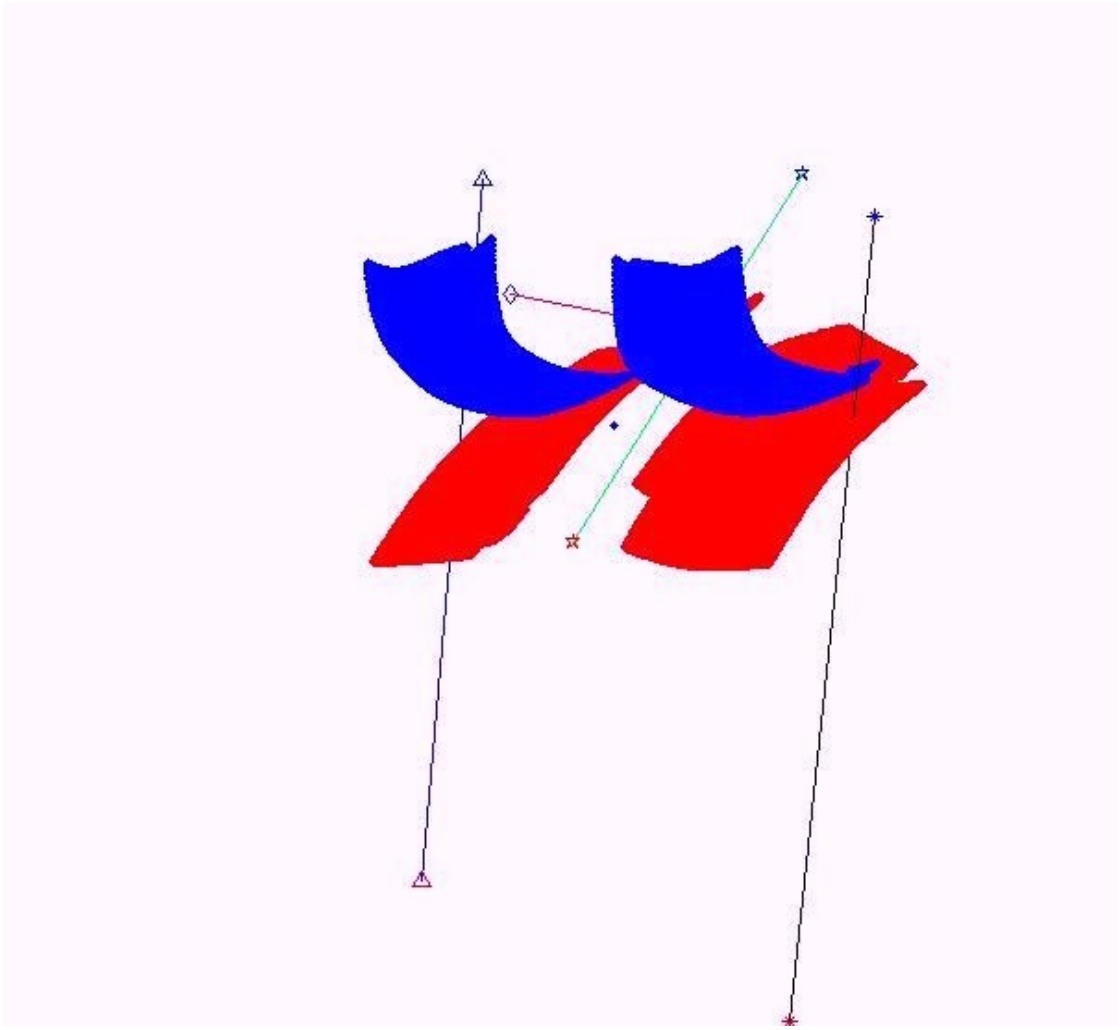

Figure 3.11: A representation of the femur and tibia with the ligaments.

3.4.6 Analysis

The equilibrium analysis was performed with a FORTRAN optimization routine from the Minpack optimization package (Argonne National Laboroatory). The software uses a hybrid form of Powell method for non-linear equations. Two subroutines (artcart.for and ligament.for) were used to quantify the contact and ligament forces and the moments in the femur for a given position of the tibia. The contact subroutine estimates contact forces,

moments and stresses on the femur which comes into contact with one point on the tibia. The shortest distance for a point on the femur to the tibia was used to determine the point of contact on the tibia, from that the forces and moments were calculated. The ligament subroutine determines the forces and moments in the ligament corresponding to the strain due to the relative position of the femur and the tibia.

There are two important parameters within the optimization software which decide the progression as well as successful completion of the iteration, called 'factor' and 'epsfcn'. Factor can be defined as a positive input variable used in determining the initial step bound in each of the six degrees of motion. After the initial step bound, the value is set to the product of factor and the euclidean norm of diag*x if nonzero, or else in the case of euclidean norm of diag*x being zero to the factor itself. The general range of the factor is (.1 to 100.), whereas 100 being a recommended value. Epsfcn is another input variable used to determine a suitable step length for the forward-difference approximation. This approximation assumes that the relative errors in the functions are of the order of epsfcn. If epsfcn is less than the machine precision, it is assumed that the relative errors in the functions are of the order of the machine precision.

The surface of the femur and the tibia were divided into three equal regions on both medial and lateral sides corresponding to posterior, central and anterior regions. Each region was then assigned their respective thickness and modulus. The values were taken as the averages for each region from the mechanical testing of the cartilage at 2 and 4 weeks and for the 4 week contralateral controls.

The muscle forces were estimated in a study of rabbit gait at five different hopping phases [46]. At 20% stance the quadriceps force was 75 N [46] and was decreased in steps of 5N for our simulation till we attained equilibrium. Finally, a compressive force of 15 N was also applied to simulate bodyweight. The location of the patella was taken approximately from the cadaveric studies, about which the moments were calculated. The thickness, length, and width of the patella were measured using a caliper and it was assumed that the patella is in contact with the femur during higher flexion angles. Then the center of the patella was calculated which was assumed as an approximate patella position.

During the optimization analysis it was found that the variable 'factor' was very large (factor=100), and it led to huge jumps in all the directions moving the surfaces out of contact. With the subsequent reductions in value the jumps were reduced but the optimization process led to results in the flexion angles around 60^0-70^0, which was not the accepted range. Therefore the value of the factor had to be reduced significantly (10^{-3}) which led to smaller step bounds, resulting in an increased time for estimating the optimized joint contact loads.

Chapter 4

RESULTS

μ-CT, indentation and histology tests were performed on the 6 locations of 8 rabbits (4 each 2 week and 4 week loaded and contralateral). The six locations included posterior, central and anterior aspect for both medial and lateral on femur and tibia for both loaded and contralateral control.

4.1 μ-CT & Indentation:

Properties of the sub-chondral trabecular bone were determined at 6 locations under tibia and femur, where indentation and needle tests were performed. In order to determine the statistical analysis to be performed, a test of the normality of the data was performed. Both histograms and Anderson-Darling tests were performed to ascertain the normality of the data and it was found that data was normal. Hence, paired Student's t-test was utilized to determine significance between the loaded and unloaded contralateral side.

In the 2 weeks loading period BMD was found to be significantly different between control and contralateral control only for the whole tibia (Mean = 378.637 gm/cc) and tibial medial side (Mean = 383.7 gm/cc). BVF was found to be significantly different for femoral lateral (Mean = 0.485) and femoral medial sides (Mean = 0.496). Tb.T and Tb.N were not found to be significantly different in the femur or the tibia. Tb. S was found to be significantly different in the femoral lateral side (Mean =0.192). The mean and standard deviations for each of the location in the femur and tibia for the two week loaded specimens (Table 4.1) and contralateral specimens (Table 4.2) are tabulated below.

Location	BMD (mg/cc)		BVF		Tb. T (μm)		Tb. N		Tb. Sp (μm)	
	Mean	SD	Mean	SD	Mean	SD	Mean	SD	Mean	SD
FLA	356.02	61.06	0.464	0.04	0.165	0.03	2.837	0.41	0.193	0.03
FLC	397.35	81.66	0.484	0.06	0.177	0.03	2.719	0.35	0.195	0.04
FLP	414.58	55.35	0.509	0.04	0.190	0.02	2.683	0.38	0.189	0.04
FMA	381.39	56.56	0.461	0.05	0.187	0.02	2.485	0.43	0.226	0.06
FMC	423.90	66.62	0.494	0.05	0.177	0.01	2.773	0.37	0.188	0.04
FMP	481.64	89.15	0.532	0.03	0.178	0.02	3.045	0.55	0.159	0.04
TLA	321.20	42.58	0.422	0.08	0.119	0.01	3.506	0.55	0.172	0.06
TLC	364.78	76.29	0.478	0.09	0.209	0.05	2.364	0.62	0.240	0.09
TLP	434.74	28.82	0.537	0.03	0.244	0.11	2.448	0.75	0.206	0.08
TMA	321.61	36.53	0.425	0.07	0.127	0.01	3.347	0.61	0.180	0.06
TMC	390.17	44.69	0.481	0.04	0.235	0.03	2.046	0.17	0.256	0.02
TMP	439.32	35.69	0.546	0.04	0.293	0.05	1.892	0.22	0.240	0.03

Table 4.1: Bone properties of 2 week loaded results for both the tibia and femur. Where BMD is bone mineral density, BVF is bone volume fraction, Tb. T is trabecular thickness, Tb. N is trabecular number and Tb. S is trabecular separation. The letters in locations are F for femur, T for Tibia, L for lateral, M for medial, A for anterior, C for center and P represents posterior.

Location	BMD (mg/cc)		BVF		Tb. T (μm)		Tb. N		Tb. Sp (μm)	
	Mean	SD	Mean	SD	Mean	SD	Mean	SD	Mean	SD
FLA	340.01	65.12	0.415	0.07	0.185	0.02	2.221	0.19	0.268	0.05
FLC	376.54	50.56	0.447	0.06	0.179	0.01	2.471	0.34	0.232	0.06
FLP	411.94	42.11	0.507	0.04	0.181	0.02	2.820	0.51	0.182	0.04
FMA	396.44	29.70	0.485	0.04	0.177	0.01	2.739	0.41	0.194	0.04
FMC	492.33	51.98	0.555	0.02	0.209	0.03	2.675	0.37	0.170	0.03
FMP	506.27	50.16	0.561	0.02	0.188	0.03	3.018	0.46	0.148	0.02
TLA	333.10	28.16	0.489	0.03	0.128	0.01	3.821	0.35	0.135	0.02
TLC	357.31	70.02	0.463	0.08	0.194	0.01	2.351	0.36	0.238	0.07
TLP	441.02	50.82	0.557	0.07	0.250	0.06	2.304	0.45	0.196	0.04
TMA	362.96	37.08	0.453	0.00	0.127	0.01	3.570	0.31	0.155	0.01
TMC	404.09	71.81	0.475	0.09	0.217	0.02	2.167	0.26	0.249	0.07
TMP	456.10	48.33	0.571	0.07	0.364	0.07	1.617	0.35	0.274	0.08

Table 4.2: Bone properties for both tibia and femur (2 week contralateral). Where BMD is bone mineral density, BVF is bone volume fraction, Tb. T is trabecular thickness, Tb. N is trabecular number and Tb. S is trabecular separation. The letters in locations are F for femur, T for Tibia, L for lateral, M for medial, A for anterior, C for center and P represents posterior.

Aggregate modulus was found to be significantly different only for the tibial medial side (Mean = 0.433) for the 2 week specimens. Poisson's ratio was found to be significant in the tibial (Mean = 0.152) (all the lateral and medial were combined for loaded vs. unloaded side) as well as tibial lateral (Mean = 0.169). Permeability was not found to be significantly different for either femur or tibia. Thickness was also found to be significantly different for tibial lateral side. The mean and standard deviations for each of the location in the femur and tibia for the two week loaded specimens (Table 4.3) and contralateral specimens (Table 4.4) are tabulated below.

Location	Thickness(mm)		Ha (MPa)		nu		k (m^4/Ns) ($X10^{-16}$)		R^2	
	Mean	SD	Mean	SD	Mean	SD	Mean	SD	Mean	SD
FLA	0.199	0.02	0.270	0.11	0.206	0.06	6.26	5.63	0.959	0.03
FLC	0.211	0.03	0.284	0.06	0.214	0.08	5.37	1.15	0.956	0.03
FLP	0.192	0.04	0.342	0.05	0.208	0.02	7.51	2.24	0.945	0.06
FMA	0.269	0.08	0.392	0.19	0.194	0.07	6.13	2.54	0.962	0.01
FMC	0.195	0.03	0.286	0.10	0.226	0.04	4.23	1.27	0.976	0.01
FMP	0.213	0.05	0.484	0.39	0.227	0.02	4.31	0.89	0.959	0.03
TLA	0.269	0.08	0.388	0.29	0.190	0.04	4.24	2.05	0.956	0.01
TLC	0.308	0.08	0.590	0.36	0.178	0.05	8.45	3.30	0.954	0.01
TLP	0.253	0.16	0.379	0.10	0.139	0.06	9.39	7.03	0.951	0.02
TMA	0.275	0.07	0.313	0.25	0.135	0.05	7.11	3.18	0.974	0.01
TMC	0.430	0.05	0.512	0.22	0.121	0.02	15.2	4.97	0.944	0.01
TMP	0.380	0.13	0.475	0.13	0.147	0.07	13.5	5.25	0.943	0.02

Table 4.3: Mechanical properties for 2 week loaded for both tibia and femur. Ha represents aggregate modulus, k presents permeability, v represents Poisson's ratio and R^2 is the coefficient of determination. The letters in locations are F for femur, T for Tibia, L for lateral, M for medial, A for anterior, C for center and P represents posterior.

Location	Thickness(mm)		Ha (MPa)		nu		k (m^4/Ns) ($X10^{-16}$)		R^2	
	Mean	SD	Mean	SD	Mean	SD	Mean	SD	Mean	SD
FLA	0.198	0.05	0.318	0.17	0.160	0.05	6.70	4.62	0.961	0.02
FLC	0.208	0.05	0.262	0.05	0.249	0.06	5.18	2.27	0.975	0.00
FLP	0.179	0.06	0.229	0.06	0.234	0.13	4.66	2.11	0.946	0.01
FMA	0.235	0.04	0.287	0.09	0.179	0.07	5.16	1.35	0.962	0.00
FMC	0.202	0.02	0.324	0.06	0.249	0.05	5.18	1.41	0.972	0.00
FMP	0.216	0.08	0.424	0.11	0.209	0.05	6.08	1.85	0.964	0.02
TLA	0.183	0.04	0.445	0.12	0.230	0.02	3.49	2.95	0.959	0.01
TLC	0.194	0.01	0.372	0.11	0.203	0.05	4.26	3.42	0.963	0.03
TLP	0.185	0.03	0.306	0.17	0.209	0.03	5.45	0.76	0.971	0.01
TMA	0.314	0.16	0.485	0.15	0.196	0.10	11.7	12.1	0.959	0.01
TMC	0.369	0.06	0.614	0.28	0.149	0.08	16.0	13.8	0.951	0.02
TMP	0.435	0.07	0.652	0.17	0.124	0.04	8.52	4.90	0.948	0.03

Table 4.4: Mechanical properties for 2 week contralateral for both tibia and femur. Ha represents aggregate modulus, k presents permeability, v represents Poisson's ratio and R^2 is the coefficient of determination. The letters in locations are F for femur, T for Tibia, L for lateral, M for medial, A for anterior, C for center and P represents posterior.

For the 4 week loading period, as expected, the results were more significantly different between the loaded and contralateral control knees. BMD was significantly different for all except the femur and tibial lateral (Mean = 440.495 gm/cc and Mean = 455.404 gm/cc for medial and lateral femur respectively and Mean = 445.923 gm/cc and Mean = 429.661 gm/cc for tibia and tibia medial respectively). The BMD was highly significantly different for the femoral medial when compared to lateral (P=0.0004 and P=0.0404 respectively). BVF values were significant for femur (Mean =0.479), lateral femur (Mean = 0.451), medial femur (Mean = 0.506), tibia (Mean = 0.547) and medial tibia (Mean = 0.537). Tb. T was found to be significantly only for tibial lateral side (Mean = 0.231 μm). Tb. N was found to be significantly different tibia (Mean = 2.185 μm) and lateral tibia (Mean = 2.44 μm) and the femoral lateral side (Mean = 2.394 μm) Tb. S was found to be significantly different for the whole femur (Mean = 0.214 μm) and corresponding lateral (Mean = 0.234 μm) and medial sides (Mean = 0.194 μm), and the whole tibia (Mean = 0.211 μm) (medial and lateral together for loaded vs. contralateral) as well as corresponding lateral (Mean = 0.183 μm) and medial sides (Mean = 0.239 μm). The mean and standard deviations for each of the location in the femur and tibia for the four week loaded specimens (Table 4.5) and contralateral specimens (Table 4.6) are tabulated below.

Location	BMD (mg/cc)		BVF		Tb. T (μm)		Tb. N		Tb. Sp (μm)	
	Mean	SD	Mean	SD	Mean	SD	Mean	SD	Mean	SD
FLA	470.88	34.64	0.471	0.03	0.202	0.03	2.339	0.34	0.232	0.04
FLC	424.26	34.44	0.444	0.08	0.190	0.04	2.310	0.18	0.244	0.04
FLP	426.35	35.29	0.439	0.08	0.173	0.04	2.533	0.34	0.227	0.05
FMA	429.62	31.13	0.495	0.04	0.201	0.01	2.456	0.09	0.207	0.02
FMC	446.37	30.19	0.514	0.03	0.200	0.01	2.546	0.13	0.194	0.02
FMP	490.22	8.63	0.510	0.01	0.188	0.01	2.733	0.13	0.179	0.01
TLA	461.79	30.74	0.532	0.04	0.209	0.01	2.541	0.21	0.186	0.03
TLC	479.49	41.90	0.577	0.03	0.246	0.03	2.351	0.19	0.181	0.02
TLP	445.28	27.16	0.562	0.06	0.238	0.06	2.428	0.32	0.180	0.01
TMA	392.83	73.02	0.475	0.06	0.208	0.03	2.103	0.62	0.235	0.05
TMC	456.71	27.67	0.574	0.03	0.309	0.02	1.863	0.18	0.231	0.04
TMP	439.44	55.53	0.562	0.04	0.318	0.05	1.822	0.43	0.252	0.07

Table 4.5: Bone properties of 4 week loaded for both the tibia and femur.

Location	BMD (mg/cc)		BVF		Tb. T (μm)		Tb. N		Tb. Sp (μm)	
	Mean	SD	Mean	SD	Mean	SD	Mean	SD	Mean	SD
FLA	371.33	15.04	0.493	0.01	0.178	0.01	2.760	0.18	0.186	0.01
FLC	407.35	37.35	0.480	0.01	0.192	0.02	2.481	0.25	0.215	0.02
FLP	398.37	26.41	0.516	0.05	0.205	0.04	2.534	0.40	0.196	0.03
FMA	479.05	42.90	0.510	0.05	0.202	0.03	2.522	0.12	0.195	0.01
FMC	510.27	28.25	0.538	0.03	0.221	0.03	2.442	0.20	0.190	0.01
FMP	527.26	55.15	0.536	0.03	0.189	0.03	2.849	0.38	0.166	0.02
TLA	421.38	22.41	0.514	0.02	0.177	0.02	2.892	0.24	0.170	0.01
TLC	453.13	23.04	0.570	0.04	0.241	0.03	2.328	0.08	0.181	0.01
TLP	474.97	19.91	0.577	0.04	0.218	0.04	2.719	0.34	0.157	0.01
TMA	469.75	64.06	0.539	0.05	0.239	0.02	2.244	0.05	0.206	0.02
TMC	522.07	77.58	0.600	0.04	0.307	0.07	2.018	0.38	0.202	0.04
TMP	509.67	53.76	0.590	0.05	0.322	0.09	1.919	0.45	0.219	0.04

Table 4.6: Bone properties of 4 week contralateral for both the tibia and femur.

Aggregate modulus was found to be significantly different for the whole femur (Mean = 0.204 MPa) and on both the lateral femur (Mean = 0.226 MPa) and medial femur (Mean = 0.183 MPa). Poisson's ratio was found to be significant in whole femur (Mean = 0.205); trends (when $p<0.10$) were observed in lateral and medial side of femur as well as lateral and medial side of tibia. Permeability was found to be significantly different on the whole tibia (Mean = 1.679E-15 m^4/Ns) and on both the lateral tibia (Mean = 1.153E-15 m^4/Ns) and medial tibia (Mean = 2.205E-15 m^4/Ns). Thickness was not found to be significantly different for either the tibia or femur but trends were found in lateral femur and whole tibia as well. The mean and standard deviations for each of the location in the femur and tibia for the two week loaded specimens (Table 4.7) and contralateral specimens (Table 4.8) are tabulated below.

Location	Thickness(mm)		Ha (MPa)		nu		k (m^4/Ns) ($X10^{-16}$)		R^2	
	Mean	SD	Mean	SD	Mean	SD	Mean	SD	Mean	SD
FLA	0.140	0.02	0.250	0.09	0.190	0.05	4.28	1.16	0.960	0.05
FLC	0.180	0.02	0.220	0.04	0.240	0.04	4.25	0.85	0.980	0.01
FLP	0.160	0.02	0.200	0.03	0.200	0.01	4.47	1.21	0.980	0.00
FMA	0.180	0.08	0.120	0.04	0.170	0.06	3.92	2.28	0.980	0.01
FMC	0.210	0.04	0.180	0.10	0.200	0.08	4.84	1.29	0.980	0.00
FMP	0.170	0.03	0.240	0.09	0.230	0.09	6.74	5.89	0.980	0.01
TLA	0.250	0.14	0.260	0.17	0.180	0.05	9.82	4.69	0.980	0.01
TLC	0.290	0.14	0.540	0.58	0.170	0.09	9.06	3.16	0.980	0.01
TLP	0.300	0.12	0.290	0.17	0.160	0.12	15.7	5.04	0.970	0.01
TMA	0.360	0.18	0.510	0.20	0.170	0.11	23.1	12.0	0.960	0.01
TMC	0.440	0.14	0.620	0.32	0.160	0.06	20.6	8.91	0.950	0.02
TMP	0.380	0.15	0.600	0.50	0.210	0.09	22.5	15.0	0.960	0.01

Table 4.7: Mechanical properties for 4 week loaded for both tibia and femur.

Location	Thickness(mm)		Ha (MPa)		nu		k (m^4/Ns) ($X10^{-16}$)		R^2	
	Mean	SD	Mean	SD	Mean	SD	Mean	SD	Mean	SD
FLA	0.139	0.05	0.408	0.30	0.306	0.08	3.60	3.26	0.980	0.01
FLC	0.149	0.04	0.323	0.15	0.301	0.10	5.02	3.44	0.978	0.01
FLP	0.142	0.02	0.403	0.16	0.167	0.03	4.49	2.03	0.983	0.00
FMA	0.166	0.06	0.288	0.20	0.222	0.07	6.75	5.84	0.978	0.00
FMC	0.190	0.03	0.447	0.32	0.231	0.04	6.46	3.31	0.980	0.00
FMP	0.179	0.03	0.827	0.23	0.246	0.12	3.33	0.94	0.972	0.01
TLA	0.180	0.06	0.266	0.19	0.236	0.10	5.76	1.91	0.982	0.00
TLC	0.205	0.09	0.466	0.21	0.243	0.12	5.66	2.47	0.977	0.01
TLP	0.236	0.09	0.364	0.13	0.203	0.09	9.76	5.68	0.978	0.01
TMA	0.269	0.11	0.539	0.47	0.188	0.03	7.23	5.88	0.972	0.01
TMC	0.501	0.02	1.162	0.53	0.068	0.04	15.7	9.35	0.949	0.01
TMP	0.366	0.12	0.838	0.67	0.170	0.12	13.0	10.1	0.958	0.01

Table 4.8: Mechanical properties for 4 week contralateral for both tibia and femur.

The % changes in each of the femur, lateral femur, medial femur, tibia, lateral tibia and medial tibia are tabulated for 4 week and two week loaded vs. respective controls (Table 4.9), between 4 week loaded and two week loaded, and between 4 week controls and two week controls.

	Four week loaded femur.			Four week loaded tibia.			Two week loaded femur.			Two week loaded tibia.		
	T	L	M	T	L	M	T	L	M	T	L	M
Ha	-54.5	-40.3	-64.8	-22.2	0.2	-31.9	11.6	10.7	12.3	-7.6	20.7	-25.8
nu	-16.4	-18.5*	-14.0	-4.5	-25.2*	28.8	-0.6	-2.8	1.6	-18.1	-21.1	-14.0
k	-3.9	-0.8	-6.3	76.4	63.3	84.1	2.6	15.7	-10.6	16.9	67.2	-1.4
BMD	-0.2	12.3	-9.9	-6.2	2.7	-14	-2.7	3.5*	-7.8*	-3.5	-0.9	-5.9
BVF	-6.5	-9	-4	-3.2	0.6	-6.8	-0.9	6.4	-7.1	-3.9	-4.7*	-3.1
Tb. T	-2.9	-1.6	-4	1.5	8.8	-3.9	-4	-2.1	-5.7*	-4	0.1	-7.3
Tb. N	-4.4*	-7.6	-1.2	-7.2	-7.8	-6.4	3.7	9.7*	-1.5	-1.4	-1.9	-0.9
Tb. S	11.9	17.8	5.4	11.5	7.8	14.4	-3.8	-16	11.9*	3.8	8.6	-0.1

Table 4.9: Comparison of the bone trabecular morphology of Ha, nu, k, BMD, BVF, Tb. T, Tb. N and Tb. S for the four and two week loaded versus the control as indicated by the sign change in terms of percentage. T indicates the total as in medial and lateral compartments combined, L stands for lateral and M for medial compartments respectively. The colored cell indicates significant changes; whereas non colored cell indicates with '*' indicates trend and plane non colored cell indicates non significant changes. The % change is calculated as (loaded -control)*100/(control).

	Loaded						Control					
	Femur			Tibia			Femur			Tibia		
	T	L	M	T	L	M	T	L	M	T	L	M
Ha	-40	-25	-53	6.5	-19	33.1	46.2	40.2	50.9	26.4	-2.5	45.0
nu	-3.4	0.4	-7.1	16.4	0.7	36.2	14.9	19.8	9.8	-0.2	6.2	-9.1
k	-16	-32	5.6	74.3	56.7	85.2	-10.0	-20.7	0.7	15.5	60.5	-0.8
BMD	9.5	13.1	6.2	17.8	23.7	12	6.7	4.3	8.7	21.1	19.3	22.8
BVF	-2.4	-7	2.1	13.6	16.3	11	3.4	8.7	-1.1	12.7	10.1	15.4
Tb. T	7.3	6	8.5	24.3	20.9*	27.3	6.1	5.6	6.6	17.6	11.3	22.7
Tb. N	-9.9	-13	-7.0*	-16	-12.0*	-21	-2.2*	3.5	-7.3	-10.8	-6.3	-15.9*
Tb. S	11.8	22.1	1.5	-2.1	-11	6.3	-3.8	-12.4	7.7	-8.8	-10.7*	-7.3

Table 4.10: Comparison of the bone trabecular morphology of Ha, nu, k, BMD, BVF, Tb. T, Tb. N and Tb. S for the four loaded specimen vs. two week loaded specimens and four week controls vs. two week controls as indicated by the sign change in terms of percentage. T indicates the total as in medial and lateral compartments combined, L stands for lateral and M for medial compartments respectively. The cell in colored indicates significant changes; whereas non colored cell indicates with '*' indicates trend and plane non colored cell indicates non significant changes. The % change is calculated as (4 week -2 week)*100/(2 week).

Correlations were found using Spearman's rank correlation test to determine if relations existed among and between the μ--CT measurements of the subchondral bone and the material properties of the articular cartilage. A non parametric test was

used because a test for normality using both histograms and the Anderson Darling test resulted with the p-values not being very significant. Hence the non parametric test was used to evaluate the correlations. The different correlations between the mechanical properties of cartilage and trabecular bone morphological properties are tabulated below (Table 4.9).

			Femur Loaded	Femur Contralateral	Tibia Loaded	Tibia Contralateral
1	Ha vs. BMD	R^2	0.04	0.052	2.00E-04	0.012
	4 Week	R^2	3.00E-06	0.03	7.00E-03	0.401 ↓
	2 Week	R^2	0.007	0.081	0.001	0.011
2	Ha vs.Tb.T	R^2	0.095 ↓	0.004	0.033	0.164 ↑
	4 Week	R^2	0.066	0.177 ↓	0.082	0.403 ↑
	2 Week	R^2	0.01	0.11	0.03	0.38 ↑
3	Ha vs. Tb.N	R^2	0.022	0.027	0.09	0.084 ↓
	4 Week	R^2	7.00E-04	0.275 ↑	0.280 ↓	0.201 ↓
	2 Week	R^2	0.007	0.039	0.014	0.026
4	Ha vs. Tb.S	R^2	6.00E-04	0.019	0.067	0.064
	4 Week	R^2	0.021	0.201 ↓	0.294 ↑	0.201 ↑
	2 Week	R^2	0.036	6.00E-04	0.001	0.091
5	nu vs. BMD	R^2	0.008	0.003	0.004	0.028
	4 Week	R^2	0.008	0.02	0.03	8.00E-05
	2 Week	R^2	0.008	6.00E-04	0.001	0.054
6	nu vs. Tb.T	R^2	0.016	0.091 ↓	5.00E-04	0.184 ↓
	4 Week	R^2	4.00E-04	0.128	2.00E-04	0.339 ↓
	2 Week	R^2	0.121	0.064	0.017	0.314 ↓

7	nu vs. Tb.N	R^2	0.007693	0.015	7.00E-04	0.122 ↑
	4 Week	R^2	0.02	0.102	0.002	0.141
	2 Week	R^2	0.041	0.048	0.007	0.138
8	nu vs. Tb.S	R^2	0.007	0.037	0.009	0.053
	4 Week	R^2	0.032	0.088	0.025	0.038
	2 Week	R^2	0.054	0.075	5.00E-04	0.111
9	k vs. BMD	R^2	0.011	0.006	0.059	0.090 ↑
	4 Week	R^2	0.022	0.052	0.079	0.125
	2 Week	R^2	0.002	2.00E-04	0.178 ↑	0.059
10	k vs. Tb.T	R^2	0.032	0.096 ↑	0.279 ↑	0.088 ↑
	4 Week	R^2	0.1	0.179 ↑	0.024	0.148
	2 Week	R^2	0.013	0.125	0.457 ↑	0.052
11	k vs. Tb.N	R^2	0.005	0.067	0.340 ↓	0.07
	4 Week	R^2	0.017	0.077	0.12	0.103
	2 Week	R^2	0.023	0.016	0.434 ↓	0.031
12	k vs. Tb.S	R^2	0.002	1.00E-04	0.166 ↑	0.008
	4 Week	R^2	0.002	6.00E-05	0.133	0.017
	2 Week	R^2	0.011	0.009	0.201 ↑	0.011

Table 4.11: A correlation table between mechanical and bone properties, where the cells filled with blue being significant and the arrow direction pointing +ve for up arrow and –ve for down arrow. For e.g. with increase in k there was an increase in Tb. S for four week tibia.

4.2 Histology

After the staining and mounting was complete the grading was done by two observers. The average of both the scores was presented. The scores were tabulated in Table 4.12 where the comparisons were made between the loaded and unloaded with mean and standard deviation for each of them. Analysis was made using Student's t-test assuming equal variance between the loaded and contralateral controls. All results were significantly different except for 2 week lateral tibia which had a trend. Comparisons were also made between the loaded four weeks and loaded two weeks, where there were no significantly different results though there was a trend in the whole femur. Tests of significance between the controls of four week and two week resulted in significance in every comparison.

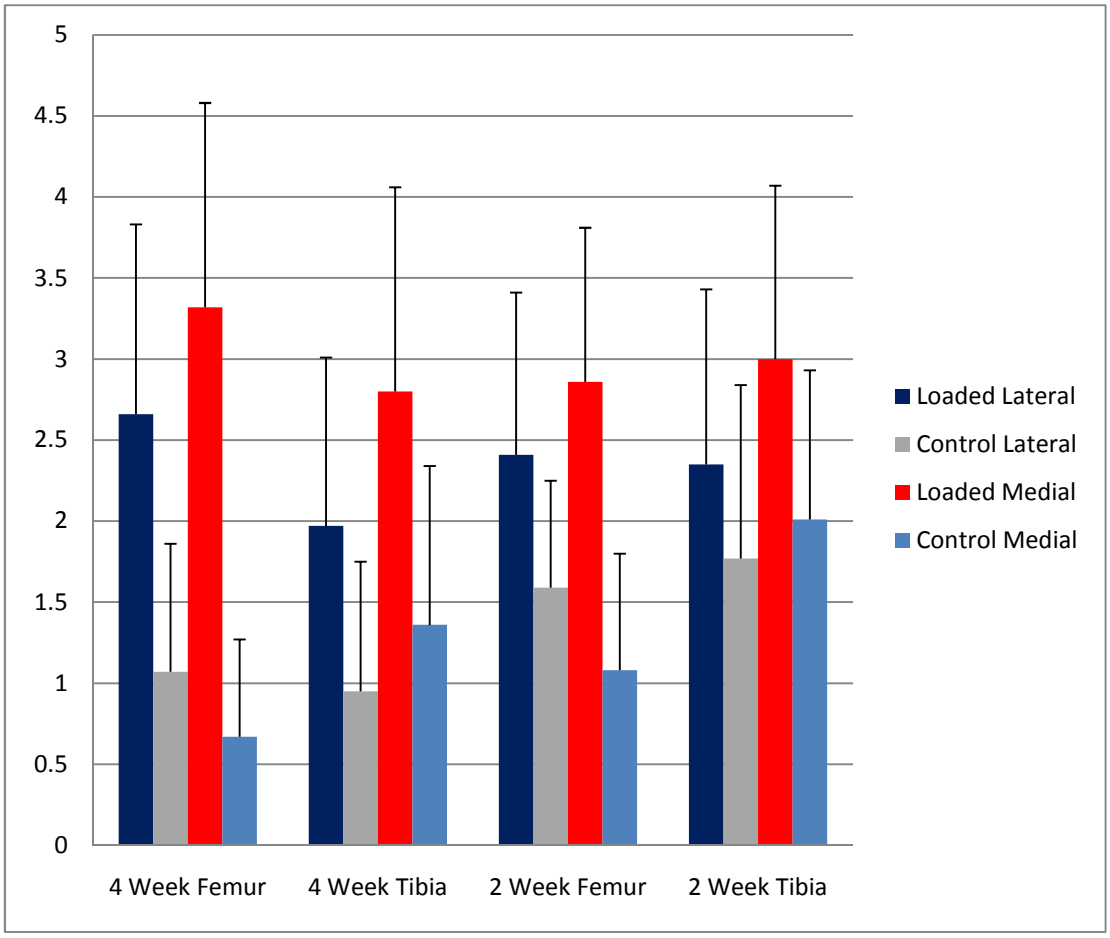

Figure 4.10: Graph represents the mean score with the error bars representing the standard deviations. The graph has four sections 4 week & 2 week, femur and tibia with the columns representing loaded lateral, control lateral, medial loaded and control medial in that order.

While looking at the gross morphology, the four week loaded femurs had a markedly reduced staining overall as well as occasional lack of staining near the cartilage with an occasional tide mark disruption and staining into the calcified cartilage region and rare surface fibrillation. There was almost no difference between the medial and the lateral sides. A picture of stained four week loaded femur is shown below as noted by decreased staining (Figure 4.1).

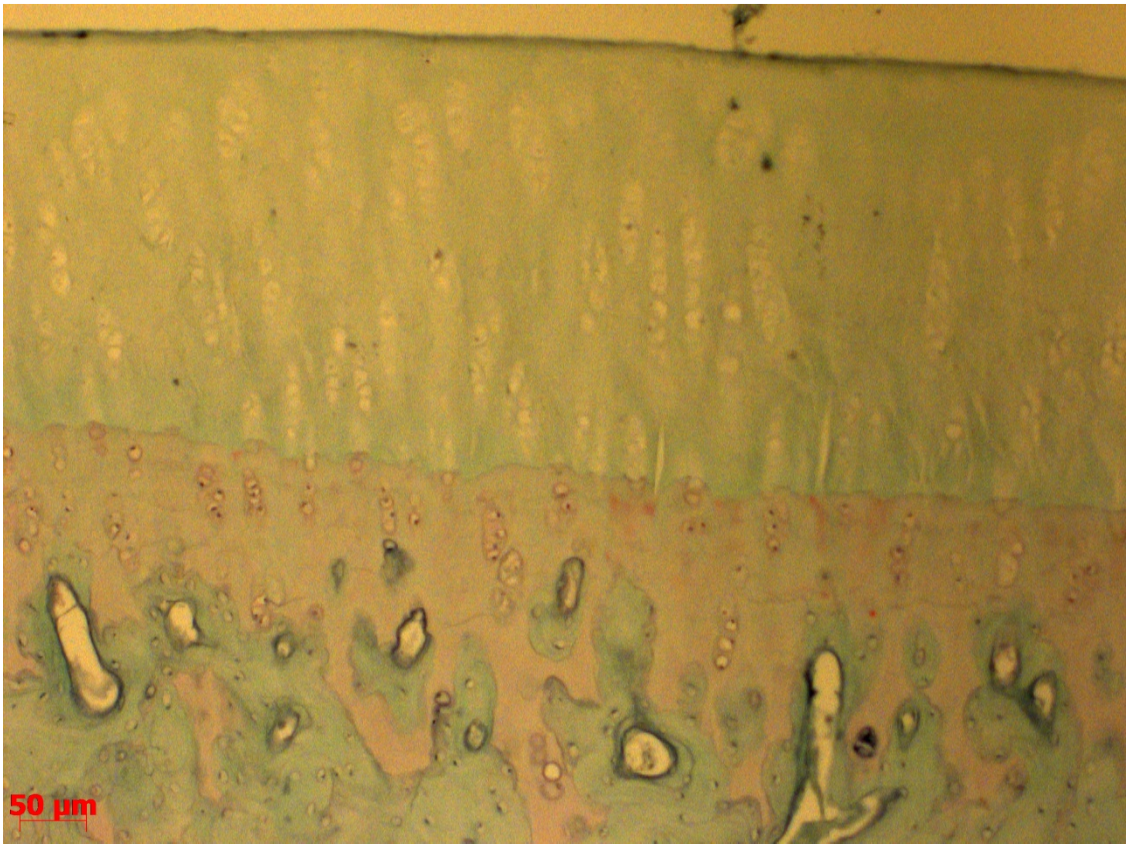

Figure 4.2: As seen by the histology side of femur loaded for 4 weeks, the staining was greatly reduced and staining past the tidemark.

The four week contralateral femurs had nothing abnormal to report with very little reduction in staining, no disruption of tide mark or staining in the zones past the tide mark. Four week loaded tibias had more interesting histological analysis. There were more pronounced surface defibrillation and fissures when compared to loaded femur, reduced staining and little staining past the tidemark. The medial side had more fissures when compared to the lateral side. The contralateral tibias at 4 weeks had nothing to report except occasional surface fibrillation which looked as if they were produced by the sectioning procedure. The staining was consistent and with a very little staining past the tidemark. The medial side and lateral sides were not different. As seen by the picture the surface is not smooth but rather jagged and few irregularities with reduced staining (Figure 4.2).

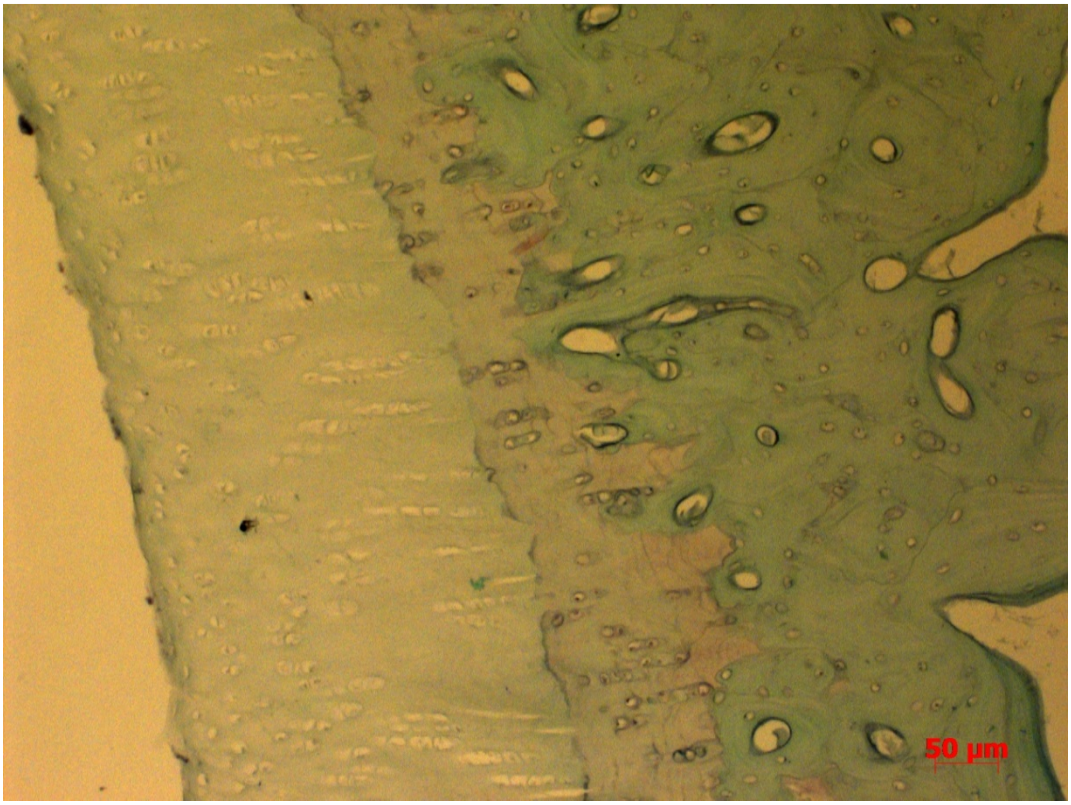

Figure 4.3: Tibia 4 week loaded had less staining, but the surface as seen was slightly fibrillated as well.

The loaded femurs at 2 weeks had reduced staining but less when compared to the 4 week loaded femurs. There was little surface fibrillation. A sparse staining was noticed past the tidemark, with the tidemark remaining intact almost every time. There was little difference between the medial and lateral sides. The contralateral femurs at 2 weeks had an occasional reduction in staining. The surfaces were intact with no fibrillation. The tidemark was intact with no staining past it and no difference between medial and lateral sides was noticed. Te loaded tibias at 2 weeks had a very slight reduction in staining, with occasional surface fibrillation. The tidemark was intact as well with no staining past the tidemark. Medial and lateral sides had no distinguishable differences. The contralateral tibia at 2 weeks was similar to the loaded, not much reduction in staining, intact tidemark and surface. In addition there was no difference between medial and lateral side. The snapshot indicates no surface irregularities with normal staining pattern (Figure 4.3).

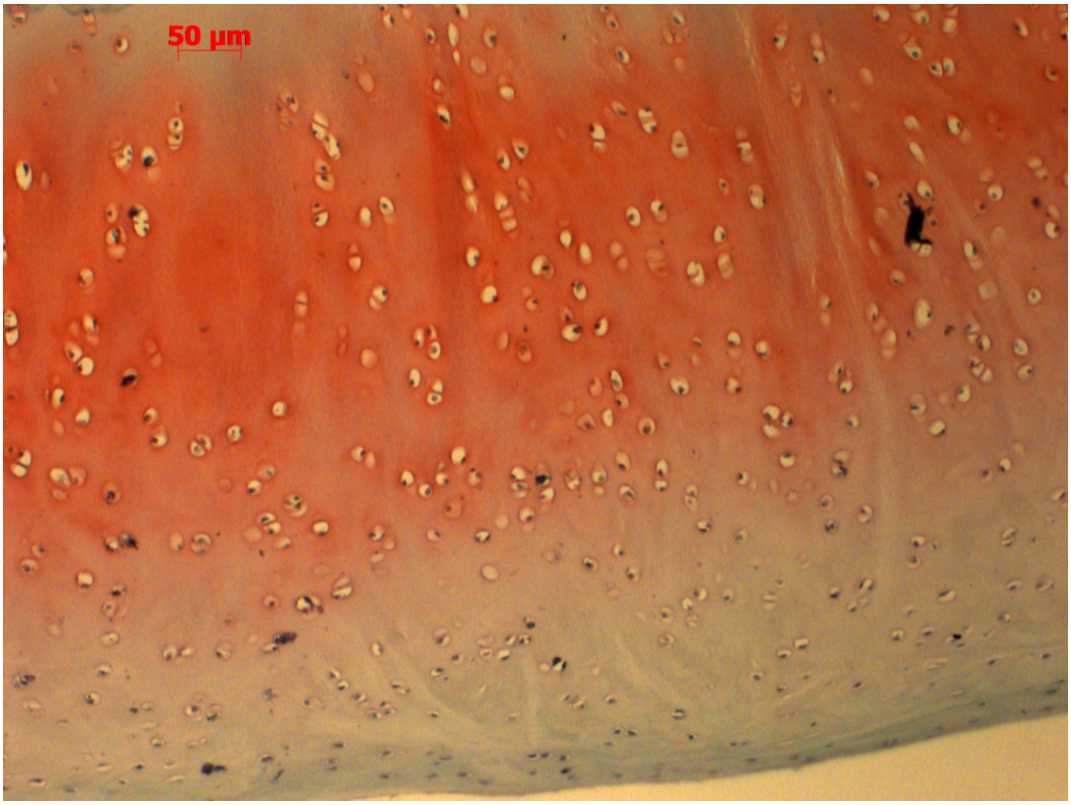

Figure 4.4: Tibia loaded 2 week had a pretty normal appearance, as seen from the well stained surface with no fibrillation.

4.3 Joint modeling

As with any optimization routine the results will converge to some set criteria and will not get better beyond a point. Hence an error margin of +/- 10% was thought as a good enough point to stop. Error for force was defined as the ratio of sum of all forces to sum of the absolute values of individual forces, similarly for moment too. After the optimization process was completed for the four week loaded model, the force on medial femur was found to be 78.331 N and on the lateral side 40.269 N. A screenshot of the results at the end of optimization is shown below (Figure 4.3). On the left as marked by 1, 2, 3, 4, 5 and 6 is the current coordinates of the tibia indicating translation x, y, z, and rotation z, x and y coordinates respectively, where as the numbers on the right side corresponding to the coordinate is resultant sum of forces and moments in x, y and z direction respectively. As seen from the tolerances the moments were very well balanced and force was also balanced except in z-

direction and a bit in y-direction, as a result of which the moment in the x-direction was slightly off.

Table 4.12: Values of the tolerances obtained from optimization routine for the four week loaded specimen; expressed as %.

	X-Axis	Y-Axis	Z-Axis
Force	0.016228	11.77057	-30.2659
Moment	-4.95919	-0.19298	0.016876

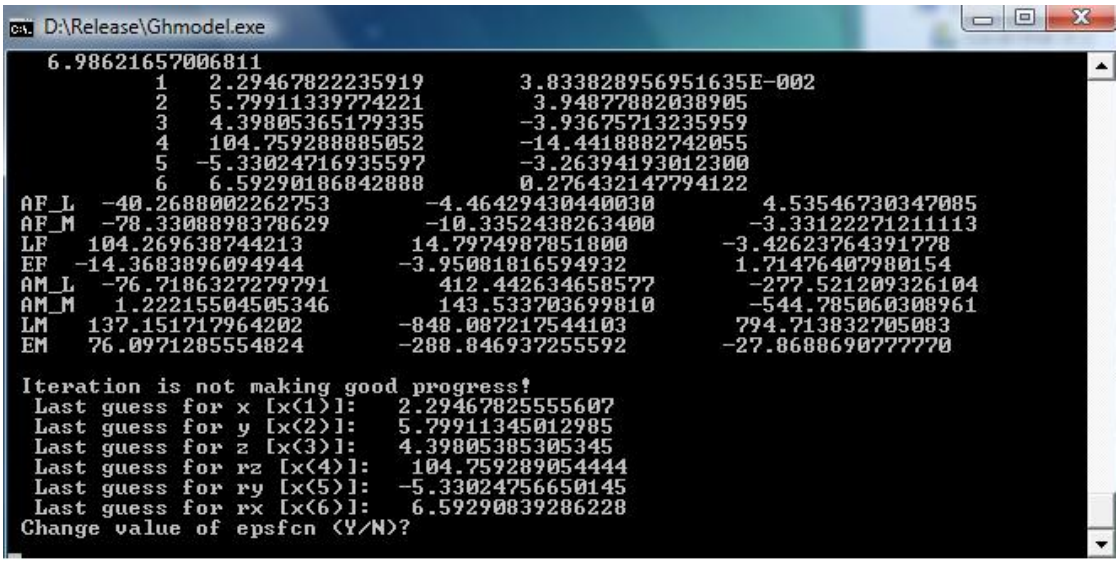

Figure 4.5: Screenshot of the optimization routine for the four week loaded specimens. While running the optimization the routine updates the screen for every iteration as means of showing us how the optimization routine is progressing.

For the two week loaded model the force acting on the medial femur was 71.451 N and on the lateral side was 41.806 N. As seen from tolerance and the screenshot the same trend as before was there moments were balanced pretty well but the forces in y-direction were higher than in four week loaded model.

Table 4.13: Values of the tolerances obtained from optimization routine for the two week loaded specimen; expressed as %.

	X-Axis	Y-Axis	Z-Axis
Force	1.599493	21.76932	-27.0828
Moment	-5.92078	-0.1457	0.091657

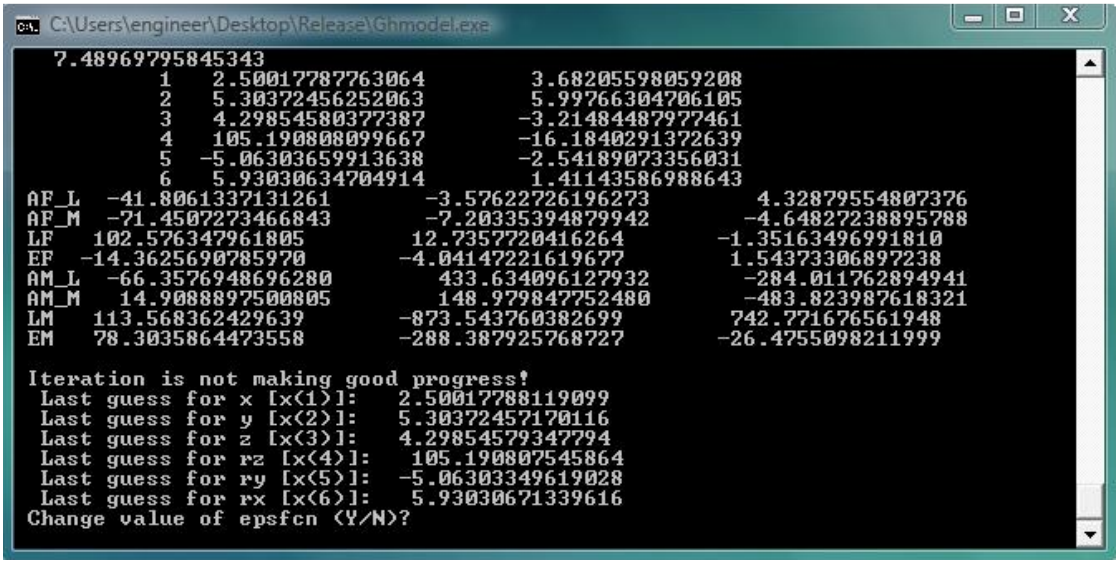

Figure 4.6: Screenshot of the two week results. Force in y-direction was off a bit which resulted in the x-direction moment to be off by a slight bit.

For the contralateral side the model was simulated as if it was loaded. The optimized force for the medial femur side was 68.9355 N while the lateral side experienced 42.821 N. As seen from the tolerances everything was well balanced.

Table 4.14: Values of the tolerances obtained from optimization routine for the four week contralateral specimen; expressed as %.

	X-Axis	Y-Axis	Z-Axis
Force	0.495181	-3.63524	-2.65395
Moment	3.728254	-0.90592	-2.07849

Figure 4.7: Screenshot of the optimization routine for the four week contralateral specimens.

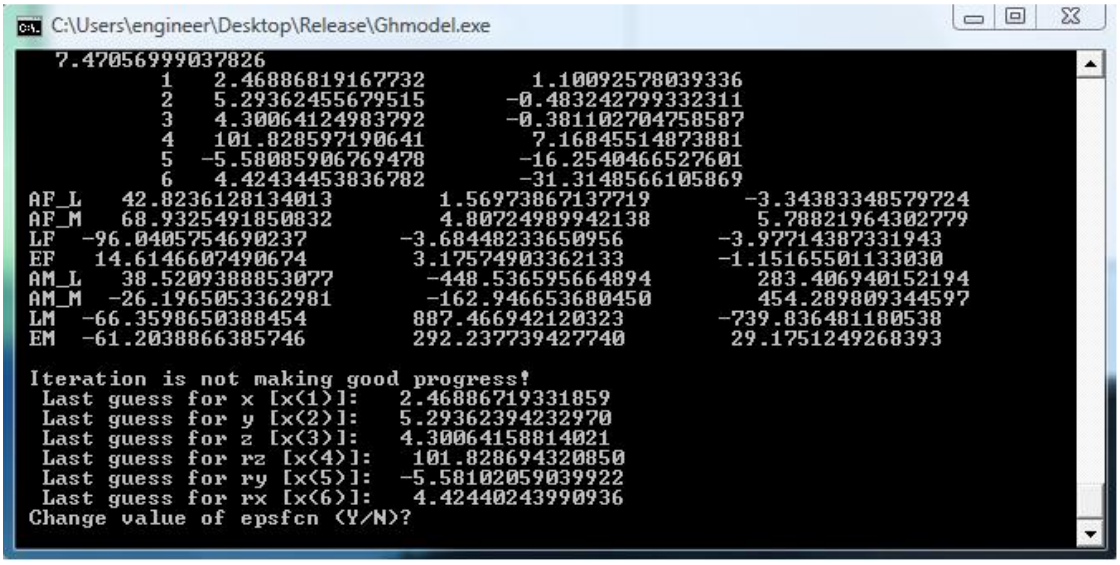

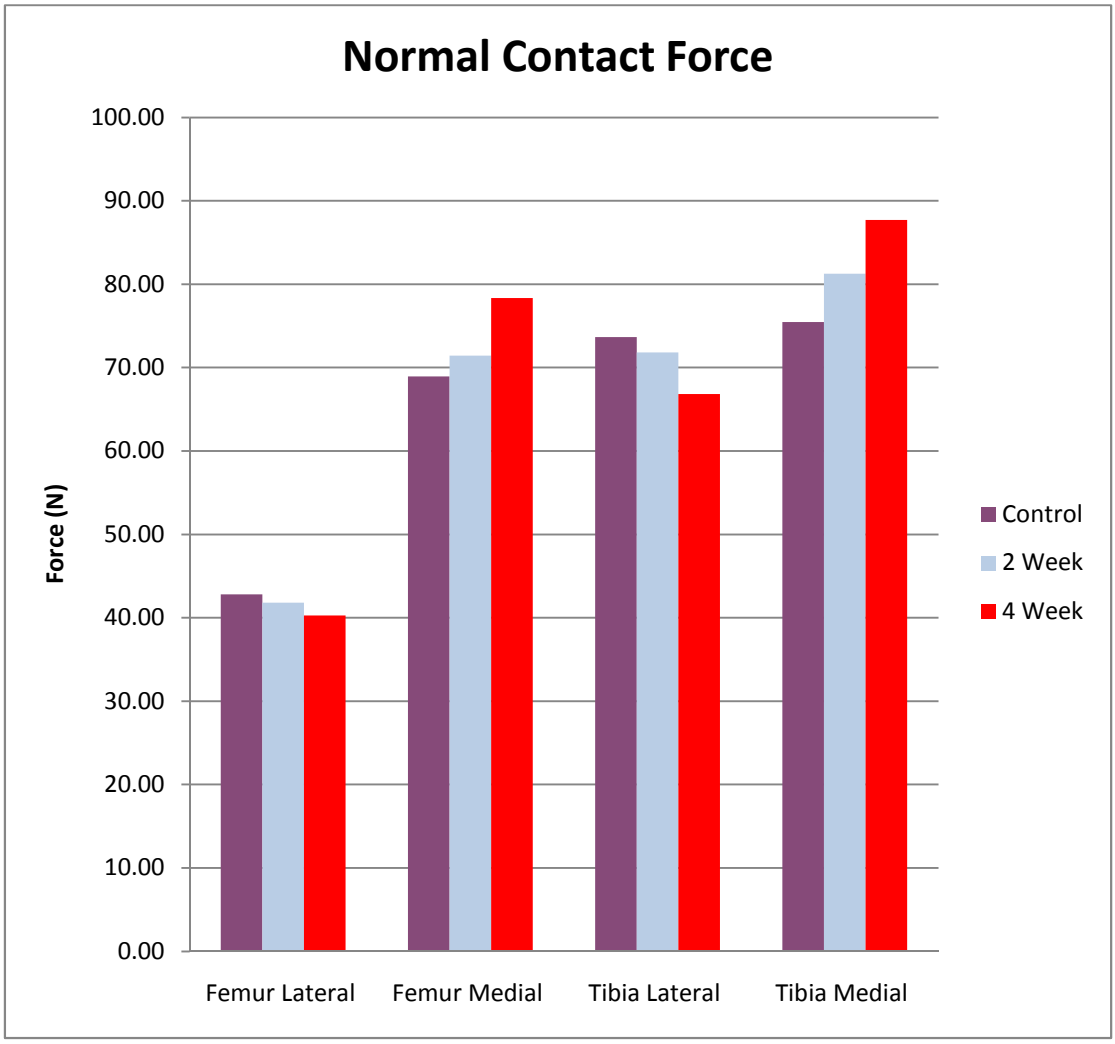

Figure 4.8: The graph represents Normal Contact forces has four sections femur lateral, femur medial, tibia lateral and tibia medial. Each has three columns, first column is control, second one is 2 week loaded and third one is 4 week loaded.

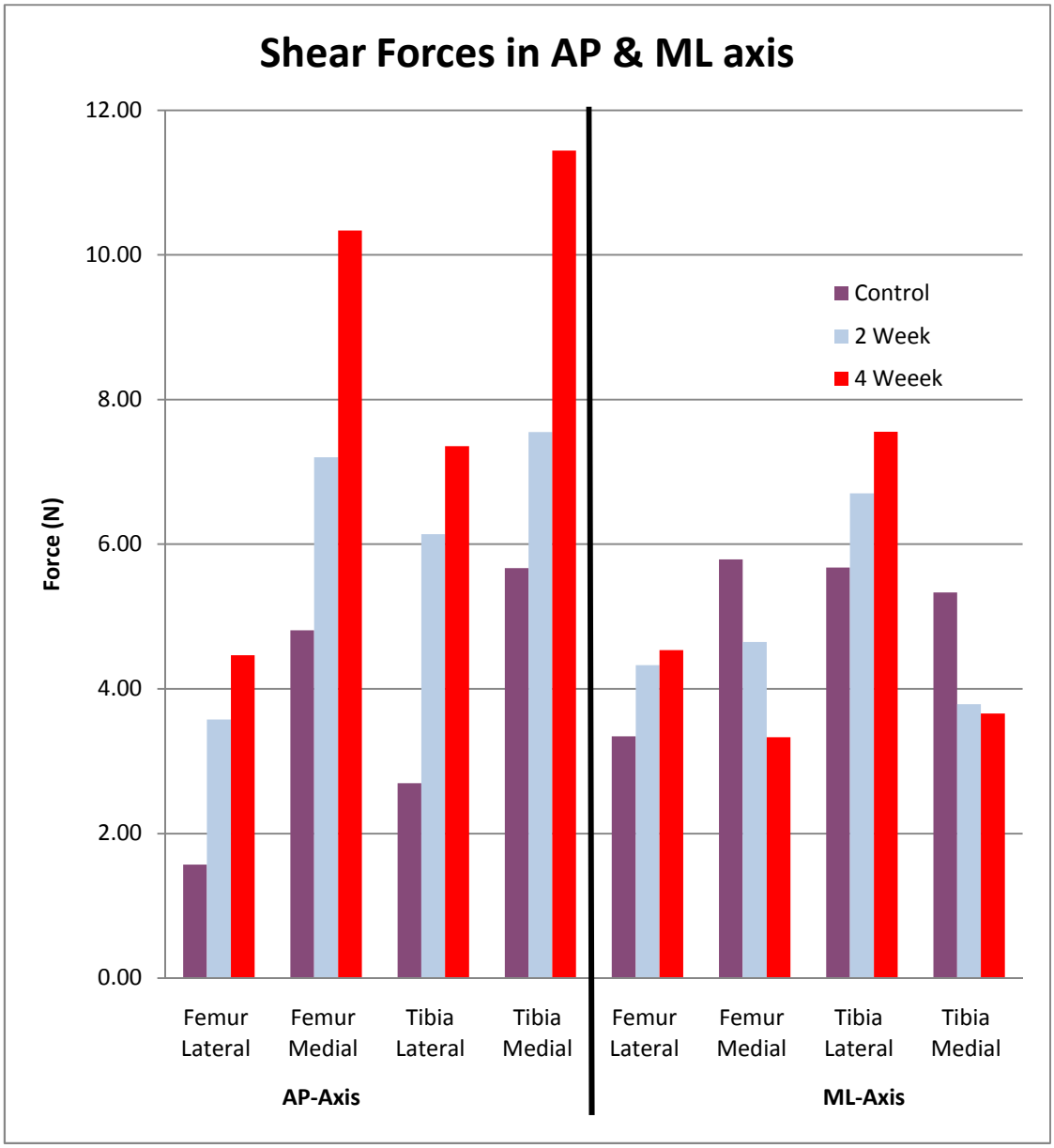

Figure 4.9: Graph represents the shear forces forces along the anterior posterior and medial lateral axis. Graph has four sections femur lateral, femur medial, tibia lateral and tibia medial. Each has three columns, first column is control, second one is 2 week loaded and third one is 4 week loaded.

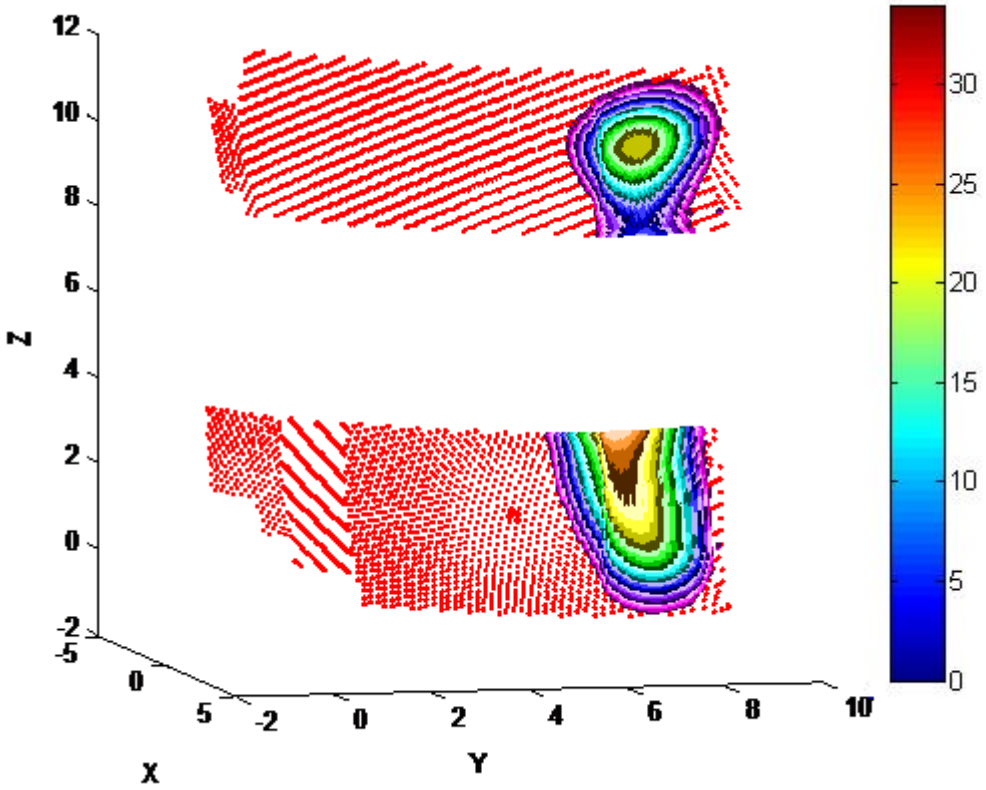

Figure 4.10: Contact stresses on femur for the 4 week loaded model.

As indicated by the contour map the stresses on the medial side are a lot greater than the lateral side for the 4 week loaded medial femur (max 26.6 N/mm^2). For the contralateral side the max stress was 18.6 N/mm^2.

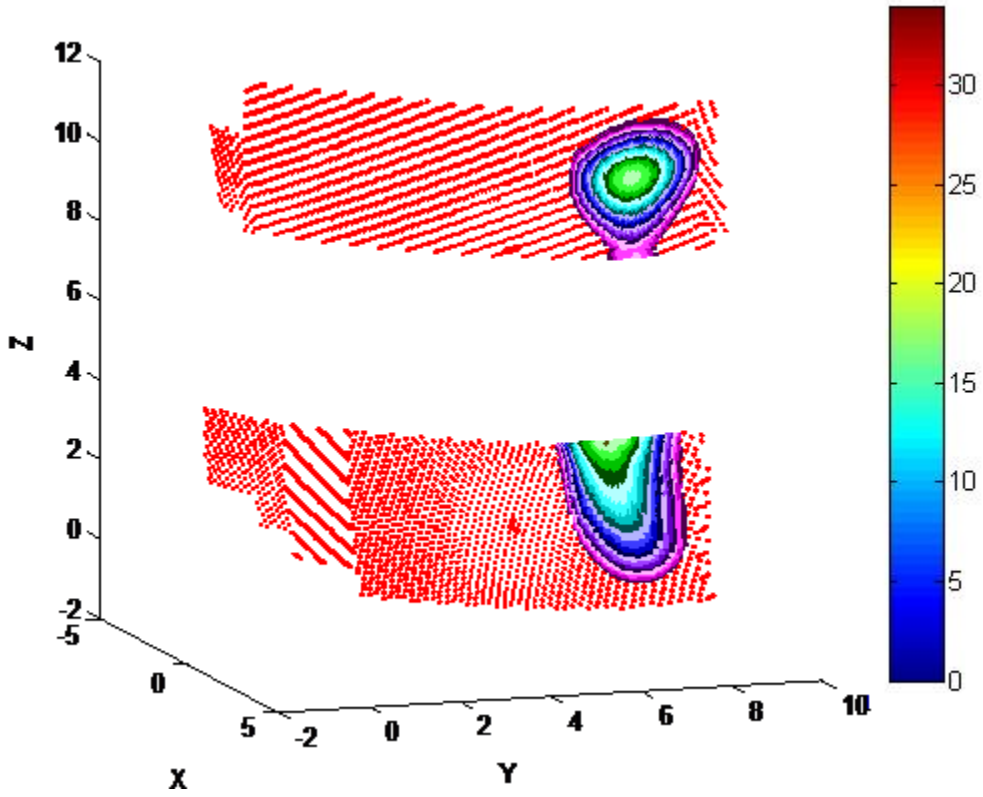

Figure 4.11: Contact stresses on femur for the 2 week loaded one.

When compared to the 4 week loaded model the contact stresses are less than the 2 week loaded model (max 20.2 N/mm^2).

Chapter 5

DISCUSSION

5.1 Biomechanical properties results

As indicated by the results at the end of four weeks there were significant changes in the biomechanical properties of the loaded joints. Mechanical properties as determined by the indentation tests clearly show that there was a significant decrease in stiffness of the articular cartilage in both the femur and tibia. Previous studies have shown that the aggregate modulus or compressive modulus decrease in both humans [47], [48] and rabbits [34]. There were decreases of 65% in the aggregate modulus on the medial femoral side and a decrease of 40% in the lateral femoral side and a total decrease of 55% throughout the femur when compared with the contralateral side at the end of four weeks. The average value of the modulus of the four week medial contralateral side was about 0.521 ± 0.332 MPa which was comparable to the one obtained by controls of the anterior cruciate ligament transection surgery 0.75 ± 0.28 MPa [34].

The modulus in four week medial tibial side had a decrease of about 31% with a trend towards difference rather than significance. We expected the effect of the applied moment to have an impact on the tibial plateau as well. The four week contralateral medial tibial plateau had an average aggregate modulus of about 0.846 ± 0.573 MPa which was comparable to 0.78 ± 0.24 MPa as obtained by a previous research [49]. The high standard deviation was attributed to one of the rabbit where the aggregate modulus was significantly higher than others.

The two week rabbits did not follow the patterns of the four week animals. There was an increase of 12% and 10% in the aggregate modulus of the femoral medial condyle and lateral condyle respectively with an overall increase of about 11% in the femur when compared with contralateral femoral side. One probable theory is that an internal repair mechanism such as repair by the articular cartilage might be working to prevent the effects of

the loading. In the case of two week tibia there was a significant decrease of about 25% and an increase of 20% in the medial and the lateral compartments respectively. The increase in the modulus of the lateral compartment is an anomaly and probably be explained by the internal repair mechanism.

In the canine model of OA based on transection of the anterior cruciate ligament, there was a decrease of about 27-31% of the aggregate modulus in the tibial plateau when compared with the control at the end of 6 and 12 weeks following the surgery [50]. In the rabbit model of OA based on meniscectomy the aggregate modulus decreased by 20-30% at the end of 8-26 weeks of surgery [51]. In the goat model of chemically induced OA there was a decrease of about 69% in the aggregate modulus of the tibial plateau [52]. The aggregate modulus represents the stiffness of articular cartilage in compression in equilibrium when all the fluid motion has ceased. Higher the modulus leads to lower deformation in the tissue under a given load. With the degradation of the tissue the normal stress bearing mechanism is disturbed and hence the tissue becomes more compliant or easily deformable. This may lead to changes in the stress distribution. These changes as reflected by decrease of aggregate modulus are an indicator of the progression of OA.

Permeability was found to significantly higher in the four week tibia about 84% in the medial compartment and 63% in the lateral compartment. Even though the increase seems large in terms of percentage change, the order of the permeability is 10^{-15} – 10^{-16}. In the four week femur there was very slight non significant increase in the permeability was noticed in both medial and lateral condyles. Significant increase of about 67% in permeability of the two week tibial lateral plateau was noticed and a non-significant decrease in the medial tibial plateau was determined. In the two week femoral lateral side there was a non-significant increase of about 15% was found and a 10% decrease in the medial side.

The average value of the femoral permeability in the control of the rabbit based ACL transection model 0.639 ± 0.279 10^{-15} m^2 / Pa-s [34] was similar to the values obtained here 0.494 ± 0.276 10^{-15} m^2 / Pa-s, but slightly lower than 2.0 ±1.6 10^{-15} m^2 / Pa-s, values obtained by Bonassar [53]. The permeability is also an important factor in assessing the frictional interactions between interstitial fluid flow and the solid matrix. Permeability in simple terms, of a tissue can be defined as a means of flow of water flow through tissue with some resistance. The compressive forces cause the cartilage to be loaded, resulting in the fluid to exude out and the solid matrix to be compressed. The rate of efflux depends on the permeability. With higher the permeability there is higher the rate of efflux, which in turn causes less load sharing

in by the fluid in the cartilage and more load is carried by the solid matrix. Similarly the lower the permeability, the lower the rate of efflux, and more load is borne by the fluid which decreases the pressure of the solid matrix. Higher permeability is also an indicator of the progression of OA.

When comparing the loaded results of the 4 weeks and 2 weeks there was a decrease in the aggregate modulus as expected. With increased loading the articular cartilage's normal functioning is disrupted and will result in the changes of the mechanical properties. Nothing was significant in the results of tibia and Poisson's ratio of either femur or tibia. The permeability however decreased in the 4 week loaded lateral femur when compared to the 2 week loaded samples. One reason might be that the load decreased on the lateral femur in 4 week specimen. As the aggregate modulus decreased (0.226 MPa for 4 week vs. 0.299 MPa for 2 week) one would expect the permeability to increase. An increase in permeability would lead to the increase in the load shared by the solid matrix but even though the modulus decreased it did not decrease much in terms of magnitude hence a decrease in the load might have resulted in the decrease in the permeability. The permeability increased significantly in the whole tibia, lateral tibia and medial tibia as the loading increased.

One would expect that there will not be any change or any significant difference between the controls of 4 weeks and 2 weeks but the results indicate otherwise. The aggregate modulus increased by significant amount in the four week controls of whole femur, medial femur and lateral femur. It might indicate some kind of internal systemic control through a endocrine related response. As the animal experiences increased load on the loaded side, it tries to repair the control side also. Significant contralateral responses have been noted in other animal studies of the anterior cruciate ligament, where material properties changes were seen [53].

5.2 Trabecular bone morphology results

Bone properties indicate changes occurring at the subchondral level which in turn depend on the stress acting on the cartilage. One of the important bone properties is BMD which indicates the amount of actual mineral per volume. In the four week loaded femur there was a significant 12% increase in the lateral side, a significant decrease of 9% in the medial side and overall non-significant decrease of 0.2%. The four week tibia had a similar trend,

where in the lateral side had a slight non-significant increase of 2.7% and the medial side had a significant decrease of 14.1% with overall significant decrease of 6.1%. Usually high BMD is correlated with the progression of disease [54] but there have been cases where the BMD initially decreased and then increases [55] and a case where there has been a decrease in the BMD content [56]. The average value of BMD of normal femur was 448.93 ± 68.66 mg/cc which was close to 341.1 ±28.8 mg/cc the values obtained by MacNeil [57]. The BMD of two week loaded femur had 3.4% increase in lateral side and 7.7% decrease in the medial side with strong trends in both the compartments. Two week loaded tibia had a significant decrease of 5.89% in the medial side and whole tibia with a non-significant decrease in the 0.9%.

One explanation to the decrease in the BMD would be that during initial load bearing, one compartment of the knee received increased stresses compared to the other [53]. Here the medial plateau being the compartment with lesser BMD hence higher stress and the lateral side may have been stress shielded. Another paper also cited that during the initial stages of OA there was a decrease in the BMD due to incomplete mineralization of trabecular structure [58]. The amount of the decrease at 12% in the medial side with the four week femur clearly indicated increased stresses in that compartment.

The other bone properties such as Tb. T (Trabecular Thickness), Tb. N (Trabecular Number) and Tb. S (Trabecular Separation) all depend on BMD in one way or another. BVF or bone volume fraction decreased significantly in the four loaded femur and tibia and their compartments individually as well except lateral tibia. In the two week loaded lateral femur had a significant increase and a significant decrease medial femur and tibia as a whole. It has been shown in a guinea pig based OA model that initially there was a loss of BVF and later in the advanced OA there was an increase in the BVF [59]. Four weeks of loading is can easily be considered as initial stages considering the surgery based models going up to 40 weeks.

Tb. T or trabecular thickness and Tb. N or trabecular number are interrelated with Tb. S or trabecular separation. If Tb. T and Tb. N decrease then Tb. S will increase which is what the results from the four week loaded femur and tibia represent. The guinea pig based model also concluded that Tb. T decrease initially and increased towards the later stages in OA [Layton et al., 1988]. Another paper cited during the initial stages of OA in humans the Tb. S increase significantly and Tb. N and Tb. T decreased significantly [60]. The results obtained here are concurrent with their findings indicating the presence of early OA.

Comparisons were made between the 4 week loaded and 2 week loaded for femur and tibia. The BMD increased significantly in whole femur, lateral femur, whole tibia, lateral tibia and medial tibia. Previous studies have shown that increased loading results in an increase in the BMD in the later stages of OA [4]. This trend can be seen in the results even when compared to the controls where there was a decrease in the BMD. When compared to 2 week loaded specimens, in the 4 week samples Tb. T increased significantly in whole femur, medial femur, whole tibia and medial tibia with a strong trend in lateral tibia. In the 4 week specimens, Tb. N decreased significantly in the whole femur, lateral femur, whole tibia and medial tibia with a strong trend in medial femur and lateral tibia. In previous studies, it was indicated that increased trabecular thickness and decreased trabecular number may be indicators of the progression of OA [Sharma and Berenbaum, 2007]. With an increase in the duration of loading, the amount of damage to the tissue is expected to increase which will in turn affect the trabecular structural parameters.

One would expect that there would not be any significant differences between the 4 week and 2 week controls, but the results indicate otherwise. There have been changes in the mechanical properties of the articular cartilage in the controls between the 4 week and 2 week loading periods. This is bound to have an effect on the trabecular bone morphology. In the 4 week controls, the BMD increased significantly except in medial femur. BVF increased significantly except in whole femur and medial femur. There is a possibility that the animal might be trying to adapt to a posture which might lead to less loading on the loaded leg. Also an internal, systemic control might be working within these animals which might have increased BMD and BVF. Any one of these reasons could have led to the changes in these bone trabecular morphological parameters.

5.3 Histology results

The scores were calculated on the guidelines provided in Table 3.1. In our case, the major component of the scores was either reduced amount of staining or clefts and fissures or both or sometimes disruption of the tidemark. The histological scores of the stained samples indicate that there have been a definitive changes occurring at the tissue level of the articular cartilage. The 4 week loaded medial femur (Mean=3.22) had significantly higher score when compared to the unloaded medial (Mean=0.67). The 4 week loaded lateral femur (Mean=3.06) had also significantly higher score when compares to the unloaded lateral femur (Mean=1.07).

These results coupled with the gross morphological analysis from the 4 week loaded femur (which signifies less staining and in turn points to a decrease in the proteoglycan content) indicate the restructuring of the tissue. A decrease in proteoglycan content has been shown as an important factor associated with progression of OA [61]. The gross morphology also indicated changes such as occasional disruption of tidemark and staining into the calcified region. The rare fibrillations indicate the surface of cartilage is degrading. One explanation to the decrease in staining is the decrease in the aggregate modulus. The decrease in aggregate modulus might have resulted in the restructuring of the cartilage and a decrease in proteoglycan content is directly related to decrease in the aggregate modulus. Negatively charged proteoglycan provides the resistance to the compressive loads by repulsion among the other proteoglycan molecules. These changes again point to the observation that the 4 week loaded cartilage structure is no longer same when compared to the normal cartilage.

The 2 week loaded femur medial (Mean=2.86) and lateral (Mean=2.41) were also significantly higher when compared to the unloaded medial femur (Mean=1.08) and unloaded lateral femur (Mean=1.59) respectively. The gross morphological changes consisted of very rare disruption of tidemark and very slight reduction in the staining indicative of minor changes in the tissue level. Very slight reduction in the staining signifies reduction in the proteoglycan content.

The 4 week loaded medial tibia (Mean=2.80) had a significantly higher grade than the unloaded medial tibia (Mean=1.36). The 4 week loaded lateral tibia (Mean=1.97) was also significantly higher than the unloaded lateral tibia (Mean=0.95). The gross morphological analysis for tibia was similar but slightly more staining when compared to femur indicating loss of proteoglycan. The surface was more irregular and slight tears and occasional clefts indicate that the tibial cartilage was undergoing a faster rate of degradation. The scores although were less than corresponding for the femur but the major component of the scores included grade for fibrillation and clefts rather than the decrease in the staining, which was a major component in the score of the femur rather than fibrillation or clefts on the surface of cartilage. The aggregate modulus did not decrease much and as a result of which there is not much restructuring in the cartilage which could explain the slight reduction in the staining.

The 2 week loaded medial tibia (Mean=3.00) was higher than 4 week loaded medial femur, which can only highlight the problems associated with grading process. As discussed before, there were few slides which had clefts and fissures which were caused by sectioning

procedure, rather than degradation. It is possible that those slides belonged to these groups of 2 week loaded medial tibia and 2 week loaded lateral tibia. The average was high because of the grade only due to clefts rather than decreased staining; which further seems to indicate the presence of the above mentioned samples. The same factor seems to effect the control of this group; medial tibia (Mean=2.01) and lateral tibia (Mean=1.77).

5.4 Joint modeling results

The joint modeling results clearly indicate that the loads were increasing with time and so were the stresses. The loaded four week simulation had higher contact loads acting on femur and forces in other directions increased as well. The four week loaded ones had higher varus angle at which the optimization was terminated (6.6^0) when compared with two week (5.9^0) and control (4.42^0). As the varus angle increases so does the load transmitting through the medial compartment.

	Four Week Loaded		Two Week Loaded	
	Lateral	Medial	Lateral	Medial
X-Force	-5.96142	13.6293	-2.37061	3.64857
Y-Force	184.141	114.964	127.552	49.8231
Z-Force	35.7013	-42.4563	29.5065	-19.7076

Table 5.1: The % change in the loads of the femur for four weeks and two weeks subjects when compared with the control loads.

The table indicates that the there was an increase of 13.6% in the medial contact load which is 9.39 N approximately 19% increase of body weight of the rabbit. These loads will cause increased stresses and will lead to degradation of the cartilage and subchondral bone remodeling as indicated by the changes in the stiffness values and the BMD values. Even though the forces in Y direction have increased by 184.1% and 114.9%, the load values have

increased by 2.8 N and 5.2 N in lateral and medial compartments. The loads in Z direction have increased in the lateral compartment direction but decreased in the medial compartment. The loads in Y and Z direction can be assumed as the shear forces where as the load in X direction is the compressive contact force. The increase in shear can also be accounted for the degradation of cartilage surface as the cartilage is not that stiff in shear when compared to the compression. The increase in the loads in medial direction can also explain the decrease in the BMD and decrease in the loads of the lateral direction led to an increase in the BMD in the lateral compartment, as increased loading causes bone resorption and vice-versa, which in turn explain the increase in the Tb. S.

	Four Week Loaded		Two Week Loaded	
	Lateral	Medial	Lateral	Medial
X-Force	-9.243	16.231	-2.451	7.659
Y-Force	172.989	101.756	127.829	33.151
Z-Force	33.112	-31.392	18.111	-28.978

Table 5.2: The % change in the loads of the tibia for four weeks and two weeks subjects when compared with the control loads.

The loads in the tibia for the 4 week contralateral (Medial= 75.467, Lateral= 73.643) are similar to 77.57 N (Medial) and 87.07 N (Lateral) obtained by Grover et al [46]. In another study by Lerner et al., [62] the medial joint contact load (femur + tibia) for the neutral loading pattern (varus loading pattern in our case) was 300% of the body weight. Which is similar in our case, 68 N (Femur) + 75 N (Tibia) =153 which is around 300 % of 50 N body weight of the rabbit. The increase in the medial tibia loads of the 4 week loaded tibia can be a reason for the changes in the properties of the articular cartilage and as well as for the trabecular bone morphology. The shear force in the medial tibia was slightly higher than the medial femur (11.42 vs. 10.353). This slight increase in shear force might be the reason for the damage caused to the surface of the tibia resulting in the clefts and fissures; as found from the

histology results. There was a decrease in the lateral forces as well. That can be the reason there is an increase in the aggregate modulus.

5.5 Limitations

5.5.1 Animal model

The major limitation with this animal model of study is that the number of animals used for the study was limited. We used 8 animals in total; in the previous studies of involving rats the number is usually around 40 or higher. It is difficult to handle so many rabbits and also the cost involving such number would be high. More resources would be needed for taking care of them and handling during the loading time. Another limitation associated with the study was limited time periods for testing. We had just two time periods 2 weeks and 4 weeks. Generally in animal testing the time periods consist of 2, 4, 8, 12, 16, etc up to 38 weeks and more. The variability factor amongst the animal is another limitation to consider even though we used animals from the same litter and sex.

5.5.2 Mechanical testing

There are limitations associated with the mechanical testing too, the limited precision associated with the load cells and the indenter tip was not always straight. There could have been computational errors in the FEM calculations. The indentation tests were very sensitive to disturbances such as vibrations; we conducted most of the tests in the night and leave the lab till the test was completed. But still vibrations from the building were hard to dampen.

5.5.3 µ-CT

The problem with the µ-CT is that the resolution was limited to 27 µm, which is still small; that is the best we have in our University. Also while doing the bone analysis the ROI was a cube and sometimes it didn't fit exactly and we had access to only two shapes rather than complex shapes that would have fit much better.

5.5.4 Histology

There were difficulties with specimen preparation such as embedding and sectioning; we did sectioning from anterior to posterior and when we were reaching the end of sectioning we were unable to maintain the same degree of integrity. We picked sectioned samples from different intervals; there is a possibility that we might have missed an important sample. The major drawback with the grading technique was the variability in the scores. Different scores occasionally seem to only highlight the flaws associated with this methodology.

5.5.5 Modeling

The model which we used is not the most accurate representation of the articular surface. We used Bird system to generate the geometry which is susceptible to disturbances from vibrations and from other unknown sources. These limitations might have also caused changes in the insertions of the ligaments. The model didn't include any menisci and just one muscle. The major limitation with this model is that we used averaged material properties as input, rather than individual specimen properties.

Chapter 6

CONCLUSIONS AND FUTURE WORK

6.1 Articular Cartilage and Trabecular Bone Morphology

A mechanical model of early stage uni-compartmental OA was established through the previously designed device. The results indicate joint degeneration with changes resulting in trabecular bone morphology. The changes associated with this model are similar to the changes associated with early stages of OA. The decrease in aggregate modulus is major has always been associated with the progression of OA both in early stages and advance stages of OA. The decrease in the BMD in the loaded side when compared with the controls has been indicated as a marker in early stages of OA. The BMD increase in the 4 week compared to 2 week is a step in the direction of the progression of OA. Histology does not indicate a drastic collapse of the articular cartilage as seen in some other models of OA, and thus, early biological changes, and the study of the effects of treatment might be possible.

The future work will include increased joint loading duration as well as change in the amount of loading. This would determine the sensitivity of the intervention to modulate degeneration. One thing of particular interest would be to see how different amount of loading versus different loading duration would affect the changes in both the articular cartilage properties and trabecular bone morphology. In order to further test the progression of OA, the tests such as water content determination and aggrecan or proteoglycan content testing would establish the presence of OA. The advantages of a mechanical model of OA when compared with any other surgery or chemical based model of OA, is that the mechanical model does not affect the joint capsule in any manner. The surgical models induce OA in a manner unnatural to the disease progression in humans. Further tests of changes in chondrocyte biology and gene expression would be of interest.

6.2 Joint Modeling

The increase in the stresses and the loads has been known to cause destabilizing and damaging effects on any structure. With the help of joint load analysis we have shown that there has been a significant increase in the amount of loads passing through femur and tibia. The effect can be clearly seen in terms of the changes occurring at the articular cartilage and trabecular bone morphology. Increased varus loads have been cited as a reason for the progression of uni-compartmental OA. This is a first study that studies the correlation between the loads and the effects on the properties of articular cartilage and trabecular bone morphology. An increase in the joint contact loads has led to decrease in the aggregate modulus and decrease in the BMD of the trabecular bone; both the signs of early stage OA.

Future work would include a more accurate model for the analysis of the joint as well as inclusion of the menisci and more muscles. As the model does not employ a deformable mesh a finite element study of the joint will yield more accurate results of the joint analysis. Also we used averaged properties of aggregate modulus in each location; instead we would like to use individual properties for each rabbit to better understand the loading pattern.

REFERENCES

[1] J. A. Buckwalter and J. A. Martin, "Osteoarthritis," Adv Drug Deliv Rev, vol. 58, pp. 150-67, May 20 2006.

[2] L. Sharma, et al., "The role of knee alignment in disease progression and functional decline in knee osteoarthritis," JAMA, vol. 286, pp. 188-95, Jul 11 2001.

[3] J. A. Barrios, et al., "Walking shoes and laterally wedged orthoses in the clinical management of medial tibiofemoral osteoarthritis: a one-year prospective controlled trial," Knee, vol. 16, pp. 136-42, Mar 2009.

[4] S. Cahue, et al., "Varus-valgus alignment in the progression of patellofemoral osteoarthritis," Arthritis Rheum, vol. 50, pp. 2184-90, Jul 2004.

[5] T. P. Andriacchi, "Dynamics of knee malalignment," Orthop Clin North Am, vol. 25, pp. 395-403, Jul 1994.

[6] L. Sharma, et al., "Knee adduction moment, serum hyaluronan level, and disease severity in medial tibiofemoral osteoarthritis," Arthritis Rheum, vol. 41, pp. 1233-40, Jul 1998.

[7] O. D. Schipplein and T. P. Andriacchi, "Interaction between active and passive knee stabilizers during level walking," J Orthop Res, vol. 9, pp. 113-9, Jan 1991.

[8] B. W. Lim, et al., "Does knee malalignment mediate the effects of quadriceps strengthening on knee adduction moment, pain, and function in medial knee osteoarthritis? A randomized controlled trial," Arthritis Rheum, vol. 59, pp. 943-51, Jul 15 2008.

[9] J. Martel-Pelletier, et al., "Cartilage in normal and osteoarthritis conditions," Best Pract Res Clin Rheumatol, vol. 22, pp. 351-84, Apr 2008.

[10] M. Del Carlo, Jr. and R. F. Loeser, "Cell death in osteoarthritis," Curr Rheumatol Rep, vol. 10, pp. 37-42, Jan 2008.

[11] X. L. Lu and V. C. Mow, "Biomechanics of articular cartilage and determination of material properties," Med Sci Sports Exerc, vol. 40, pp. 193-9, Feb 2008.

[12] P. H. Byers, "Folding defects in fibrillar collagens," Philos Trans R Soc Lond B Biol Sci, vol. 356, pp. 151-7; discussion 157-8, Feb 28 2001.

[13] T. Yasuda, et al., "Peptides of type II collagen can induce the cleavage of type II collagen and aggrecan in articular cartilage," Matrix Biol, vol. 25, pp. 419-29, Sep 2006.

[14] M. W. Holmes, et al., "Hyaluronic acid in human articular cartilage. Age-related changes in content and size," Biochem J, vol. 250, pp. 435-41, Mar 1 1988.

[15] G. Cs-Szabo, et al., "Large and small proteoglycans of osteoarthritic and rheumatoid articular cartilage," Arthritis Rheum, vol. 38, pp. 660-8, May 1995.

[16] M. Zhang, et al., "Estimating the effective Young's modulus of soft tissues from indentation tests--nonlinear finite element analysis of effects of friction and large deformation," Med Eng Phys, vol. 19, pp. 512-7, Sep 1997.

[17] W. C. Hayes, et al., "A mathematical analysis for indentation tests of articular cartilage," J Biomech, vol. 5, pp. 541-51, Sep 1972.

[18] C. G. Armstrong, et al., "An analysis of the unconfined compression of articular cartilage," J Biomech Eng, vol. 106, pp. 165-73, May 1984.

[19] J. M. Coletti, Jr., et al., "A comparison of the physical behavior of normal articular cartilage and the arthroplasty surface," J Bone Joint Surg Am, vol. 54, pp. 147-60, Jan 1972.

[20] V. C. Mow, et al., "Biphasic creep and stress relaxation of articular cartilage in compression? Theory and experiments," J Biomech Eng, vol. 102, pp. 73-84, Feb 1980.

[21] A. F. Mak, et al., "Biphasic indentation of articular cartilage--I. Theoretical analysis," J Biomech, vol. 20, pp. 703-14, 1987.

[22] A. M. Bendele and J. F. Hulman, "Effects of body weight restriction on the development and progression of spontaneous osteoarthritis in guinea pigs," Arthritis Rheum, vol. 34, pp. 1180-4, Sep 1991.

[23] A. Bendele, et al., "Animal models of arthritis: relevance to human disease," Toxicol Pathol, vol. 27, pp. 134-42, Jan-Feb 1999.

[24] M. Walton, "Degenerative joint disease in the mouse knee; radiological and morphological observations," J Pathol, vol. 123, pp. 97-107, Oct 1977.

[25] S. Mahr, et al., "Sexual dimorphism in the osteoarthritis of STR/ort mice may be linked to articular cytokines," Ann Rheum Dis, vol. 62, pp. 1234-7, Dec 2003.

[26] J. M. Jordan, et al., "Ethnic and sex differences in serum levels of cartilage oligomeric matrix protein: the Johnston County Osteoarthritis Project," Arthritis Rheum, vol. 48, pp. 675-81, Mar 2003.

[27] E. M. Wojtys and D. B. Chan, "Meniscus structure and function," Instr Course Lect, vol. 54, pp. 323-30, 2005.

[28] K. Messner and J. Gao, "The menisci of the knee joint. Anatomical and functional characteristics, and a rationale for clinical treatment," J Anat, vol. 193 (Pt 2), pp. 161-78, Aug 1998.

[29] D. McNicol and P. J. Roughley, "Extraction and characterization of proteoglycan from human meniscus," Biochem J, vol. 185, pp. 705-13, Mar 1 1980.

[30] A. M. Ahmed and D. L. Burke, "In-vitro measurement of static pressure distribution in synovial joints--Part I: Tibial surface of the knee," J Biomech Eng, vol. 105, pp. 216-25, Aug 1983.

[31] D. Laurent, et al., "In vivo MRI of cartilage pathogenesis in surgical models of osteoarthritis," Skeletal Radiol, vol. 35, pp. 555-64, Aug 2006.

[32] M. A. LeRoux, et al., "Simultaneous changes in the mechanical properties, quantitative collagen organization, and proteoglycan concentration of articular cartilage following canine meniscectomy," J Orthop Res, vol. 18, pp. 383-92, May 2000.

[33] L. M. Wancket, et al., "Anatomical localization of cartilage degradation markers in a surgically induced rat osteoarthritis model," Toxicol Pathol, vol. 33, pp. 484-9, 2005.

[34] R. L. Sah, et al., "Physical properties of rabbit articular cartilage after transection of the anterior cruciate ligament," J Orthop Res, vol. 15, pp. 197-203, Mar 1997.

[35] T. Kikuchi, et al., "Intra-articular injection of collagenase induces experimental osteoarthritis in mature rabbits," Osteoarthritis Cartilage, vol. 6, pp. 177-86, May 1998.

[36] P. M. van der Kraan, et al., "Degenerative knee joint lesions in mice after a single intra-articular collagenase injection. A new model of osteoarthritis," J Exp Pathol (Oxford), vol. 71, pp. 19-31, Feb 1990.

[37] J. Wismans, et al., "A three-dimensional mathematical model of the knee-joint," J Biomech, vol. 13, pp. 677-85, 1980.

[38] L. Blankevoort, et al., "Articular contact in a three-dimensional model of the knee," J Biomech, vol. 24, pp. 1019-31, 1991.

[39] A. J. Baliunas, et al., "Increased knee joint loads during walking are present in subjects with knee osteoarthritis," Osteoarthritis Cartilage, vol. 10, pp. 573-9, Jul 2002.

[40] V. M. Goldberg and J. A. Buckwalter, "Hyaluronans in the treatment of osteoarthritis of the knee: evidence for disease-modifying activity," Osteoarthritis Cartilage, vol. 13, pp. 216-24, Mar 2005.

[41] V. C. Mow, et al., "Biphasic indentation of articular cartilage--II. A numerical algorithm and an experimental study," J Biomech, vol. 22, pp. 853-61, 1989.

[42] J. S. Jurvelin, et al., "Comparison of optical, needle probe and ultrasonic techniques for the measurement of articular cartilage thickness," J Biomech, vol. 28, pp. 231-5, Feb 1995.

[43] H. J. Mankin, "Biochemical and metabolic aspects of osteoarthritis," Orthop Clin North Am, vol. 2, pp. 19-31, Mar 1971.

[44] K. P. Pritzker, et al., "Osteoarthritis cartilage histopathology: grading and staging," Osteoarthritis Cartilage, vol. 14, pp. 13-29, Jan 2006.

[45] K. L. Camplejohn and S. A. Allard, "Limitations of safranin 'O' staining in proteoglycan-depleted cartilage demonstrated with monoclonal antibodies," Histochemistry, vol. 89, pp. 185-8, 1988.

[46] D. M. Grover, et al., "Biomechanics of the rabbit knee and ankle: muscle, ligament, and joint contact force predictions," J Biomech, vol. 40, pp. 2816-21, 2007.

[47] C. G. Armstrong and V. C. Mow, "Variations in the intrinsic mechanical properties of human articular cartilage with age, degeneration, and water content," J Bone Joint Surg Am, vol. 64, pp. 88-94, Jan 1982.

[48] G. Grushko, et al., "Some biochemical and biophysical parameters for the study of the pathogenesis of osteoarthritis: a comparison between the processes of ageing and degeneration in human hip cartilage," Connect Tissue Res, vol. 19, pp. 149-76, 1989.

[49] K. A. Athanasiou, et al., "Interspecies comparisons of in situ intrinsic mechanical properties of distal femoral cartilage," J Orthop Res, vol. 9, pp. 330-40, May 1991.

[50] L. A. Setton, et al., "Mechanical properties of canine articular cartilage are significantly altered following transection of the anterior cruciate ligament," J Orthop Res, vol. 12, pp. 451-63, Jul 1994.

[51] D. H. Hoch, et al., "Early changes in material properties of rabbit articular cartilage after meniscectomy," J Orthop Res, vol. 1, pp. 4-12, 1983.

[52] N. A. Le and B. C. Fleming, "Measuring fixed charge density of goat articular cartilage using indentation methods and biochemical analysis," J Biomech, vol. 41, pp. 715-20, 2008.

[53] L. J. Bonassar, et al., "In vivo effects of stromelysin on the composition and physical properties of rabbit articular cartilage in the presence and absence of a synthetic inhibitor," Arthritis Rheum, vol. 38, pp. 1678-86, Nov 1995.

[54] A. Fahlgren, et al., "Meniscectomy leads to an early increase in subchondral bone plate thickness in the rabbit knee," Acta Orthop Scand, vol. 74, pp. 437-41, Aug 2003.

[55] P. C. Pastoureau, et al., "Evidence of early subchondral bone changes in the meniscectomized guinea pig. A densitometric study using dual-energy X-ray

absorptiometry subregional analysis," Osteoarthritis Cartilage, vol. 7, pp. 466-73, Sep 1999.

[56] K. Messner, et al., "Simultaneous changes in bone mineral density and articular cartilage in a rabbit meniscectomy model of knee osteoarthrosis," Osteoarthritis Cartilage, vol. 8, pp. 197-206, May 2000.

[57] J. A. MacNeil, et al., "Preservation of periarticular cancellous morphology and mechanical stiffness in post-traumatic experimental osteoarthritis by antiresorptive therapy," Clin Biomech (Bristol, Avon), vol. 23, pp. 365-71, Mar 2008.

[58] E. A. Messent, et al., "Fractal analysis of trabecular bone in knee osteoarthritis (OA) is a more sensitive marker of disease status than bone mineral density (BMD)," Calcif Tissue Int, vol. 76, pp. 419-25, Jun 2005.

[59] M. W. Layton, et al., "Examination of subchondral bone architecture in experimental osteoarthritis by microscopic computed axial tomography," Arthritis Rheum, vol. 31, pp. 1400-5, Nov 1988.

[60] R. I. Bolbos, et al., "Relationship between trabecular bone structure and articular cartilage morphology and relaxation times in early OA of the knee joint using parallel MRI at 3 T," Osteoarthritis Cartilage, vol. 16, pp. 1150-9, Oct 2008.

[61] D. Laurent, et al., "In vivo assessment of macromolecular content in articular cartilage of the goat knee," Magn Reson Med, vol. 49, pp. 1037-46, Jun 2003.

[62] D. L. Gushue, et al., "Rabbit knee joint biomechanics: motion analysis and modeling of forces during hopping," J Orthop Res, vol. 23, pp. 735-42, Jul 2005.

[63] Zhang, L. and Szeri, A.Z. "Neutral solute transport in articular cartilage: effects of loading and particle size." Proc. R. Soc. London, A 459, 2021-2042., 2005.

[64] Marquet P. "Biomechanics of the knee: with applications to the pathogenesis and the surgical treatment of osteoarthritis", Berlin, Springer-Verlag, 1984.

[65] Van C Mow,Rik Huiskes. "Basic Orthopaedic Biomechanics and Mechano-Biology", Lippincott Williams & Wilkins, Third Edition edition, December 1, 2004.

[66] Kalker, J J. " A Course of Contact Mechanics", Delft University of Technology, Delft, The Netherlands.

[67] Christina M. Turka. Thesis- "A Model of Uni-compartmental Osteoarthritis and Experimental Measurements of Material Properties of Cartilage", 2005.

[68] Lei, Fulin. Thesis- "Modeling of articular cartilage : optimization, large deformation, and microstructure" , 2006.

[69] Bendele, A. “Animal models of rheumatoid arthritis.”, J Musculoskelet Neuronal Interact. 2001 Jun;1(4):377-85.

[70] Guilak, F et al. “Mechanical and biochemical changes in the superficial zone of articular cartilage in canine experimental osteoarthritis”, J Orthop Res. 1994 Jul;12(4):474-84.

[71] Li, M, et al. “Parathyroid hormone monotherapy and cotherapy with antiresorptive agents restore vertebral bone mass and strength in aged ovariectomized rats”. Bone 16, 629-35, 2005.

[72] K. E. Kuettner and V. M.Goldberg. “Osteoarthritic Disorders”, Illinois:

American Academy of Orthopaedic Surgeons, 1995. ISBN: 0-89203-129-8.

[73] Korhonen et al. “Comparison of the equilibrium response of articular cartilage in unconfined compression, confined compression and indentation”. J of Biomech 35 (2002) 903–909.